POLITECNICO
MILANO 1863

ADDITIVE MANUFACTURING FOR COMPOSITE TOOLING

UV-Assisted 3D Printing of Thermoset Materials Reinforced with Pristine and Recycled Glass Fibers

POLITECNICO DI MILANO

School of Industrial and Information Engineering
Department of Chemistry, Materials and Chemical Engineering "Giulio Natta"
Master of Science in Materials Engineering and Nanotechnology

Author: Luca Luzzatto
ID: 883338
Academic Year: 2017-2018

Supervisor: Prof. Marinella Levi
Co-supervisor: Andrea Mantelli

DON'T PANIC

[Douglas Adams]

Really, don't. It's never worth it.

Table of Contents

List of Figures

List of Tables

List of Charts

Glossary

#

3DP	3D Printed

A

ABS	Acrylonitrile Butadiene Styrene
AM	Additive Manufacturing
ASA	Acrylonitrile Styrene acrylate

B

BAAM	Big Area Additive Manufacturing
BMC	Bulk Moulding Compound

C

CAD	Computer Aided Design
CF	Carbon Fiber
CFR	Carbon Fiber Reinforced
CNC	Computer Numerical Control
CNR	Consiglio Nazionale delle Ricerche
CTE	Coefficient of Thermal Expansion
CVD	Chemical Vapour Deposition

D

DFAM	Design For Additive Manufacturing

DLP	Digital Light Processing
DFMA	Design For Manufacturing And Assembly
DSC	Differential Scanning Calorimetry
DMA	Dynamic Mechanical Analysis
DMD	Digital Micro-mirror Device
DMTA	Dynamic Mechanical Thermal Analysis

F

FDM	Fused Deposition Melting
FRP	Fiber Reinforced Polymer
FT-IR	Fourier Transform Infrared Spectroscopy

G

GFRP	Glass Fiber Reinforced Polymer

I

IPN	Interpenetrating Polymer Network

L

LCP	Liquid Crystal Polymer
LDM	Liquid Deposition Modeling
LED	Light Emitting Diode
LSAM	Large Scale Additive Manufacturing

M

MEKP	Methyl Ethyl Ketone Peroxide

N

NC	Numeric Control
O	
OM	Optical Microscopy
ORNL	Oak Ridge National Laboratory
P	
PA	Polyamide
PC	Polycarbonate
PEI	Polyether Imide
PEEK	Polyether Ether Ketone
PEKK	Polyether Ketone Ketone
PETG	Polyethylene Terephthalate Glycol
PHR	Parts per Hundred Resin
PLA	Polylactic Acid
PAEK	Polyaryletherketone
PPS	Polyphenylene Sulphide
PPSU	Polyphenylsulfone
Q	
R	
RTM	Resin Transfer Moulding
S	
SEM	Scanning Electron Microscope
SLA	Stereolitography

SLS	Selective Layer Sintering
SMC	Sheet Moulding Compound

T

TGA	Thermogravimetric Analysis
TMA	Thermomechanical analysis

U

UTS	Ultimate Tensile Strength
UV	Ultraviolet
UV-DSC	Differential Scanning Photocalorimetry

V

VARTM	Vacuum Assisted Resin Transfer Moulding
VOC	Volatile Organic Compound

Abstract

Composite materials play a major role in modern industry. During the last decades, their use has greatly increased, and the market predictions do no foresee any imminent changes in this trend. The currently biggest hurdles to overcome for an even wider adoption of these extremely promising materials are the very high costs and slow production times of the necessary tooling. Additive manufacturing technologies are considered a viable solution, since they offer a cheaper and faster alternative to traditional technologies for the production of the necessary moulds, jigs, mandrels and fixtures. However, the currently existing techniques, based on thermoplastic polymers, present certain drawbacks related to the materials' high coefficients of thermal expansion and intrinsic sensitivity to the high temperatures typical of the most demanding autoclave cycles. This work addresses this issue by proposing an alternative technology based on thermoset photopolymers manufactured on a Liquid Deposition Modelling (LDM) system. Given the importance of sustainability and circular economy, the performance of these polymers are enhanced by the addition of various types of not only pristine, but also recycled glass fibers obtained within the framework of the European FiberEUse project. Novel composite materials suitable for these applications are identified, their mechanical and thermal properties are thoroughly characterized and their applicability to the aforementioned tooling issues is demonstrated.

1. Introduction

1.1 Composite Materials

Composite material: the result of the combination of two or more materials. Certain properties are enhanced compared to those of the precursors.

Figure 1.1 Vestas Sailrocket 2, an experimental sailing machine currently holding the world record for speed sailing, at 65.45 knots (121.21 km/h) on a 500 m run. It makes extensive use of composite materials, without which its realization would have been impossible. [1]

Composite materials are everything but a new idea. The first traces date back to 3400 B.C, when the Egyptians glued papyrus plant strips at different angles, creating what would now be called an asymmetric cross-ply laminate [2]. Paintings in Egyptian tombs document the manufacturing techniques for mud and straw bricks [3], and the Romans made extensive use of concrete, with many structures still standing today [4]. Technological process in the field proceeded at a somewhat slow pace until the end of the XIX century, when the polymer revolution struck the world of chemistry and materials science [5]. New synthetic resins were developed at an astonishing pace. As ground-braking as they were, however, these materials still lacked the strength of classical structural materials, such as steel and aluminium. In

1935, Owens Corning developed the first glass fiber [6], and the era of modern composite materials as we know them began. WWII brought glass fiber-reinforced polymers (GFRP) from research to production: by 1945, more than 3000 tons of GFRP had been used, mainly for military marine applications [7]. In 1953, the Chevrolet Corvette entered the market as the first mass-produced car that made extensive use of GFRP [8]. In 1958, boron fibers appeared in literature [9]; in 1961, the first patent for carbon fiber was issued [10]; in 1965, DuPont developed an aramid fiber currently best known under its commercial name, Kevlar [11]. While the marine market was the largest consumer of glass fiber-based composites, the ones where stiffness to weight ratio played a vital role, such as aerospace, racing and sporting goods, quickly started to make extensive use of more advanced composite materials, effectively fuelling great amounts of research in this field [12].

As of today, fiber-reinforced polymers (FRP) are more common than ever. They are considered one of the key materials of the industry of the future, since they allow levels of structural optimization, and thus weight reduction, far higher than what traditional materials have to offer [13]. If we consider the rapidly growing awareness towards ecological issues displayed by both public opinion and legislative bodies around the world, we can easily see how this is of paramount importance for those sectors where there is a strong dependence of energy consumption on mass, such as transportation (especially land- and air-). The use of these composite materials, however, is far from limited to purely technical applications. They are greatly appreciated for their strong aesthetic appeal and the intrinsic feeling of quality, durability and luxury they transmit to the final consumer, which makes them ideal for design applications. It is more and more common to encounter composite materials while shopping for furniture, luggage, watches, pens, accessories such as phone covers, and much more.

Now that we have briefly reviewed the current and future role of FRP, a description of the main materials and manufacturing techniques is due.

1.1.1 Materials for Fiber Reinforced Polymers[1]

FRP are made of fibers embedded in a polymer matrix. Depending on the application, fibers can have different sizes and arrangements; in any case, they usually have very high strength and stiffness, and act as reinforcement, bearing most of the loads. The matrix keeps them in place, distributing the stress between them and effectively giving the final shape to the component. The fiber volume fraction, v_f, is one of the most important characteristics of an FRP, as it directly governs the mechanical properties of the final material. As we will see, many of the most advanced production methods focus on maximizing this parameter.

1.1.1.1 The matrix

Various types of polymers are used as matrix, both thermoplastic and thermoset. Each of them has its own unique characteristics and is optimally suited for certain applications. Table 1.1 and Table 1.2 summarize the key information about the most common ones.

Polyester

Polyester resins are one of the most commonly used matrixes, mainly due to their very good performance to cost relation, which makes them perfectly suited for a whole variety of low- and midrange applications. They are based on unsaturated polyesters dissolved in a reactive monomer, such as styrene. Free radical initiators induce a cross-linking reaction that leads to a three-dimensional network. The polyester to monomer ratio controls the final cross-linking density. Different monomers, monomer contents, and additives, can greatly change the properties of the final product, influencing a wide range of parameters, such as heat, UV, fire or corrosion resistance.

[1] Unless otherwise noted, the information contained in this section is sourced from E. Barbero's excellent *Introduction to Composite Materials Design* book [69].

Vinyl ester

Vinyl ester resins are a better performing alternative to polyesters, having better elongation and corrosion properties, and good overall chemical resistance. They provide a cheaper alternative to the epoxies used for high-end applications and maintain the versatility typical of polyesters.

Epoxy

Epoxy resins are widely used for highly demanding applications. They have the highest mechanical properties, combined with excellent corrosion resistance, electrical insulation, low shrinkage and the highest maximum working temperatures. On the other hand, they have comparatively very high prices: therefore, their use must be justified by the requirements of the project.

Phenolic

Phenolic matrixes are less common. They have very low flammability and smoke production, and are, thus, often chosen for those applications that underly strict regulations regarding fume emissions, such as aircrafts or building interiors.

Thermoplastic

Thermoplastic matrixes do not undergo any chemical transformation during processing. They rely on heat to transfer to the liquid phase and impregnate the fibers, and return to the solid state after cooling down, forming the final composite. They can undergo this reversible transition any given number of times, meaning that repairs and modifications are much easier than for their thermoset counterparts. On the other hand, liquid thermoplastic polymers have very high viscosities, compared to liquid resins. This leads to a more difficult impregnation process; additionally, the very high shear stresses damage the fibers, effectively reducing their length and, thus, the mechanical properties of the composite.

Some of the most commonly used thermoplastic polymers for FRP are polyamide (PA) polyether ether ketone (PEEK), polyetherimide (PEI), poly sulfone (PSU) and polyphenylene sulphide (PPS).

	Polyester	Vinyl ester	Epoxy	Phenolic [14]
Tensile modulus [GPa]	2.8-3.4	3.0-3.7	2.6-4.0	2.7-4.1*
Tensile strength [Mpa]	20-75	40-90	55-100	35-60*
ε [%]	1.5-3.3	5.0-6.0	1.7-5.2	1.8-4.3*
T_g [°C]	60-130 [15]	80-130*	150-200	70-130*
CTE [10^{-6}/K]	30	40*	55	35*
Price [€/Kg]	1-5*	5-10*	2-15*	5-10*

*Table 1.1 Overview of the properties of the most common thermoset polymers for FRP matrixes. *Sourced fron "Composites Manufacturing,: Materials, Product and Process Engineering"* [14]

	PA	PEEK	PEI	PSU	PPS
Tensile modulus [GPa]	1.3-3.5*	3.2	3.0	2.5	3.3
Tensile strength [MPa]	55-90*	100	105	70	82
ε [%]	70-80*	50	60	75	5
T_g [°C]	70*	143	217	190	90
CTE [10^{-6}/K]	52*	47	56	56	49
Price [€/Kg]	5-15*	100-150*	80-130*	40-80*	50-100*

*Table 1.2 Overview of the properties of the most common thermoplastic polymers for FRP matrixes. * Sourced fron "Composites Manufacturing,: Materials, Product and Process Engineering"* [14]

1.1.1.2 The fibers

A first classification of fiber reinforcements can be made based on their size, differentiating between continuous and discontinuous fibers. Continuous fibers maximize the mechanical properties of the final composite. Discontinuous fibers, however, are cheaper to produce and are suited for a wider range of manufacturing processes. Great effort has been put into improving the performance of discontinuous fiber composites, reaching up to 50% strength and 90% stiffness of continuous fiber composites with the same reinforcement-matrix combination.

The subsequent, obvious, distinction is based on the material.

Glass fiber

Glass fibers are processed from bulk glass, and are, thus, mainly made of silica (SiO_2). Changes in the composition lead to the many types of glass fiber currently available, each aimed at a specific application. Glass fibers exhibit good chemical resistance, hardness, flexibility and corrosion resistance. These overall good properties, combined with their very low price, make them the most common reinforcement in the industry, by far.

Carbon fiber

Carbon fibers are a lightweight, stiff and strong type of reinforcement, and currently dominate the market of advanced applications. Their structure is based on crystalline graphite and amorphous carbon chains. The crystalline to amorphous volume ratio and the alignment of the atomic structures in relation to the fiber axis control the mechanical properties of the fiber. Both these parameters can vary greatly: thus, it has been possible to develop a great variety of carbon fibers with very different characteristics, ranging from high strength and low stiffness to low strength and high stiffness, and covering almost every other combination in-between.

The use of carbon fiber is somewhat limited by its low shock resistance, due to its high stiffness and fragility, poor chemical resistance, especially in oxidizing environments at high temperatures, and the high price.

Boron fiber

Boron fibers are an alternative to carbon fiber for advanced applications. Elemental boron is deposited by CVD on thin tungsten wires. This slow and complicated procedure leads to one of the most expensive reinforcements currently available, limiting its application to those rare cases where the use of boron fibers instead of carbon is justified.

Aramid fiber

Aramid fibers are the most prominent example of organic reinforcement. Liquid crystal polymers (LCP) such as these show very high mechanical properties, often comparable to those of carbon fiber. This is mainly due to the macromolecular anisotropy that arises in the metaphase during manufacturing, with preferential alignment of the bonds along the fiber axis. The first aramid fiber was developed by Dupont in 1965, is commercially known as Kevlar, and is still widely used. Aramid fibers exhibit very high toughness, and are, therefore, particularly well-suited for applications that require high levels of energy absorption, such as impact or ballistic protection. They have a low density which leads to favourable strength and stiffness to weight ratios, and they do not ignite in normal oxygen concentrations below 500 °C. They do, however, lose mechanical resistance with increasing temperature, absorb moisture, creep, are sensitive to UV radiation, and have low compressive strength.

	E-Glass	S-Glass	Carbon	Boron	Aramid
Tensile modulus [GPa]	72-85	86-93	230-965	395-410	62-179
Tensile strength [MPa]	3300-3450	4700-4800	1900-7100	2700-4000	1100-3800
ε [%]	2.6-2.8	5.2-5.3	0.3-2.0	0.7-0.8	1.9-4.4
CTE [10^{-6}/K]	4.9 -5.1	2.8-3.0	(-1.5)-(-0.6)	4.4-4.6	(-2.0)-(-6.0)
ρ [g/cm^3]	2.55-2.60	2.49-2.50	1.75-2.20	2.41-2.61	0.97-1.56
Price [€/Kg]	2-5*	5-10*	15-100*	120-200*	30-40*

*Table 1.3 Overview of the properties of the most common fiber reinforcements. *Sourced fron "Composites Manufacturing,: Materials, Product and Process Engineering"* [14]

1.1.2 Manufacturing techniques[2]

The creation of a composite part comprises two basic steps: the combination of the reinforcement with the matrix, and the shaping of the material through specialized tools. For those processes that rely on pre-processed materials such as prepregs or compression moulding compound, the two steps are separated. Nonetheless, the procedure is conceptually still the same. Through time, a wide array of techniques has been developed, ranging from relatively cheap processes with low hardware requirements, to extremely expensive, high-performing techniques with huge overhead costs.

[2] Unless otherwise noted, the information contained in this section is sourced from E. Barbero's *Introduction to Composite Materials Design* book [69].

The main differences between the different techniques are the imperfection content of the final part (for example voids, excessive resin or not impregnated fibers) and the obtainable shapes, fiber volume fractions and surface finish. While the cheaper methods I will now describe surely achieve satisfactory results, the more expensive processes introduce unarguable benefits that greatly justify their use in those industries that can afford such high investments.

1.1.2.1 Hand lay-up

This is the most basic composite production technique, often chosen by amateur manufacturers or for one-off or very small series production of parts with relatively low performance demands, due to its low cost and low hardware requirements. It is usually combined with thermoset resins and cloth fiber-reinforcement. Obtainable fiber volume fractions vary greatly and depend mainly on the operator's ability. In any case, they are rarely higher than 40%.

The starting point is a mold (or tool), which can be male or female, depending on the specific case and on the preferences. Male molds are usually easier to produce, but female molds may guarantee a better aesthetic result, since only the face of the component in contact with the tool will have a good surface finish. The fiber-reinforcement is cut to the right size and the resin is prepared. Resin and fibers are alternatively deposited inside of the mold and pressed, so as to fully impregnate the fibers. The part is left to cure, usually at room temperature. It is finally removed from the mold and undergoes finishing operations such as trimming or polishing.

1.1.2.2 Vacuum bag

Vacuum bags are an affordable improvement to the hand lay-up procedure. The initial procedure is the same; instead of leaving the part to cure in the mold as-is, however, it is covered with a sheet of peel ply, one of breather/bleeder, and put in a sealed bag connected to a vacuum pump. The pressure differential drives the excess resin out of the fiber and improves the adhesion to the mold, increasing the fiber volume fraction, eliminating dry spots, reducing the void content and improving the surface finish. The part is left to cure in the vacuum bag, usually at room temperature.

1.1.2.3 Autoclave

Autoclaves are specialized pressure vessels that extremize the vacuum bag concept and allow the production of extremely complex, high-quality components. The part is vacuum bagged and put inside of the autoclave, which fills up with gas and pressurizes up to 5-7 bar while heating to a certain temperature. The additional pressure differential further increases the fiber volume fraction and reduces the void content, while curing at high temperature improves the thermal resistance and mechanical properties of the matrix. Composite autoclaves can reach diameters of nearly 10 meters [16], and their very high cost justifies their use only for those industries which are able to amortize the huge investments. The biggest autoclaves are used for aerospace and marine applications.

1.1.2.4 Compression moulding

The compression moulding process involves the use of two complementary male and female dies, normally made of metal. A certain amount of loading compound (resin and fiber) is loaded into the mold. A hydraulic press closes the two halves and applies pressure and heat, initiating the cure process. The part is finally extracted and undergoes all necessary post-processing operations, such as trimming, flash removal or post-curing. Compression moulding is a simple, well-established process. It is highly repeatable, requires minimal set-up and minimizes waste production. It needs little manual labour and is easily automated, allowing high production rates and excellent part uniformity. Compression moulding materials do not allow high contents of continuous fiber and are therefore poorly suited for structural components. The most commonly used loading compounds are Bulk Moulding Compound (BMC) and Sheet Moulding Compound (SMC). BMC is a dough-like material with fiber content in the 20-50% range, and it can contain different types of fillers, such as glass, cotton, cellulose or other fibrous materials. SMC uses longer reinforcements and has higher fiber contents than BMC. It is produced in sheets containing all the necessary reinforcements, additives and catalysts. These sheets are cut into suitable sizes and charged into the press.

1.1.2.5 Bladder moulding

Bladder moulding is utilized for all those applications aimed at manufacturing hollow components with female molds. It guarantees very high final dimensional accuracy of the component, unachievable with a classical mandrel lamination process, and an excellent surface finish. The set of molds is used in combination with an inflatable rubber bladder. The material, usually prepreg, is precisely cut according to the requirements and positioned inside one of the molds. The bladder is positioned and partially inflated, allowing the operator to wrap the plies around it. The mold is closed, the bladder pressure is increased, typically to around 4-6 bar, and heat may be applied to complete the curing process.

1.1.2.6 Resin Transfer moulding (RTM)

Similar to compression moulding, RTM uses male and female dies, equipped with resin inlets and air outlets. The dry reinforcement, usually cloth, is charged inside the mold. A closed-circuit system pumps liquid resin inside the mold while allowing air to escape, wetting out the fibers and filling the tool. The pump is then disconnected, the inlets and outlets are sealed, and heat is applied to cure the component. Once the cure is completed, the mold is opened and the composite part is removed. The RTM process can produce large, complex parts with intricated shapes with relatively low cycle times. The dry placement of the reinforcement allows for a better control over the process, allowing precise fiber positioning. This implies better and more predictable behaviour of the final part, low defect presence and very good part uniformity. Additionally, the completely sealed process minimizes the Volatile Organic Compounds (VOC) emissions. On the other hand, RTM produced parts are limited in thickness to about 12 mm by the resin transfer mechanisms. Waste production is relatively high, since it is difficult to maintain uniform fiber volume fractions at the corners and the components tend, thus, to require abundant trimming. Mold design is crucial, especially the placement of inlets and outlets, in order to avoid dry spots.

1.1.2.7 Vacuum Assisted Resin Transfer Moulding (VARTM)

In VARTM, only one tool is used, usually female, and the resin is drawn into the mold only by vacuum. Since one of the two dies used in RTM is substituted by a

vacuum bag and the usually lower pressures allow for simpler tools made of cheaper materials, the process is less expensive than RTM. Cycle times can range from a few minutes to hours, depending on the dimension and complexity of the part and on the chosen resin chemistry. VARTM is typically used for the production of very large and complex parts, such as boat hulls. Similarly to RTM, fiber volume fractions as high as 60% and very low void contents can be obtained, and the VOC emission is virtually inexistent compared to wet lay-up techniques.

1.1.2.8 Pultrusion

Pultrusion is a continuous manufacturing process used to create constant cross-section components, principally beams and shafts. It is a highly automated, low cost technology, that uses simple continuous fibers and resin as starting materials. The fibers are constantly pulled through the machine, impregnated, shaped and cured inside of a heated chamber. An additional winder allows to add reinforcement at an angle ($\pm\theta$), a feature particularly useful for driveshafts. Many types of resin and reinforcements are used for pultrusion, but polyester and vinyl ester combined with glass fibers dominate the market because of their low cost. The fiber volume fraction seldom exceeds 40%, with typical values around 30%. A minimum solid content is necessary to facilitate the operation, around 70-75% in weight. It is achieved through the addition of fillers, which also contribute to driving down the overall cost of the matrix. The wall thickness is limited to around 12 mm. Standard production rates are about 2 m/min for standard beam cross-sections and 20 m^2/min for panels.

1.1.2.9 Filament winding

Filament winding is mainly used for the fabrication of revolution surfaces, such as pressure vessels. Continuous reinforcement is impregnated and spun on a mandrel at a certain, variable angle, θ, until the desired thickness is achieved. Just like pultrusion, the process is highly automated and only requires dry fibers and resin as starting materials: the overall cost is accordingly low. There are some limitations regarding shape, fiber disposition, curvature radii and thickness. The consolidation of the composite is not as good as that achievable in, say, an autoclave. The void content is higher, and the mechanical properties are lower.

It is evident, by now, that among the many technologies that have been developed for the manufacturing of composite materials, each has its own defining characteristics and is better suited for a well-defined subset of applications. The requirements of each process are different under all aspects, both hardware (tooling, machinery, fixtures, etc.) and software (design, manual labour, post-processing, etc.). Some of these processes may benefit greatly from the adoption of additive manufacturing technologies. I will identify these processes, investigate the main problematics of the adoption of such technologies, research viable solutions and analyse their possible impact on the industry.

First, a quick overview of additive manufacturing. I will classify and review the current technologies, describing the underlying principles, the materials currently in use and the fields of application.

1.2 Additive manufacturing

Additive manufacturing is the term used to describe the family of processes able to create solid objects from virtual models via material addition. Contrary to those widely used, well known techniques that rely on material subtraction or forming, such as milling or casting, respectively, additive technologies start from an empty build space and add material in a step-wise procedure. The results are almost non-existing process planning requirements and a great modelling freedom. Without the need for specific planning, it is possible to change the design of parts with little to no additional expenses or delays: prototyping processes and fast-changing industries may benefit greatly from this. The traditional Design For Manufacturability and Assembly (DFMA) rules that drove complexity out of the design, taught the limitations of conventional manufacturing methods and raised the consciousness of cost and govern the shapes of today's parts do not apply anymore. The time and cost of production depend much less strictly on the complexity of the part and much more on the volume of material to be fabricated: the arising principles of Design for Additive Manufacturability (DFAM) ditch simplicity as the main guideline and focus on accurate optimization procedures instead, exploiting the almost limitless geometrical freedom of AM [17]-[18]. Unless otherwise noted, the information

contained in the remaining parts of section 1.2 is taken from Gibson's book on additive manufacturing, *Additive Manufacturing Technologies* [19].

1.2.1 History of AM

It is difficult to precisely assign a creator and a creation date to AM technologies. Parallel to the development of computers around the 50's and 60's, many research groups worldwide started imagining novel manufacturing techniques based on layer by layer approaches. As the surrounding technology caught up with the concepts (lasers, graphic processing units and graphic user interfaces, controllers, etc.), the first patents were filed: in 1984, four distinct requests were deposited in France (Andre et al. [20]), Japan (Marutani [21]), and in the USA (Masters in July [22] and Hull in August [23]-[24]). All of them described similar processes to selectively add material to fabricate a final component. Charles Hull's patent had the greatest commercial success and is generally recognized as the most influential of those initial four. Hull founded 3D Systems, the first AM company, and started selling stereolitography machines. As of today, 3DS is still one of the most prominent players of the AM world. Another crucial patent for the commercial development of additive technologies is the one filed by Scott Crump in 1989 for the Fused Deposition Modelling (FDM) process [25]. Crump went on to found Stratasys, the current leader of AM for industrial applications.

1.2.2 AM Principles

AM always starts from simple CAD data, not different from those that have been used for almost every industrial manufacturing process for the last decades. The three-dimensional model is converted to the stl. Format (STereoLitography interface format, also known with the backronym Standard Triangulation Language), which tessellates the geometry into triangles. This data is fed into dedicated software, known as slicing software or slicer, which generates the final data, almost always in G-code. G-code is the most widely used numerical control (NC) programming language. It completely defines the movement of the machine head (toolpath, speed, acceleration, ecc.) and is used not only for AM, but in virtually all machine tools - mills, lathes, measuring instruments and much more. The data is finally read by the

machine, which generates the part accordingly. With exclusion of some (currently) experimental technologies, all AM procedures create the part one layer at the time. This means that the three-dimensional model is approximated by two-dimensional layers of defined thickness, which add up to form the finite part. As opposed to other technologies that require multiple iterations, AM is a single-step process, regardless of the complexity of the model. It is possible, of course, to have additional post-processing operations, such as support material removal, polishing, precision machining, coating, or more; in any case, however, the core of the manufacturing process still takes place inside the machine in a single step.

Ever since the first prototypes of additive manufacturing machines were shown to the public in the 80's, researchers around the world have developed and experimented with many different techniques. I will now give a brief description of the various types of AM currently in use and the underlying principles, following the very clear classification given by Pham [26] and reported by Gibson in his book.

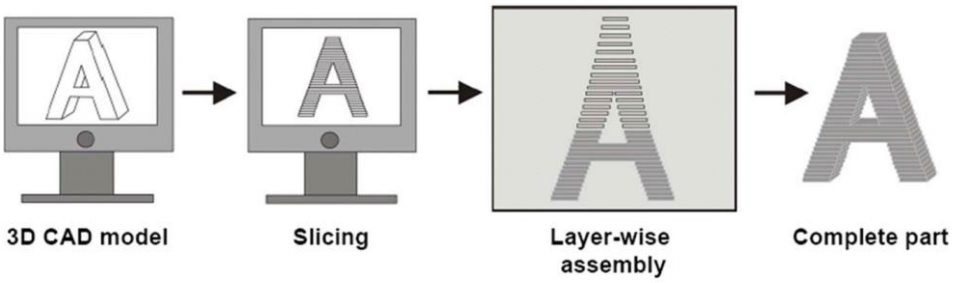

Figure 1.2 Schematic representation of the AM process. The CAD model is fed to the slicing software, which separates the part in horizontal layers and plans its step-wise construction. [27]

1.2.3 AM Classification

It is important to notice that AM has all but reached full maturity and is under continuous development. New technologies arise constantly, and what seem like true and consolidated facts now, may not hold much value tomorrow. This means that the following classification, which seems complete and adequate today, may not be satisfactory tomorrow, as newly developed processes may not fit clearly inside either of the described categories. For the sake of simplicity, however, I will limit my

description of AM to the current state of events, leaving aside those speculations about the future that do not directly affect my research.

	0D Channel	2x0D Channels	1D Channels	2D Channel
Liquid Polymer				
Discrete Particles				
Molten Material				
Solid Sheets				

Table 1.4 Gibson's classification of additive manufacturing technologies

The classification has been made according to a two-dimensional method. One dimension relates to the special fabrication logic of the part -more specifically, the geometrical disposition of the working interface (i.e. tool heads, lasers, etc.) of the machine with respect to the build space. The first technologies utilized a single point source to draw the layers. Successive developments increased the number of sources to increase the fabrication speed. Double sources, such as for dual beam sintering machines, simply double the channels. Arrays of one-dimensional sources work in a similar fashion to normal 2D printers, with the channels moving along one axis, scanning the whole build surface and activating according to the model, and are used, for example, in droplet deposition technology machines. Further improvements are possible with the use of two-dimensional array technologies, based, for example, on Digital Micro-mirror Devices (DMDs) and high-resolution displays. In these cases, the machines produce one full layer at the time. Such a distinction, however, would group together very dissimilar technologies. Thus, the introduction of the second dimension, based on the raw material. Pham defines four classes: liquid polymer, discrete particles, molten material and laminated sheets. Some solutions may not fit directly into either of these categories. More exotic materials -even the ones this research revolves around, one could argue, even though I consider them to be part of the liquid polymer family- blur the lines and could be somewhat difficult to insert into one of these four classes. New technologies, such as the latest 3D-based production method described by Kelly et al. [28] do not clearly fit inside either of the contemplated fabrication logics (even though one could say

that this specific process is, in fact, based on a two-dimensional array). In any case, it is important to remember that this classification is not fixed. More categories can and will be added, as soon as new technologies leave the experimental phase and become relevant enough to justify their introduction. The logic underlying this classification is solid and flexible enough to accommodate many future variations without losing in significance.

1.2.3.1 Liquid Polymer

Liquid polymers are a very popular material. In fact, the very first commercial AM machine, invented by Charles W. Hull in 1984, used a stereolitgraphy (SLA) technique based on liquid photopolymers. Most liquid polymer system in use today are still based on photopolymers. This classification should not be restricted to those materials, however, as many other technologies based on different processes have been developed. Hydrogels, for example, currently used in many experimental set-ups [29]-[30], fit into the liquid polymer category, and so do other systems based on different polymerization techniques.

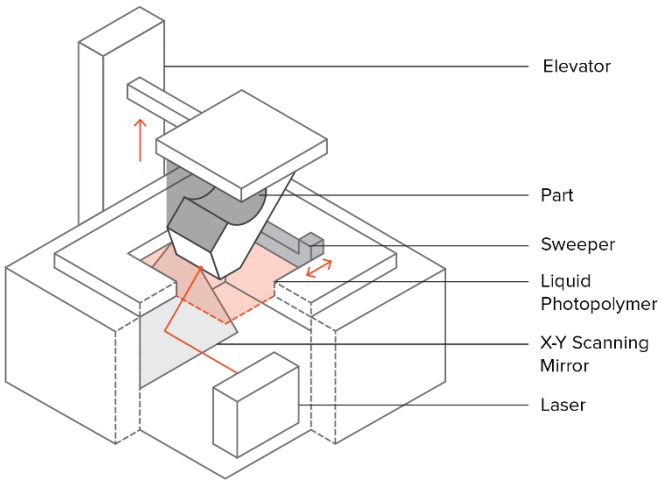

Figure 1.3 Schematic representation of an SLA system, an example of a 0D liquid polymer based technology. The UV-crosslinkable resin is cured layer by layer by a scanning laser. The part is slowly lifted by the elevator. [31]

1.2.3.2 Discrete Particles

Discrete particles are, usually, powders graded into a relatively narrow size and shape distribution. The sources can, for example, deliver energy to the powder, which may adhere according to different mechanisms. Thermoplastic polymers and metals can be molten with lasers, for example, while other materials may be primed with specific binders, which are activated by the source and promote the adhesion. It is also possible for the sources to directly deliver the binder, instead of energy: this is the case, for example, of droplet printing technologies, where the binders (glues, usually), are printed onto the powder bed, causing the particles to stick together and form the final 3D structure. This technique can be used for a wide array of materials, ranging from low-cost polymer powders combined with inexpensive glues to high-performance ceramic materials and binders for specific applications.

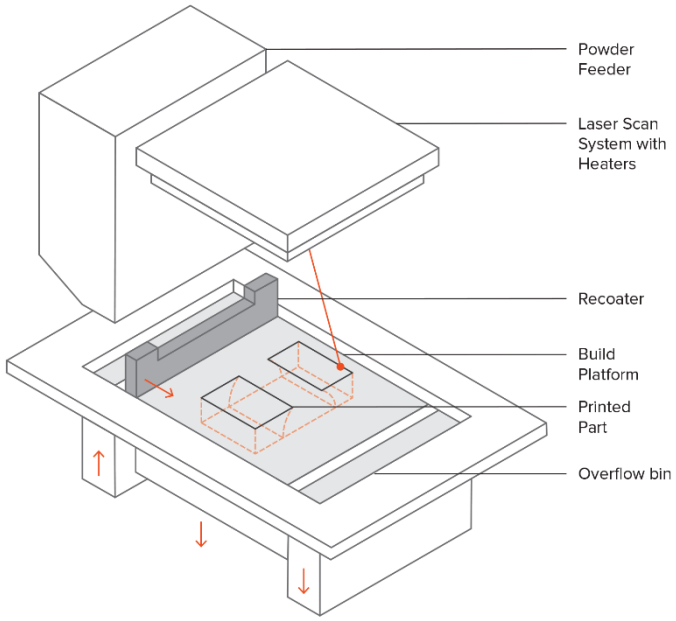

Figure 1.4 Schematic representation of a selective laser sintering (SLS) system, an example of a 0D discrete particle based technology, in which a laser selectively melts the polymer powder. [32]

1.2.3.3 Molten Material

Molten materials systems are characterized by sources equipped with a pre-heating chamber that raises the temperature of the material to the melting point, allowing it

to flow through a delivery system and be extruded onto the build surface. This technology is commonly known as Fused Deposition Modelling (FDM) and was developed by Scott Crump, the founder of Stratasys, in 1989. The majority of Stratasys' key patents on FDM lapsed in 2009 and the great competition that arose led to a tremendous decrease in prices, effectively contributing to the widespread adoption of FDM machines in the 2010's, a now common sight inside every hobby enthusiast's home. FDM systems are characterized by relative ease of use and are compatible with a wide array of thermoplastic polymers, that can, eventually, be complemented with different types of fillers, additives or pigments to suit different needs. An engineer wanting to test the form and fit of a design before approving it, for example, (or an enthusiast wanting to build a Yoda model figure for his bookshelf) may use cheap, biodegradable polylactic acid (PLA), while a company looking to manufacture a functional prototype supposed to resist to certain mechanical, thermal or chemical stresses may choose more expensive, technical polymers, such as polyether imide (PEI) or polyether ether ketone (PEEK).

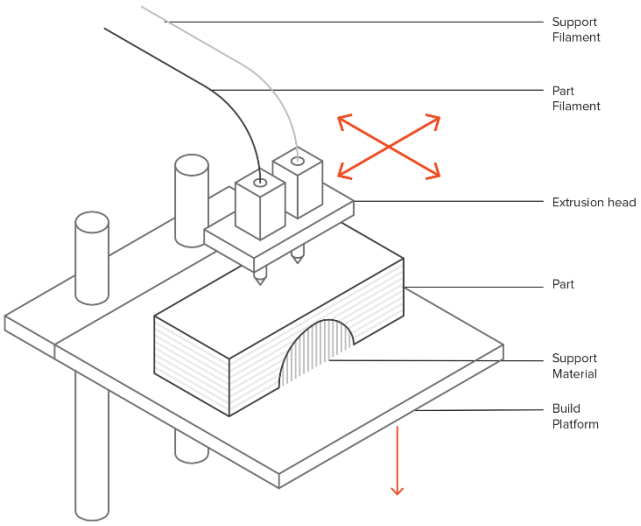

Figure 1.5 Schematic representation of a fused deposition modeling (FDM) system, example of a 2x0D (often 0D) molten material based technology. The heated extruders deposit the molten polymer, which rapidly cools down, solidifying. [33]

1.2.3.4 Solid Sheet

The Laminated Object Manufacturing (LOM) system was one of the earliest AM technologies. It was developed in 1991 by Helisys. A laser cut out profiles of sheet paper provided by a continuous roll. These profiles constituted the layers of the part and were bonded by a heat-activated resin that coated one surface of the paper. After the process, the user removed the excess paper, exposing the final part. Other companies, such as the Israel-based Solido 3D and the Japanese Kira tried to follow the same road. Currently, however, these techniques are not having great commercial success, and both the Kira and the Solido machines have been discontinued, mainly due to the high material wastage and excessive need for manual post-processing.

1.2.3.5 Hybrid systems

A solution that has been explored by various research groups is combining additive and subtractive technologies to combine the benefits of both worlds. Sanders and Objet machines, for example, complement the additive process with a planar milling step after every layer, drastically reducing the z-axis inaccuracy and thus cumulative defects. Others, such as Thermwood with their Large Surface Area Manufacturing (LSAM) machine, use a fully-fledged 5-axis mill head integrated in the printing head to trim the part, increasing both accuracy and surface finish [34]. These solutions exchange part of the simplicity of the additive processes for additional precision, while keeping a low waste production compared to full subtractive manufacturing and not jeopardizing the other benefits of AM. They have shown promising results and are seeing great interest from the industry.

1.2.3.6 Liquid Deposition Modelling (LDM)

LDM 3D-printers are a particular type of 0D liquid polymer systems that share the structure and the underlying deposition mechanisms with FDM machines. The differences lie in the material and the extruder: LDM uses various materials such as clay, cements or hydrogels, for example. Instead of working with thermoplastic polymers and relying on heat to decrease their viscosity, the materials are liquid at room temperature and undergo different hardening mechanisms once they are extruded

1.2.3.7 The standards: ASTM F42/ISO TC 261

Pham's two-dimensional classification can precisely categorize every different AM technology. There are cases, however, where it is beneficial to sacrifice some detail to gain in ease of comprehension. Stucker and Janaki Ram proposed a technology-based classification, which has been subsequently refined and adopted for the international ASTM/ISO standards for AM. This scheme uses seven categories to describe all currently existing AM technologies. An understanding of these seven classes should enable any person accustomed with the general AM concepts to quickly understand an unfamiliar process by comparing its characteristics with the other processes in the group it falls in. The identified categories are the following:

- Vat photopolymerization: liquid photopolymer contained in a vat is processed by selectively delivering energy to cure specific regions of material.
- Powder bed fusion: a container filled with powder is processed by selectively applying an energy source, usually a laser or electron-beam.
- Material extrusion: material is extruded through a nozzle that typically scans a pattern to produce a part cross-section. FDM is the most prominent example, even though other processes fall into this category.
- Material jetting: ink-jet printing processes.
- Binder jetting: a binder is selectively printed into a powder bed.
- Sheet lamination: the material is deposited in sheet form one layer at a time.
- Directed energy deposition: simultaneous deposition of both material (usually powder or a wire) and energy through a single emission device.

Now that the main AM technologies have been described, it is time to discuss the focus of my work: the application of AM to composite materials manufacturing processes. To do this, I will first give a brief overview of manufactured products in general and describe a reference system useful for defining those cases that could benefit of the application of AM. I will, then, analyse the position of composite manufacturing processes inside this reference system, and identify those cases that are compatible with AM.

1.3 When does AM make sense?

The world of manufacturing is broad and comprises products with immensely different characteristics. When does it make sense to apply AM to a process? This is one of the key questions in today's industry, and to answer it, Conner et al. [35] have developed a reference system for manufactured products.

1.3.1 3D Manufacturing space

Among all aspects of manufacturing, they have identified three key attributes: production volume, customization and complexity. Production volume simply refers to the number of parts produced in a certain timespan and can range from the billions of bricks produced in a year, to the production of a single satellite module. Complexity refers to the number, geometry and position of features in a certain component. For traditional manufacturing methods (subtractive and formative), the higher the complexity, the more difficult it is to fabricate the part, if not impossible. Customization involves the amount of changes and personalization. It ranges from small variations such as the different colour options for a car body, up to fully unique builds, such as a personalized knee-replacement implant. These three attributes form the basis of our reference system, the cube in Figure 1.6. Its eight regions group every manufacturing process according to its relevant characteristics.

Figure 1.6 3D space of manufactured products [35]

Region 1: Mass manufacturing

Ever since Henry Ford introduced the concept of assembly line, mass manufacturing has been one of the driving forces of the industry. It focuses on the highly optimized, fast production of components with little to no changes. Substantial initial investments and long lead times are necessary for the set-up of the production sites,

and very large volumes are needed to amortize the overhead costs. It is clear that with the current, well established operational models for mass manufacturing, products in this region are not suitable for the application of additive technologies. There is, however, the opportunity to integrate additive manufacturing into mass manufacturing processes by applying it to tooling production, as shown in Region 2.

Region 2: Manufacturing of the few

There are instances where components with low complexity and low customization are needed in small volumes. Many processes of the aerospace industry, for example, fall into this category. In this case, the costs for tooling and fixtures have a substantial impact and are not absorbable by the low number of built parts. This region also includes auxiliary tools and prototypes for subsequent high-volume manufacturing processes. The first application of AM was, in fact, the production of visual prototypes to aid design and marketing; as the technologies improved and the properties of additively manufactured products increased, these processes started being applied to functional components. For small production volumes, additive manufacturing can prove advantageous. Hopkins and Dickens [36] analysed the costs of fabrication of a small plastic component by additive laser sintering and conventional injection molding. Ruffo et al. [37] further improved the model, and both studies showed that for production volumes under 10.000 parts, AM led to a lower unit cost. As mentioned before, additive technologies can also be indirectly applied to conventional mass manufacturing if used for the production of tooling and fixtures, which typically fall into this second region.

Region 3: Complexity advantage

This region describes low volume production of parts with high complexity levels, justified by aesthetic or functional reasons. With conventional manufacturing processes, this additional complexity leads to higher costs. In the case of subtractive manufacturing, for example, the number of necessary operations increases. The set-up time may be higher due to the need for part repositioning, and it may even be necessary to acquire additional tooling or switch to more capable and expensive machinery, such as 5- or 6-axes mills instead of traditional 3-axes ones. With formative manufacturing, factors such as undercuts, cooling rates and thermal stresses require accurate process planning and complex molds. Fabricating the part

by joining together simpler components increases labour costs and lead time and may reduce the lifespan and the mechanical properties of the final product by adding sensitive, defect-prone connections. On the other hand, complexity is virtually free for AM, and the limitations imposed by classical manufacturing technologies are removed. The complexity can be increased at will, allowing to fully exploit the properties of the material to optimize the performance or to increase the aesthetic appeal. General Electric's LEAP engine nozzles, for example, were initially composed by twenty titanium parts welded together. The adoption of 3D laser melting into the manufacturing process allowed to redesign the whole nozzle into a single cobalt-chromium part, with increased durability and a 25% weight reduction [38].

Region 4: Mass complexity

These products are not customized, but the complexity is still high, and the volumes are larger than in the third region. One example are acetabular cups, the part of a hip implant in charge of connecting the ball socket to the hip bone. These components are not customized, as they are produced in few standard sizes, and the production volumes are rather high (in the US there are almost 440.000 hip replacement surgeries per year). Traditionally, acetabular cups are produced via a complex multi-step manufacturing process that includes forging, machining and coating of a titanium part, a notoriously difficult material to work with. Alternatively, Arcam AB has made use of a powder bed fusion process to produce them in a single step [39].

Region 5: Customized for the individual

This region comprises low volume products with low complexity but highly customized. It includes everything from personalized key chains to engraved phone covers. Excessive costs and lead times dictated by tooling and fixtures fabrication limit the opportunities for traditional manufacturing methods. Most items produced on desktop 3D printers, on the other hand, fall into this category.

Region 6: Mass customisation

This is surely one of the most challenging tasks for conventional manufacturing, and one where AM processes can easily thrive. One of the most prominent instances of the commercial success of AM in this region is Align Technologies, a company that has sold 17,2 million customized clear dental braces in 2012 -a clear example of mass

customization. Photographs, dental impressions and X-rays of the patients are used to assess the situation and extrapolate the necessary data. Stereolitography machines are subsequently used to produce a set of molds, which is used to thermoform the final braces [40].

Region 7: Artisan product

As already mentioned before, conventional manufacturing techniques follow the classical DFMA guidelines, which heavily favour symmetry, regular shapes and easy geometries. Being free of these limitations, AM offers a great tool to artists and designers, expanding their manufactural freedom and allowing them to create more with less [41]. Art is not the only field in this region that can benefit from the adoption of AM, however: highly customized, complex, low volume products are necessary for various applications. Motorsport disciplines such as Formula 1 or MotoGP, for example, make extensive use of complex aerodynamic appendices, which are often customized according not only to the driver's preferences, but also to the racetrack and its condition on the race day. In these cases, AM may allow to drastically reduce costs and, most importantly, shorten lead times -the major limiting factor in these scenarios [42]-[43].

Region 8: Complete manufacturing freedom

Complete manufacturing freedom is the nirvana of the industrial world. Achieving it with traditional manufacturing methods is a daunting task, to say the least. It has been possible, so far, to maximize two factors, sacrificing the third. One could, for example, design a manufacturing process with high complexity and high customizability; this, however, would necessarily imply low production volumes, due to the extremely long lead times necessary for the manufacturing of such products. It would be possible, in theory, to achieve complete manufacturing freedom by creating a very large array of such processes, countering the high lead times with sheer numbers. This is, however, not practically feasible with the very large volumes of certain sectors. There are no business plans or industrial models that could prove sustainable under the current boundary conditions. AM technologies are also unable to satisfy the requirements of this region, since the currently available processes are limited by geometric build volume, production rate and usable materials. Additional research, however, could lead to positive results, since the existing technologies are

relatively recent, compared to traditional manufacturing, and the continuous advancement in the field seems to indicate that there is great room for improvement. Moreover, new technologies are continuously being developed, some of which display great potential. If complete manufacturing freedom will be achieved, the chances that AM will play a pivotal role in it are very high.

1.3.2 Additive manufacturing and composite materials

Where in this manufacturing space are composite materials positioned? As seen before, FRP are manufactured with many different techniques and can be used for a wide array of applications. Even though some technologies manage to achieve relatively high production rates, such as pultrusion, filament winding or compression moulding, the majority of FRP processes are still characterized by low to medium production volumes. Let us take Adler Group's factory at Airola, for instance. It is dedicated to the realization of the CFRP chassis for Alfa Romeo's latest sports car, the 4C, and it is the biggest automotive CFRP manufacturing plant in Italy [44]. Despite being relatively huge, however, it has a maximum productivity of about ten pieces per day, which is, unarguably, a very low value for the car industry (as reference for what is usually considered as high-volume production in this field, FCA's plant at Pomigliano D'arco produces about 800 chassis per day for the Fiat Panda [45]). Boeing's latest product, the 777X, a new generation airplane that makes extensive use of various types of advanced FRP, has a planned production rate of a few tens of planes per year [46]. In general, it is possible to say that while there are some instances of high volume FRP productions, mainly when cheaper materials are combined with simpler geometries, there is a clear trend towards smaller volumes, especially as the materials become more expensive and the geometries more complex. This is the case of most advanced FRP applications, that usually combine highly optimized designs with materials specifically selected for optimal performance, despite higher costs. We will focus on these processes, from now on, since they are the most promising candidates for the application of AM, and set aside the remaining highly optimized, high-output, manufacturing processes.

1.3.2.1 Direct composite materials manufacturing

Based on the manufacturing space regions they fall into, it is clear that composite materials are a good candidate for direct application of AM. In fact, some very interesting technologies have been developed for the additive manufacturing of long fiber reinforced composites, with different types of reinforcements and matrixes, both thermosetting and thermoplastic [47]-[48]. However, even though I am confident to say that these technologies will have an important role in the future of composite materials, the performances are still not comparable to traditionally manufactured FRP, and conventional techniques are often preferred.

Among the most notable examples of direct composite material manufacturing are Markforged [49] and -to remain in house- MOI Composites, a startup born between these walls in 2018.

1.3.2.2 AM for composite tooling

However, the direct production of FRP is not the only way to integrate AM in the field of composite materials manufacturing. The tools needed for most of the processes also fall into the same manufacturing space regions, and are, thus, a viable candidate for AM. Such an introduction would be beneficial under many aspects. Since the production volumes are so low, the costs for traditional molds and fixtures are not amortized by the small numbers and have a heavy impact on the total expenses: AM would reduce these costs to a fraction of what they currently are. The lead times for conventional mold manufacturing are very long, since an accurate design is of paramount importance and the different manufacturing steps themselves are very time-consuming: AM would give a decisive time-advantage, crucial in the high-paced environments typical of many FRP applications. Additionally, AM-based tooling production would be a less disruptive change compared to direct fabrication of the final component. The manufacturers would rely on the same, well known technologies: the learning curves would be minimal, there would be very little need for changes to the set-up of the production plant, and it would not be necessary to dismantle expensive equipment. Finally, as already mentioned before, there would be no change to the final performance of the components: this is a crucial aspect especially for those advanced FRP applications that cannot compromise under this aspect.

Conclusively, AM applied to the tooling for conventional composite material manufacturing processes could lead to great time and cost savings, without altering the performance of the final components, while smoothly adapting to the existing industrial infrastructure.

It is the aim of this research to analyse the role of AM in this specific field. In the next chapters, I will break down the problem into some key issues and evaluate the currently available solutions. I will, then, propose a novel technology and discuss its potential from different point of views.

1.4 AM for composite tooling today

The idea of applying AM to rapid tooling -and, more specifically, composite tooling- has been around ever since additive technologies reached the necessary level of maturity to move from merely visual applications to the fabrication of functioning components. Since then, various research groups have tackled this problem, and their work has led to the development of an array of different solutions. I will now give an overview of these techniques, analysing the main aspects of each of them.

1.4.1 Stratasys

Stratasys is one of the leading companies for industrial FDM technologies. Through the years, they have acquired great expertise in the field of technical thermoplastic polymers for AM and have developed solutions specifically aimed at composite tooling [50]. The following table comprises their most relevant products for tooling applications:

	σ_y/UTS [MPa]	Tensile modulus [GPa]	T_g [°C]	CTE [10^{-6}/K]
Ultem 1010	-/64	2,77	215	47
Ultem 9085	47/69	2,15	186	65
Antero 800NA	-/93	3,1	149	53
PPSF	-/55	2,10	230	55
PC	40/57	1,94	161	68
ASA	29/33	2,01	108	88
ABS-M30	31/32	2,23	108	88

Table 1.5 Overview of some of Strasys' FDM materials for composite tooling applications.

Ultem products are member of the polyetherimide (PEI) family. PEI is an amorphous thermoplastic polymer. The repeating unit is $C_{37}H_{24}O_6N_2$ and has a

molecular weight of 592,61 g/mol. It has good mechanical and thermal properties. It is, however, very expensive. [51]

Antero 800NA is a polyetherketoneketone (PEKK) based materials. PEKK is a semy-crystalline thermoplastic of the polyaryletherketone (PAEK) family, with high thermal and chemical resistance and excellent mechanical properties. Its repeating unit is $C_{20}H_{12}O_3$, with a corresponding molecular weight of 300,30 g/mol. [52]

Polyphenylsulphone (PPSF or PPSU) is an amorphous polymer composed by aromatic rings linked through sulphone (SO_2) groups. It exhibits very good thermal and chemical properties. [52]

Polycarbonate (PC), acrylonitrile styrene acrylate (ASA) and acrylonitrile butadiene styrene (ABS) are more widespread, cheaper polymers with good enough properties to be used for less demanding tooling applications [52]. PC can withstand low curing temperatures, while ABS/ASA are only suited for room temperature applications. In fact, special care must be taken choosing the composite's resin system, since the high exothermic behaviour of certain resin systems may be enough to damage the tool.

All materials commercialized by Stratasys are meant to be used in combination with their FDM machines, which exploit the company's patents on hot chamber systems (among others) to print the most thermally demanding materials.

Figure 1.7 Strasys' Fortus 900 MC FDM 3D printer and an Ultem 1010 tool for the lamination of a winglet printed with it. This hot chamber machine is able to print Stratasys' complete material range and has a 916x610x916 mm build plate. [79]-[80]

Figure 1.8 Carbon/epoxy UAV propeller manufactured via compression moulding on an Ultem 1010 tool (356x102x102 mm upper and lower molds combined) produced by Stratasys. The total production time was 30 h and the cost was 50% of the estimate for traditional technologies. [50]

1.4.2 Oak Ridge National Laboratory

Oak Ridge National Laboratory (ORNL) is a US research institution that has been working on the development of novel solutions for AM during the last years, usually in partnership with different companies that later went on to commercially exploit the obtained results. Their initial project was a joint effort with Cincinnati Incorporated aimed at the development of the Big Area Additive Manufacturing (BAAM) machine, an industrial-size FDM system with an output of almost 40 kg/h, equipped with a vibrating head for porosity reduction and precise bead dimension, able to print a wide range of materials [53]. This machine allowed to carry out the first trials on tooling applications.

An initial feasibility test was conducted with low-tech, short carbon fiber reinforced ABS (CF-ABS) [54]. The fabricated tools were evaluated based on the number of completed pulls. After the first pull, all models exhibited major surface finish deterioration, induced by the relatively high temperature (~93°C) reached by the methyl ethyl ketone peroxide (MEKP) initiator during the curing of the selected vinyl ester resin. The molds started showing excessive degradation even for applications where the surface finish is not a decisive factor after a maximum of 4 pulls for the most resistant surface finishes.

After this first testing phase, ORNL started collaborating with Techmer PM on the development of technical materials dedicated to composite tooling processes, to be printed in the BAAM machine [55]. Their conjoined efforts led to the commercialization of two polymer blends:

- Electrafil PPS 3DP: a PPS/CF 50 wt% blend. Polyphenilene sulphide (PPS) is a polymer very similar to PPSU. The main difference is in its semi-crystalline nature.
- Electrafil PPSU 3DP: a PPSU/CF 25 wt% blend.

Techmer PM has not released any information regarding the mechanical, thermal and chemical properties of these blends. Given their similar nature, however, their behaviour should be similar to Stratasys' own PPSU blend, with some possible improvements due to the presence of carbon fiber reinforcement.

1.4.3 Thermwood

Thermwood further developed BAAM's technology, developing the Large Scale Additive Manufacturing (LSAM) machine [34], which integrates additive and subtractive manufacturing to achieve precise fabrication of very large components with a good surface finish. They also collaborated with Techmer MP to expand the previous research line on materials for tooling, relying on different polysulfone/CF blends. They have managed to fabricate multiple large tools for various applications.

Figure 1.9 Two examples of the LSAM applied to composite tooling. A tool made in collaboration with Boeing for the 777X program and a boat hull mold being fabricated. Both parts are made from ABS with 20 wt% carbon fiber. [46]-[47]

Figure 1.3 Thermwood's LSAM machine. Its build volume is 3 m wide and 1.5 m high and features a modular length that can reach up to 30 m. in addition to the classical extruder, it features a second head equipped with a 5-axis CNC router for machining. [83]

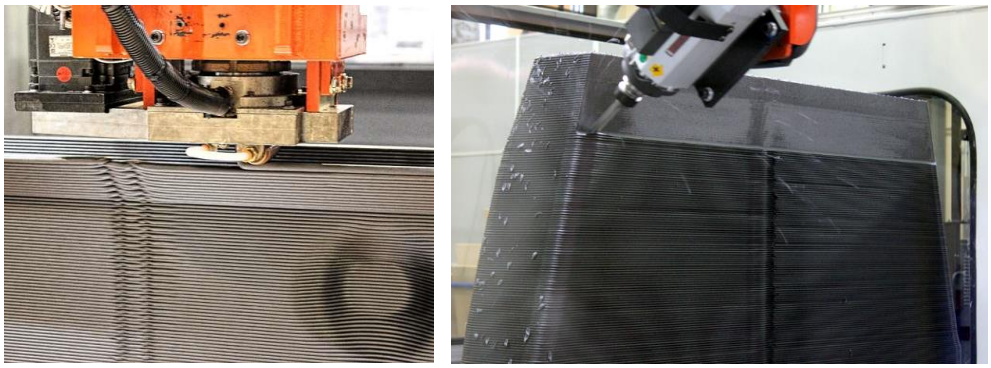

Figure 1.4 A close-up of the printing and trimming process. The very large bead dimension can be noted. [84]-[34]

It is interesting to notice how all major research works on this topic up to now has been limited to FDM-based techniques. Even though many valid solutions have been proposed, some with excellent results, thermoplastic materials still suffer from certain intrinsic limitations when it comes to high temperature applications, such as those found in advanced composite materials processes. The application of other technologies to the problem of composite tooling seems to be a still uncharted territory -an intriguing niche, whose exploration could lead to interesting results.

1.5 Photopolymers[3]

Photopolymerization-based technologies make use of liquid resins (photopolymers) as their primary material. The polymerization process is initiated via different methods of energy delivery; UV radiation is by far the most common one. Photopolymers were developed in the 1960s and have been widely used in many areas ever since, and it is while experimenting on these materials that Charles Hull had the idea that finally gave birth to stereolitography and, consequently, AM as a whole.

1.5.1 Photopolymer Chemistry

Photopolymers can be composed by many different ingredients. It is possible, however, to categorize them all in three categories: monomers, the building blocks of the final polymer chains, initiators, chemical species in charge of absorbing the delivered energy and initiate the polymerization reactions, and additives, which can be of different nature: plasticizers, stabilizers, moisture scavengers, inert fillers, various types of reinforcement, or more. The polymerization mechanisms can be of various natures. Virtually all relevant photopolymers, however, are based on one of the following two.

---

[3] Unless otherwise noted, the information contained in this section is take from Gibson's previously cited book, *Additive Manufacturing Technologies* [19]

1.5.1.1 Free-radical photopolymerization

Free-radical polymerization is mainly used in combination with acrylate resins. The initiator absorbs the radiation's energy and undergoes cleavage, generating radicals which initiate chain growth. Theoretically, a radical polymerization process may propagate unchecked, leading to extremely long chain polymers. In practice, multiple chain-terminating reactions take place and the final chains are usually of moderate length. The three causes leading to chain termination are recombination, disproportionation or occlusion. Recombination occurs when two reactive radical sites on two polymer chains join. Disproportionation is a redox reaction in which two reactive sites cancel each other out without merging. Occlusion occurs when the radical site remains active but increasing polymerization level in the compound and low chain mobility cause it to remain trapped in the polymer network, effectively preventing it from contributing to the chain growth process. Radical reactions are tolerant of a wide range of functional groups, impurities and solvents. The generating photopolymers are very stable and easy to work with, and, thus, widely used in chemical industry. On the other hand, free-radical polymerization processes used in combination with acrylates are characterized by oxygen inhibition and high curing-related shrinkage values, usually around 5-10%, which can lead to dimensional inaccuracy and residual stresses.

1.5.1.2 Cationic photopolymerization

Cationic photopolymerization processes are somewhat similar to their free-radical counterparts. The main difference is in the type of initiating species, which is, as the name itself suggests, a cation. These reactions are limited to certain types of monomers, specifically alkenes with electron-donating substituents and heterocycles, and are, therefore, mainly used for epoxies and vinylether resins. Cationic polymerization received little interest from both the scientific and industrial community until new high-performance initiators were developed, especially iodonium salts. The resulting shrinkage for epoxies is very low (1-2%) and these reactions do not suffer from oxygen inhibition; they are, however, highly sensitive to the presence of impurities, solvents and moisture.

1.5.1.3 Photopolymer-based AM processes

Photopolymers for AM are mostly limited to vat-photopolymerization processes. Only few different technologies have been proposed in literature [56]-[57]. While many instances of non-structural applications for additively manufactured photopolymers can be found, such as microsensors, cell-growth scaffolds, microactuators or jewellery [58]–[60], to name a few, applications in scenarios demanding high mechanical properties on large scale are limited.

.

2. Materials and methods

2.1 Thermoplastic materials

2.1.1 Carbon fiber filled polyamide

1.75 mm diameter FDM carbon fiber filled polyamide filament provided by Treedfilaments, commercially sold as Carbonium Nylon.

2.1.2 Polyphenylene sulphide

1.75 mm diameter FDM polyphenylene sulphide filament provided by 3DXTech Advanced Materials. It was given as a preproduction sample and has not yet been commercialized at the moment of writing.

2.2 Resin system

2.2.1 Ethoxilated bisphenol A diacrylate

Ethoxilated bisphenol A diacrylate is a monofunctional acrylic monomer especially developed for free-radical UV and electron beam curing applications, commercially known as SR349 and supplied by Sartomer. It has a hydrophobic backbone for complete alkali solubility and exhibits good chemical resistance, hardness, heat resistance, abrasion resistance, impact strength and relatively low shrinkage.

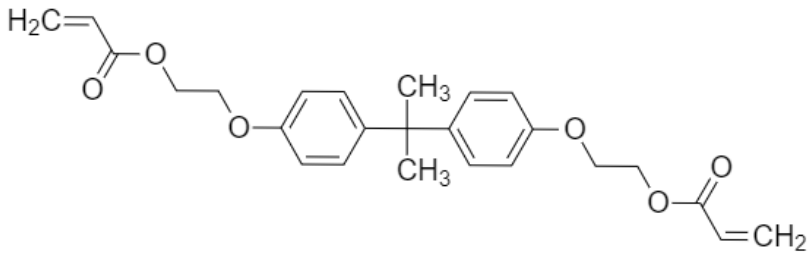

Figure 2.1 Ethoxilated Bisphenol A diacrylate.

2.2.2 Ethyl 2,4,6-trimethylbenzoyl phenylphosphinate

Ethyl 2,4,6-trimethylbenzoyl phenylphosphinate, commercially known as Lucirin TPO-L and supplied by Lambson, is a liquid type I photoinitiator absorbing in near-UV wavelengths[4]. The homolytic cleavage produces benzoyl and phosphinyl radicals that can initiate polymerisation processes of acrylates, unsaturated polyesters and styrene. It exhibits various advantageous properties, such as low yellowing, low volatility and low odour.

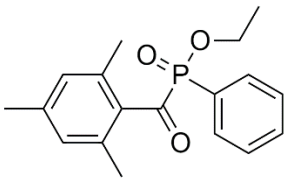

Figure 2.2 Ethyl 2,4,6-trimethylbenzoyl phenylphosphinate.

2.2.3 2-Hydroxy-2-methylpropiophenone

2-Hydroxy-2-methylpropiophenone, commercially known as Darocur 1173, is another type I photoinitiator absorbing at near-UV wavelengths whose efficacy and efficiency in comparison to Ethyl 2,4,6-trimethylbenzoyl phenylphosphinate was tested. The homolytic cleavage produces benzoyl and 2-hydroxyl-2-propyl radicals.

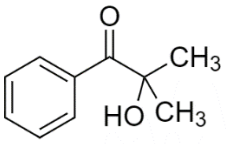

Figure 2.3 2-Hydroxy-2-methylpropiophenone.

[4] Type I photoinitiators are unimolecular free-radical generators; that is, upon the absorption of UV-light a specific bond within the initiator's structure undergoes homolytic cleavage to produce free radicals. Homolytic cleavage is a bonding pair of electron's even scission into two free radical products.

2.2.4 1,4-butanediol dimethacrylate

1,4-butanediol dimethacrylate is a low viscosity dimethacrylate monomer, commercially known as Bisomer BDDMA, supplied by GEO Specialty Chemicals. It is a non-toxic, low-odour diluent.

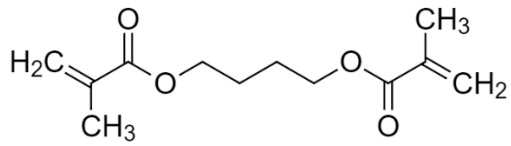

Figure 2.4 1,4-butanediol dimethacrylate.

2.2.5 Dicumyl Peroxide

Dicumyl peroxide is a thermal free radical initiator, supplied by Sigma Aldrich. The homolytic cleavage produces to alkoxy radicals.

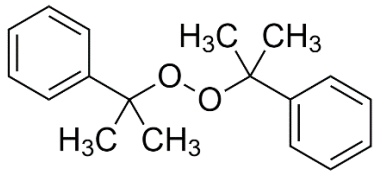

Figure 2.5 Dicumyl peroxide

2.3 Fillers

2.3.1 Italdry Fil 100

Hammer milled, unsized S-glass fibers with a 13 μm nominal diameter and a 100 μm screen size[5]. The Young's modulus is estimated at 90 GPa, taken from AZO Materials' S-glass datasheet [61].

2.3.2 Owens Corning 737BC

Hammer milled Advantex® glass fibers (patented boron-free E- and E-CR glass reinforcement with 80 GPa of elastic modulus) treated with Owens Corning's proprietary silane sizing. Nominal diameter of 16 μm and 400 μm screen size.

2.3.3 Rivierasca

End-of-life product obtained from dismissed E-glass/polyester corrugated panels, supplied by Rivierasca S.p.A. in the framework of the European FiberEUse project. The Young's modulus is estimated at 75 GPa, taken from AZO Materials' E-glass datasheet [62].

2.3.4 Gamesa

End-of life product obtained from dismissed E-glass/polyester wind turbines, supplied by Siemens Gamesa and hammer milled at CNR with an 80 μm screen size. It was obtained in the framework of the European FiberEUse project. Again, the Young's modulus is estimated at 75 GPa.

[5] The screen size describes the hole diameter of the hammer mill screens and not the actual fiber length. The milling process produces a distribution of length, related to the screen size.

Figure 2.6 Rivierasca (left) and Gamesa (right) recycled materials. The red hue of Rivierasca's material and the darker colour of the one supplied by Gamesa are clearly visible.

2.4 Formulations and mixture preparation

Resin system A: SR349 monomer with 3 PHR (Parts per Hundred Resin) TPO-L photoinitiator.

	Resin system A [wt%]	Italdry Fil 100 [wt%]
SR50V/SR50VTT	50	50
SR60V/SR60VTT	40	60
SR70V	30	70

Resin system B: SR349 monomer with 3 PHR TPO-L photoinitiator and 0,3 PHR dicumyl peroxide thermal initiator.

	Resin system B [wt%]	Italdry Fil 100 [wt%]
SR70VT	30	70

Resin system C: 80 wt% SR349 monomer and 20 wt% BDDMA diluent with 3 PHR TPOL photoinitiator and 0,3 PHR dicumyl peroxide thermal initiator.

	Resin system C [wt%]	Rivierasca [wt%]
20DR45	55	45

	Resin system C [wt%]	Gamesa [wt%]
20DR57G/20DR57GTT	43	57

SR70VT, 20DR45 and 20DR57G samples underwent a thermal post-curing for 2 hours at 140 °C in an MMM Incucell V 55 oven.

The TT suffix indicates a final thermal treatment of 1 hour at 200 °C in an MMM Incucell V 55 oven.

The formulations were prepared by mixing the resin system in a beaker covered with aluminium foil under an unlit fume hood, to minimize UV-light exposure. The fillers were subsequently added and mixed by hand with a spatula until a homogeneous fluid was obtained.

Rivierasca's recycled glass fiber exhibits low wettability with the used resin systems. Thus, an additional automated mixing step was added for the formulations that used this filler. A Brabender twin-screw shear mixer was used, with two consecutive cycles of 20 minutes at 60 rpm and 15 minutes at 30 rpm respectively, both at 25 °C.

2.5 The machines

Two different experimental LDM machines were set up for this research. The first one was built to prove the functionality of the technology and manufacture various test pieces. The second was the subsequent scale-up: the printing volume increased, and various improvements were made, allowing the printing of functional, more complex models. The custom parts produced were mainly made in house through AM on a commercial FDM machine (Prusa MKII) from polyethylene terephthalate glycol (PETG), chosen for its good mechanical properties and ease of use. Some components with special requirements or that had to be made from metal were

manufactured in the university's mechanical workshop via traditional subtractive technologies.

2.5.1 3DRag – V1

The first set-up was developed by fellow researcher Gabriele Natale based on a commercial 3DRag FDM machine by Futura Elettronica. It is a cartesian 3D-printer with a Z-head mechanical arrangement, meaning that the X- and Y-axis movements are delegated to the plate, while the small and slow Z-axis movements are left to the head. This arrangement is very favourable in case of bigger and heavier extruders, since the limited accelerations do not cause any inertia-related issues. This, the open source nature of the machine and its great hacking potential are what motivated the choice of this 3D printer as a starting point. The electronics and the mechanics were left unaltered. The main changes were on the extruder: the old system was completely removed, and a proprietary system was installed in its place. The fulcrum of the build is a commercial plastic syringe. A threaded rod, powered by a stepper motor through a 2:1 reduction, actuates the syringe's piston, extruding the material. The extrusion speed is controlled by the printer firmware. Since the material feed is radically different, however, the motor steps per extruded filament millimetre relation commonly used for FDM materials does not hold anymore. To address this issue, the generated G-codes are changed accordingly to mirror the new steps/mm relation, and the filament diameter is set equal to the syringe's internal diameter. This allowed an approximately correct extrusion rate. Further fine tuning was done adjusting the flow settings through the slicing software. Three 395 nm LEDs supply the electromagnetic radiation necessary for the activation of the polymerization reaction. They are powered by an independently controlled dimmer and are mounted on an additional support with adjustable height, meaning that the LEDs can always be positioned to correctly point at the material bead, no matter the length of the currently used nozzle. Three light sources proved to be the necessary number to avoid shadow zones on the printed geometry that could lead to subpar polymerization. Three fans with adjustable speed cool the LEDs, extending their life and preventing damage to their supports, made from thermoplastic PETG.

2.5.2 3Drag – V2

During my work, the 3DRag system was further improved by modifying the first extruder design. A four-start trapezoidal leadscrew was installed for improved precision, the gear ratio was increased to 4:1 for more torque and the syringe holding system was redesigned for improved stability and compatibility with multiple syringes. Mounting points for LED supports were added, and the system was designed with additional UV-shielding of the syringe in mind.

2.5.3 Delta 40x70

While satisfactory for material testing and minor part production, the 3DRag system was meant as a technology demonstrator and its manufacturing possibilities were limited by many factors. To better exploit the potential of the developed materials and really push their limits, a new machine was necessary. Bigger build volume, increased deposition precision and bigger material reservoirs were the main requirements. A Wasp Delta 40x70 was chosen as the starting point. Contrary to the 3DRag's cartesian geometry, this 3D-printer has a polar coordinates movement mechanism, which implies an elliptic build plate -40x70 cm, in this case. As with the 3DRag, the mechanical set-up remained unchanged, and the only modifications affected the extrusion system. A vipro-HEAD endless piston dosing unit by Viscotec was mounted in place of the standard Bowden extruder. This unit allows for very precise, constant dosing and supports retraction movements. It is connected to an external pressurized material reservoir that holds up to 360 mL, greatly extending

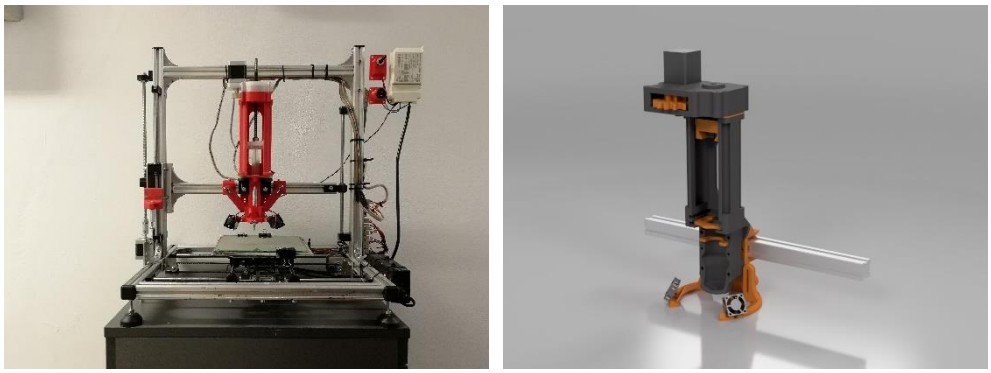

Figure 2.7 3DRag V1 (left) and a render of the 3DRag V2 (right).

the printing capabilities for bigger parts. A specifically built structure holds the extruder in place and supports the radiation sources in charge of initiating the polymerization reaction, three 395 nm LEDs (same type as the ones used for the 3DRag system).

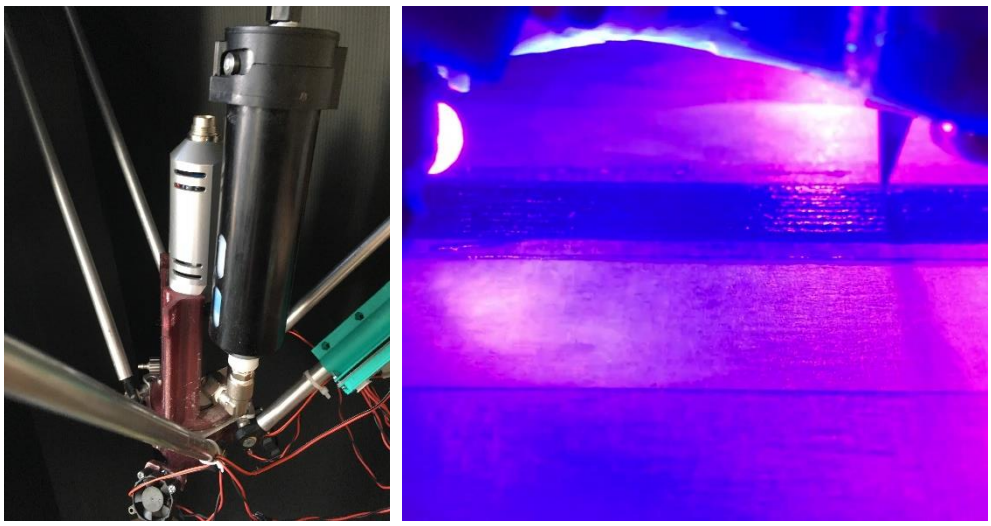

Figure 2.8 Delta 40x70 system head and a close-up image of the printing process.

2.5.4 Nozzles

Multiple Luer lock type nozzles by Viscotec were used. Their characteristics are summarized here:

	Diameter [mm]	Geometry	Material
MT18-PBN	1,041	Conical	Metal
MT21-PBN	0,609	Conical	Metal
TE71805PK	0,838	Cylindrical	Metal
TT14-RIGID-PK	1,54	Conical	Plastic

2.6 Characterization techniques

2.6.1 Gel content

Gel content measurements were used to assess the uncured resin content of the samples throughout the different processes.

A 50 ml beaker with a grade 3 paper filter and a 100 ml round-bottomed flask are dried in an oven at 70 °C for 24 h and weighed (indicated with the acronym BF and F_i in the formulae, respectively). A small sample of the material (<200 mg) is cut and placed in the paper filter inside the beaker, which is weighed again (indicated with the acronym BFS_i in the formulae). The sample is removed, placed in a metallic support and hung on a steel wire. Metal tea infusers, for example, have proven to work well. Great care should be taken while handling the sample, since the loss of even small particles could alter the results. The support is hung in a 500 ml Kumagawa boiling flask, which is filled with a precise amount of acetone calculated as a function of the sample weight according to the following equation:

$$\frac{Sample\ mass\ [g]}{250} \cdot 75 = Solvent\ volume\ [ml]$$

The sample should be fully immersed in the solvent without touching the bottom of the flask. The solution is left to stir for 24 h on a magnetic stirrer at low speed. The sample is carefully removed and placed inside the paper filter in the beaker. The flask and the support are thoroughly washed with acetone, which is filtered in the beaker in order to collect every solid particle in the filter and all the solved monomer in the beaker. The beaker's liquid content is transferred to the 100 ml round-bottomed flask. Again, the beaker should be thoroughly washed to collect all the monomer. The round-bottomed flask's content is evaporated in a rotary evaporator. The beaker, with the filter and the sample inside and the flask, are left to dry in a vacuum oven at 80 °C. Both are weighed every 24h (indicated with the acronym BFS_i and F_f in the formulae, respectively). Once the weight stabilizes, indicating complete evaporation of the solvent, the measurement is complete. The gel content can be calculated both on the solved part contained in the flask and on the unsolved part contained in the beaker, according to following formulas:

$$solid\ content\ [\%] = \frac{\mathrm{BFS_{final}} - \mathrm{BF}}{\mathrm{BFS_{initial}} - \mathrm{BF}} \cdot 100$$

$$solved\ content\ [\%] = \frac{F_f - F_i}{BCF_{initial} - BC} \cdot 100$$

2.6.2 Differential Scanning Calorimetry

Differential scanning calorimetry (DSC) is a type of thermal analysis that measures the difference in heat necessary to increase the temperature of a sample and a reference as a function of temperature. It allows to detect exothermic or endothermic physical transformations of the sample, such as phase transitions. DSC measurements were made on a Mettler Toledo DSC823e instrument at 20 K/min.

2.6.3 Differential Scanning Photocalorimetry

Differential scanning photocalorimetry (UV-DSC) measures the difference in heat flow between the sample and a reference under controlled UV light irradiation. It was used to evaluate the photoinitiated polymerization of the developed mixtures and collect information about the percentage of material that underwent polymerization and -thus- the efficacy and efficiency of the processes. UV-DSC measurements were made on a Mettler Toledo DSC823e instrument at 25 °C, with a 60 s heat flow stabilisation time, 180 s of light exposure and 60 s cooldown time. The heat measurements were normalized on the active part of the material (the resin system). 2-hydroxy-2-methylpropiophenone and ethyl 2,4,6-trimethylbenzoyl phenylphosphinate based resin samples for the photoinitiator performance evaluation were prepared with the same 3 PHR content.

2.6.4 Thermogravimetric Analysys

Thermogravimetric analysis (TGA) measures the mass change of a sample as a function of the temperature. It was used to evaluate the thermal stability of the samples and to calculate their effective fiber content. Measurements were made on a TGA Q500 by TA Instruments at 20 K/min, in air, from 0 °C to 800 °C.

2.6.5 Tensile tests

Tensile testing allows to evaluate various mechanical properties of the samples, most notably the elastic modulus, the stress at break (and eventual yield stress) and the elongation at break. Additionally, it provides information about the fragile or ductile behaviour of the sample. The examination of the fracture surface allows to determine the dominating fracture mechanisms and, in the case of composite materials and in combination with some imaging technique, the fiber-matrix adhesion.

Tensile tests were done on a Zwick Roell Z101 instrument with a 10 kN cell, with a 0.8 mm/min speed. The elastic modulus was calculated with the secant method between 0.05 and 0.2 elongation. Specimens were prepared according to the ASTM D3039 standard [63], which is more suited for additively manufactured materials than the ASTM D638 standard [64] commonly used for polymers [65]. 100x10x2 specimens were used throughout the whole work. All samples were printed at 20 mm/s, with the conical 1,54 mm plastic nozzle and a 1 mm layer height on both V1 and V2 3DRag setups and with the 0,608 mm conical metal nozzle and a 0,5 mm layer height on the Delta 40x70 setup. If necessary, the specimens were polished with medium grit sandpaper. A minimum of five samples for each formulation were tested.

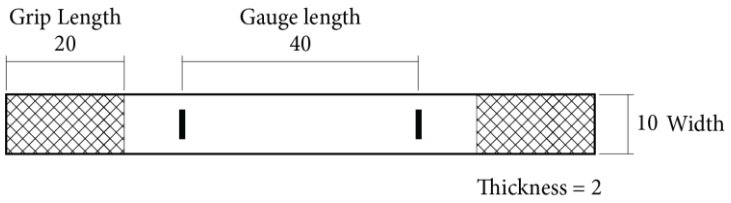

Figure 2.9 Geometry of the tensile test specimens, in accordance with the chosen standard, ASTM D3039.

2.6.6 DMA/TMA

The coefficient of thermal expansion (CTE) measurements were taken on a TA Instruments RSA3 DMA instrument in TMA mode from -30 to 200 °C with a constant preload of 5 g. The instrument had been previously calibrated according to ASTM E2113 [66] and the measurements were taken according to ASTM E228 [67]. Four 7x7 mm cross-section parallelepiped samples of every material were prepared from a single 7x7x60 mm bar, printed along the main axis at 20 mm/s on the 3DRag V1 setup (SR50V, SR60V, SR70V, 20DR45) or 3DRag V2 setup (SR60OC and 20DR57G) (see Figure 2.10). The thermoplastic samples (PA-CF and PPS) were printed on an FDM 3DRag modified by fellow Raffaele D'Addario. The sample length varied between 7.8 and 12.7 mm (see Figure 2.12).

Mean and tangent coefficients of thermal expansion were calculated according to the two following equations:

$$\alpha_{mean} = \frac{1}{L_0}\frac{\Delta L}{\Delta T}$$

$$\alpha_{tangent} = \frac{1}{L_0}\left(\frac{dL}{dT}\right)_T$$

Where

$$\frac{\Delta L}{L_0} = \frac{L_1 - L_0}{L_0}$$

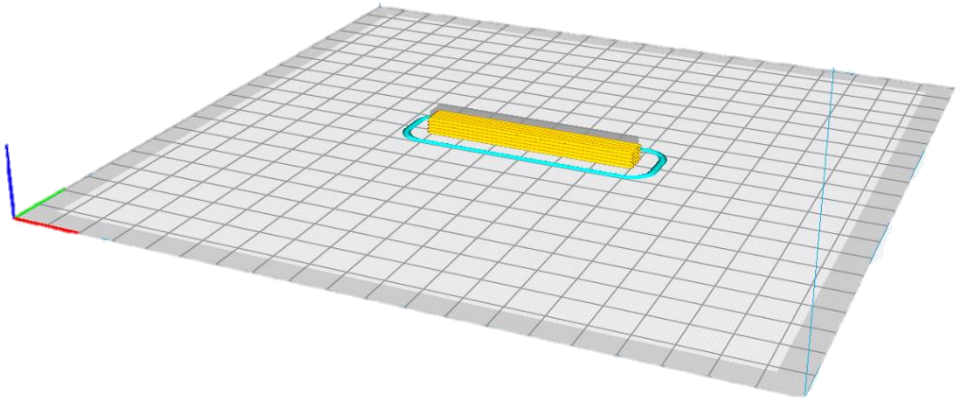

Figure 2.10 Slicer preveiew of the CTE sample. As with the tensile samples, the part is printed without bottoms, tops or walls, to mazimize homogeneity. Layer height 1 mm, nozzle diameter 1.54 mm, speed 20 mm/s.

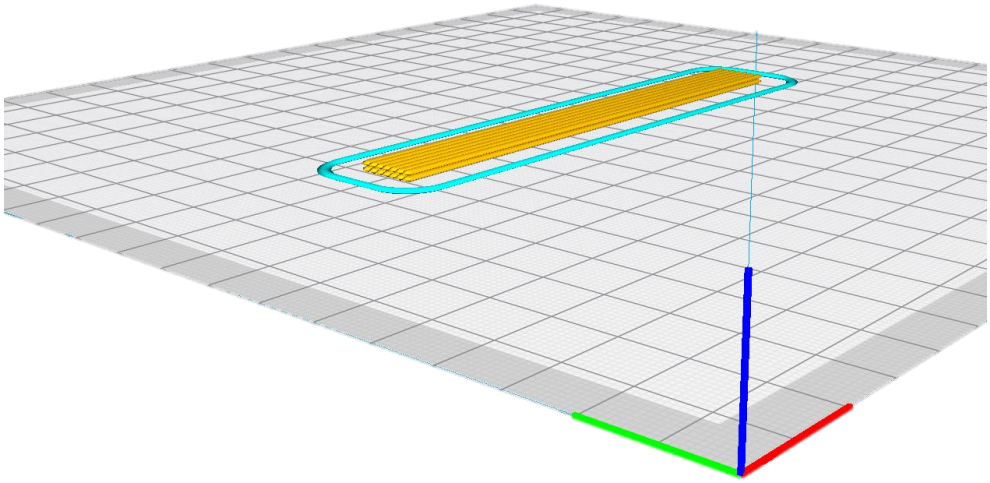

Figure 2.11 Slicer preview of a 3DRag specimen for tensile testing. The part is printed without bottoms, tops or walls to maximize homogeneity. Layer height 1 mm, nozzle diameter 1.54 mm, speed 20 mm/s.

Figure 2.12 CTE samples: CF-PA (left) and SR70V (right)

2.6.7 FT-IR

Infrared absorption measurements measure the sample's light absorption in the infrared range. The absorption peaks are linked to well-defined induced vibrations of a specific bond on an internal degree of freedom, such as stretching, bending, out of plane bending or torsion. IR analysis was used to assess the changes of the molecular structure of the thermally treated SR60TT samples in comparison to the untreated SR60V samples, to evaluate the possible thermal degradation. The samples were ground into fine powders, diluted in potassium bromide (KBr) and thin 13 mm diameter specimens were prepared by applying eight tons of pressure in a Perkin Elmer hydraulic press for three minutes. The measurements were made on a Thermo Nicolet Nexus 470 FT-IR by GMI Inc. instrument in the 4000-400 cm^{-1} range at room temperature, with 64 scans at a 4 cm^{-1} resolution. Spectra analysis was done using Omnic Spectra Software by Thermo Scientific.

2.6.8 SEM

Scanning electron microscopy images were acquired on a Cambridge Instruments Stereoscan 360 instrument. Samples were prepared by cutting specimens of around 3-4 mm height, which were subsequently metallized.

2.6.9 OM

Optical microscopy images were acquired on an Olympus BX60 instrument, with 50x, 100x, 200x and 500x magnifications, and acquired through a Luminera Infinity 2 camera used in combination with Infinity Analyze software. No cover slips were used. This partially reduced the image quality, since the uneven specimen led to some out-of-focus zones. It did, however, avoid damage on the fibers, an aspect of much greater importance.

Fiber size extrapolation

The optical microscope images were elaborated on ImageJ. This software was used to manually measure the glass fibers. Great care was put in avoiding any errors in the measurement process: to eliminate any unwanted skewing of the statistical data, it is important for the operator to make sure to thoroughly count all fibers present in an image, in order to avoid unwanted preferential selection. Additionally, it is important to analyse different zones of the microscope slide to eliminate possible size-dependent positioning phenomena of the particles.

To analyse the fibers contained in the resin mixture, a small quantity of material was extruded in a 50 ml beaker. Acetone was added, the beaker was covered and not mixed, to avoid any damage to the fibers. Once the resin was dissolved, the glass fibers deposited on the bottom of the beaker and were clearly visible. They were collected with a disposable pipette and a drop was placed on the microscope slide. As soon as the acetone evaporated, the sample was ready for image acquisition.

2.7 Vacuum Assisted Hand Lay-up

2.7.1 Materials

All material necessary for the hand-layup and vacuum bagging were acquired through Mike Compositi. All materials were prepared and used according to the manufacturer's specifications.

Epoxy resin

SX10 EVO epoxy resin system with a 3% in weight addition of SX8/10 EVO accelerator, produced by Mates Italiana s.r.l.

Carbon fiber cloth

Hexforce 200 g/m^2 3k 2/2 twill, produced by Hexcel.

Vacuum bagging equipment

HT15090T vacuum bag, 4 m^3/min vacuum pump, PP085R75 peel-ply, P1 perforated release film, AeR160100 breather film, vacuum bag sealant and vacuum bag valve, produced by Mates Italiana s.r.l.

Gelcoat

P38 epoxy gelcoat, produced by Mates Italiana s.r.l.

2.7.2 Procedure

The vacuum bag was prepared and the vacuum valve was put in place. Great caution should be taken to completely seal it, not leaving any wrinkles in the sealant through which air may pass. The resin mixture was prepared, following the A:B:accelerator 100:26:3 in weight ratio given by the manufacturer. The carbon fiber cloth was cut to size, placed on a flat, clean surface, impregnated and left to sit for approximately twenty minutes (with this amount of accelerator, pot life and gel time are around thirty and sixty minutes, respectively). Working with a resin closer to the gel point facilitates the fiber placement and avoids cloth slippage. In the meantime, the mold was thoroughly cleaned with acetone and waxed. The lamination process occurred in the following order: peel-ply, two carbon fiber cloths at 0°, release film, peel-ply, breather film. Everything was placed inside the vacuum bag. Additional breather film was placed to maintain enough free volume between the mold and the air outlet valve to facilitate internal air flow.

3. Results and Discussion

The focus of my work was the development and characterization of thermoset composite materials for LDM processes, specifically aimed at composite tooling applications. Throughout all my research, I have found great help in the people of Politecnico di Milano and the Chemistry and Materials Department “Giulio Natta”. The constant support, the help, suggestions, knowledge and technical means they have provided have been invaluable. Without these people, none of this would have been possible; this research is the result of a great team effort.

3.1 Particle size distribution

Hammer milling leads to fiber batches with wide length distributions, with the screen size indicating the typical maximum achievable fiber length. It is not possible to have precise information about the size distribution a priori, meaning that a detailed analysis is necessary, especially given the important role that the length of reinforcing fibers play in the final properties of a composite material.

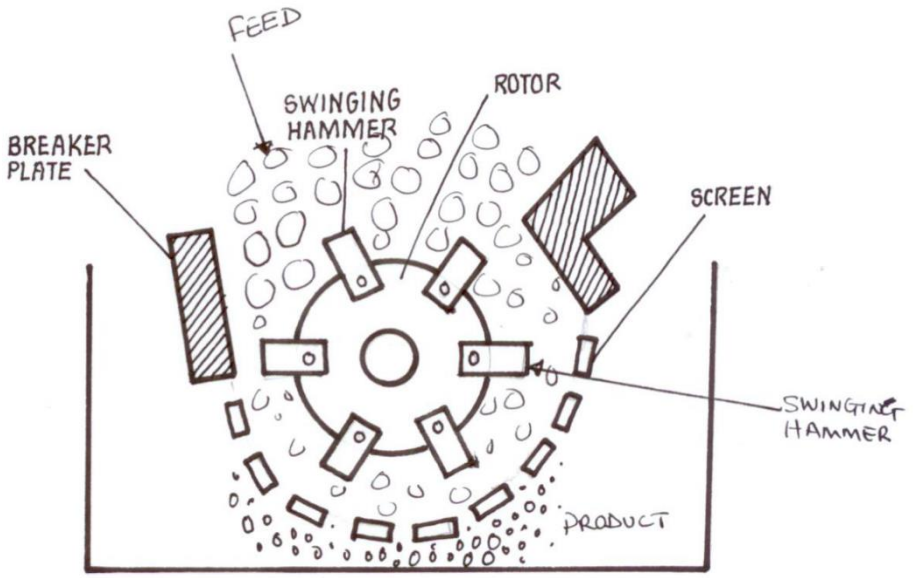

Figure 3.1 Hammer milling process scheme. The underlying principle is impact derived size reduction. The rapidly moving hammers crush the fed material untilthe particles are small enough to enter the screen holes. In case of high aspect ratio particles such as glass fibers, longer elements may pass through the screen by aligning along the main axis. [85]

Italdry Fil 100

Optical microscopy analysis revealed an average fiber length of 52,3 μm and a relatively wide distribution (61,3 μm standard deviation). The peak frequency is in the 30-35 μm range, followed by an approximately linear decline until 100 μm. It can be observed that some isolated fibers greatly exceed the average values and the screen size itself, with lengths abundantly over 600 μm. This is common for hammer milling processes, and while it does not normally cause any issues, it has to be kept in

consideration since it may lead to clogging of the nozzle in those rare, but not impossible, cases where multiple exceptionally long fibers coagulate in the extruder. A relevant amount of glass fiber powder is visible. This was probably generated by mechanical damage of the fibers during the hammer milling procedure and possibly during the following handling as well. It has a detrimental effect on the performance of the reinforcement, since it negatively affects the aspect ratio distribution of the whiskers. However, it was not possible to precisely evaluate its amount, and was subsequently left out from the calculations.

To gain insight on the damage that the fibers underwent during the different phases of mixture preparation, handling and extrusion, I repeated the same analysis on a sample of SR60V extruded from the Delta 40x70.

It is possible to observe that there is a 34,5% decrease in average fiber length during the extrusion process. Interestingly, the maximum frequency peak remains unchanged at 30-35 μm. There is, however, a notable reduction of the fiber count in the 35-100 μm range, with a very steep, non-linear decline. This phenomenon implies that the longer fibers have a higher possibility to incur in damage during extrusion. As a result, the distribution is narrower: the average length is 34,3 μm and the standard deviation is 28,1 μm.

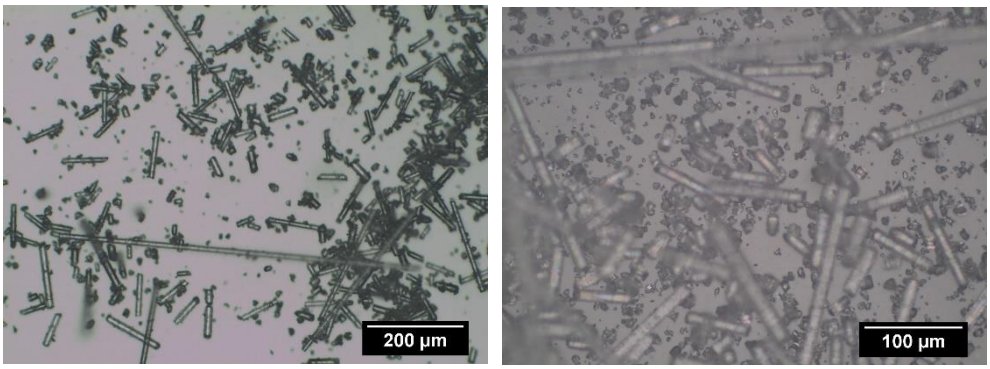

Figure 3.2 Optical microscopy images of Italdry Fil 100 glass fibers, 100x magnification (left) and 200x magnification (right). The wide size distribution is visible, with some exceptionally large fibers. Some coarse glass fiber powder is also visible, probably deriving from the mechanical size reduction procedure.

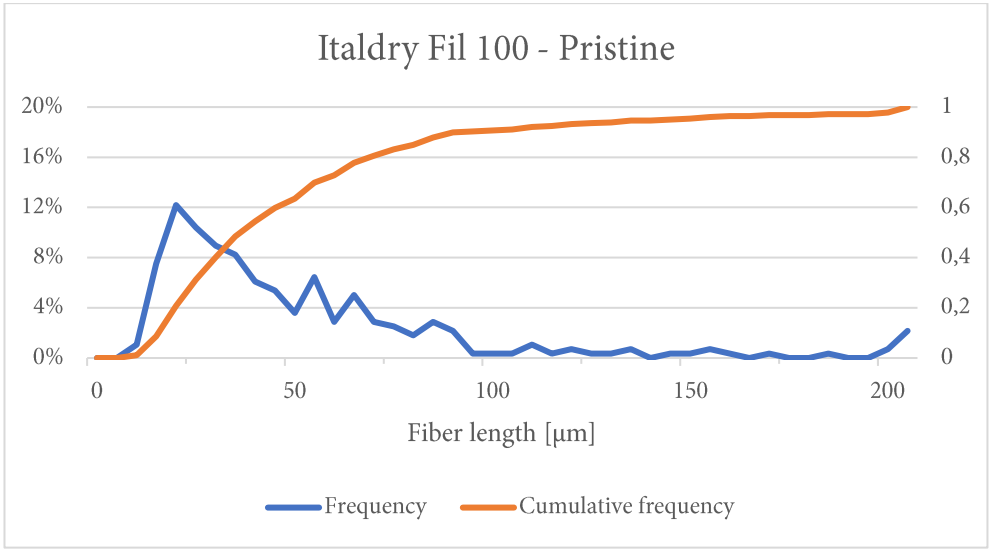

Chart 3.1 Fiber length distribution of Italdry's Fil 100 pristine fibers.

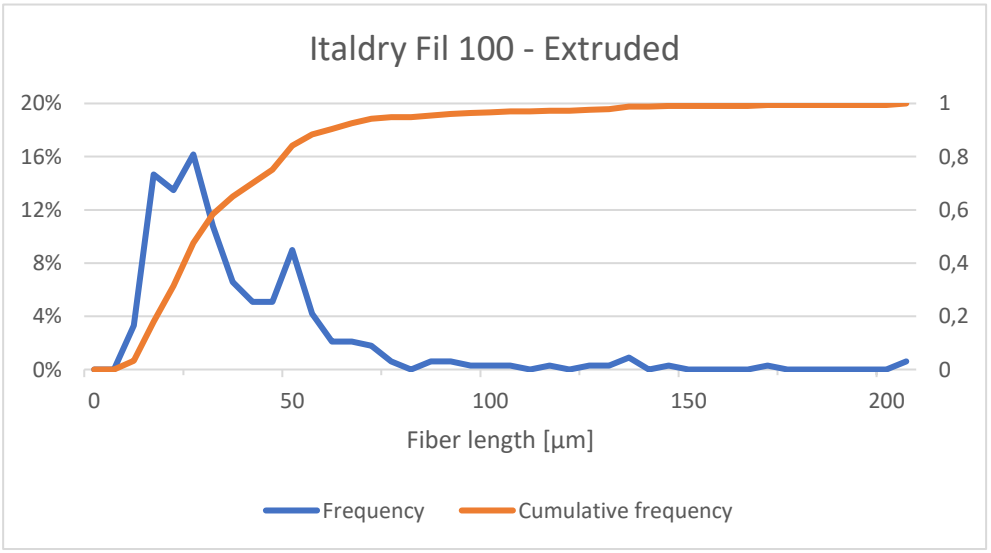

Chart 3.2 Fiber length distribution of Italdry's Fil 100 fibers after the extrusion process. The damage and subsequent average size reduction of the fibers are clearly visible.

Owens Corning 737BC

These fibers have an average length of 77,6 µm and a standard deviation of 54,3 µm. As expected, there are no notable variations in the distribution in comparison to Italdry's Fil 100, apart from the fact that the fiber size seems to increase less than linearly with respect to the screen size. This phenomenon is attributable to the increased possibility for higher aspect-ratio fibers to incur in damage during the whole post-milling handling process. Less glass fiber powder is visible, compared to Italdry Fil 100. This may be imputable to differences in the hammer milling procedure, in the handling of the fibers, or to an additional cleaning step undertaken by the manufacturer.

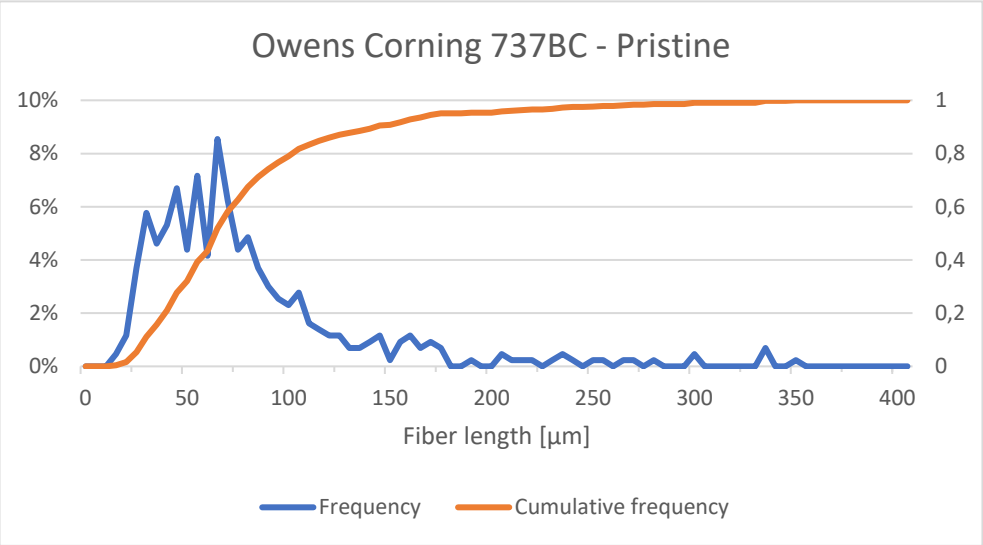

Chart 3.3 Fiber length distribution of Owens Corning's pristine 737BC fibers.

This kind of evaluation was very straightforward in the case of the virgin glass fiber samples. The recycled materials, on the other hand, required a more extensive evaluation. The manufacturing process generates a biphasic material composed by glass fibers and residual matrix polymer. Hence, the size evaluation must be done on the isolated fibers.

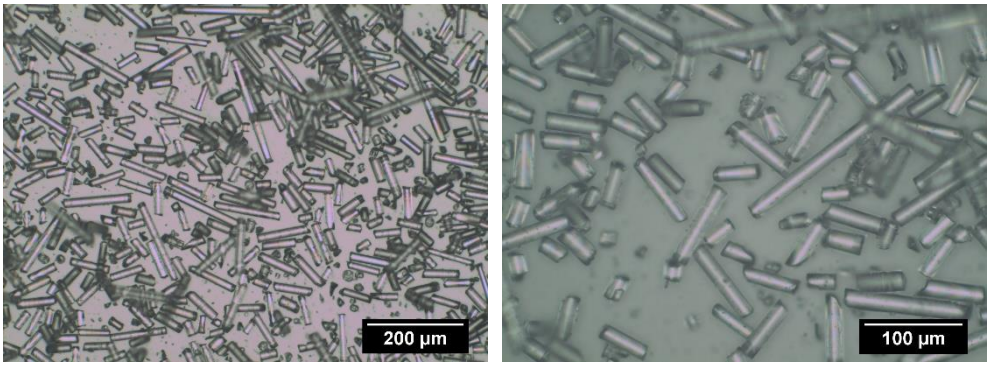

Figure 3.3 Optical microscopy images of Owens Corning 737BC fibers, 100x magnification (left) and 200x magnification (right). Contrary to Italdry Fil 100 fibers, only trace amounts of glass fiber powder are visible.

Rivierasca

In the case of Rivierasca's recycled material, the visible glass fibers were so few, as can be seen from **Errore. L'origine riferimento non è stata trovata.**, that no relevant statistical data could be extrapolated. The observed fibers had an average dimension of 136 µm and ranged from 38,5 to 225,5 µm. TGA measurements conducted by fellow researcher Luca Grandi during his previous work confirmed a low glass content of 12% in weight.

Gamesa

Gamesa's recycled material exhibits a higher glass fiber count, sufficient for statistically relevant evaluations. The average fiber length is 166,2 µm, and the standard deviation is 135,0 µm. In general, as can be seen in Chart 3.4, the distribution is very wide, and fibers commonly reach up to 500 µm. TGA showed a glass content of 70% (see appendix).

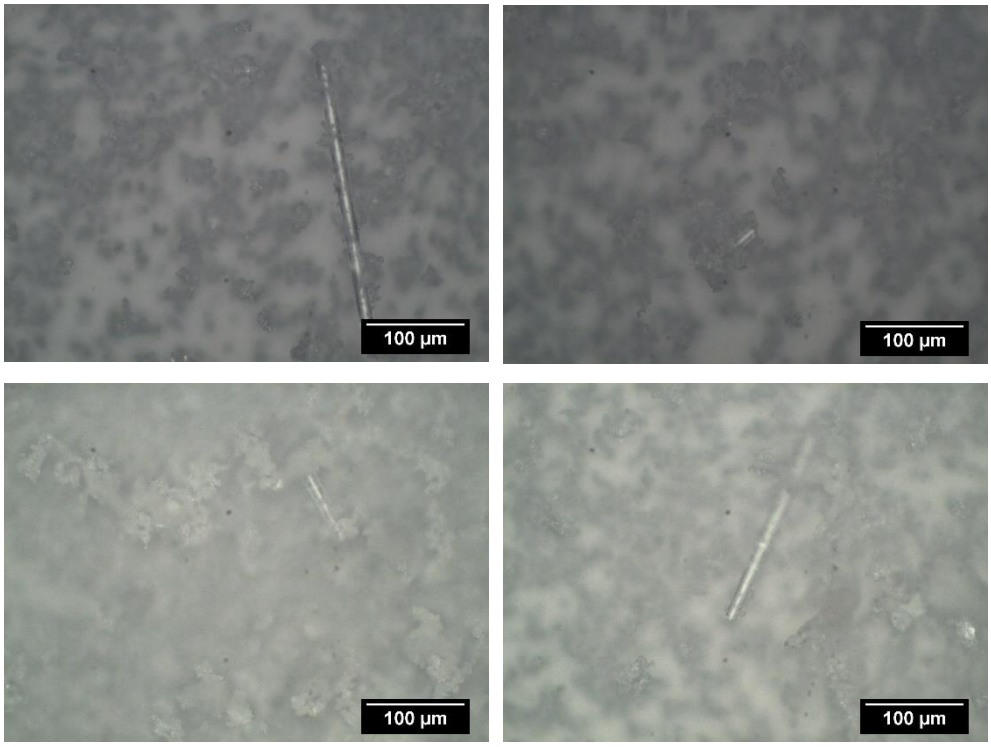

Figure 3.4 Optical microscopy images of Rivierasca's recycled material, 200x magnification. The low glass fiber content is evident. The materials is prevalently made of what appears to be residues of the polyester matrix of the original composite.

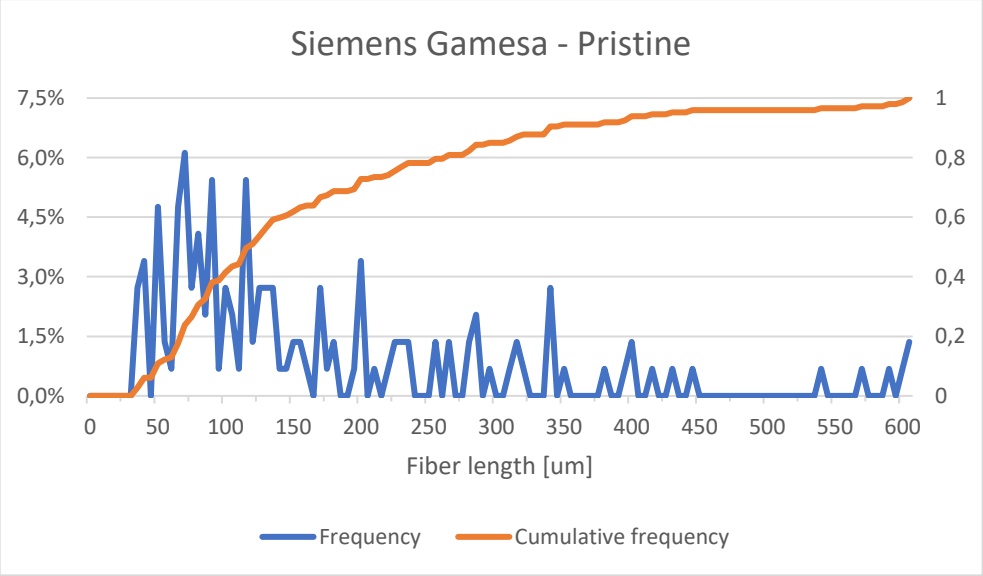

Chart 3.4 Fiber length distribution of Siemens Gamesa's recycled fiber glass.

The results are summarized in the following table:

	Average length [µm]	Standard deviation [µm]	Diameter [µm]	Glass content (in weight)
Italdry Fil 100	52,3	61,3	13	100%
Owens Corning 737BC	77,6	54,3	16	100%
Rivierasca	136	-	13	12%
Gamesa	166,2	135,0	13	70%

Table 3.1 Overview of the fiber size and glass content of the reinforcements used in this work.

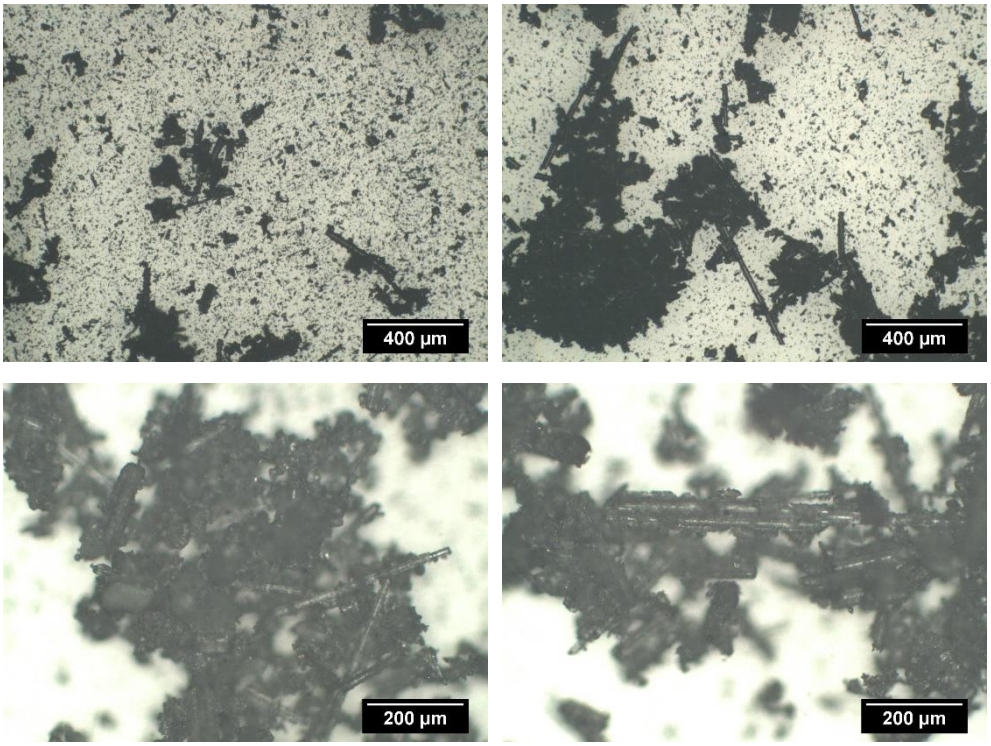

Figure 3.5 Optical microscopy images of Gamesa's recycled material, 50x magnification (top) and 100x magnification (bottom). The improved fiber content with respect to Rivierasca's material is evident. The fiber surfaces appear free of macroscopic matrix residues. Fine particles are visible, most probably poylester matrix residues.

3.2 Fiber volume fraction

While the fiber mass fraction is of practical use during the preparation of the different mixtures, all theoretical models for the behaviour prediction of composite materials depend on the volume fraction. Thus, I have calculated the volume fractions for the different materials. To do this, I needed to calculate the density of the various reinforcements. Owens Corning was the only manufacturer providing this information. I had to estimate the remaining values by making certain assumptions:

- Italdry Fil 100: 2,53 g/cm^3 Based on the average density of unsized S-glass fiber.
- Owens Corning 737BC: 2,63 g/cm^3 provided by the manufacturer.

- Rivierasca: 1,32 g/cm^3 This estimate was based on the average density of polyester resins (1,15 g/cm^3) and E-glass fiber (2,54 g/cm^3), and calculated considering a 12% glass fiber content in weight of the recycled material, obtained by thermogravimetric analysis.
- Gamesa: 2,12 g/cm^3 The underlying hypotheses were the same as for Rivierasca's recycled fibers, adjusted for a 70% glass fiber content in weight of the recycled material.

The results are summarized in the following table:

	Reinforcement	M_f [%]	Density [g/cm^3]	V_f
SR50V/SR50VTT	Italdry Fil 100	50	2,53	0,31
SR60V/SR60VTT	Italdry Fil 100	60	2,53	0,40
SR70V/SR0VT	Italdry Fil 100	70	2,53	0,51
SR60OC	Owens Corning 737BC	60	2,63	0,40
20DR45	Rivierasca	45	1,32	0,42
20DR57G	Gamesa	57	2,12	0,42

Table 3.2 Overview of the filler volume fractions of the different formulations.

3.3 Mechanical behaviour

Halpin-Tsai prediction

The Halpin-Tsai equations are a family of empirical relationships that allow to predict the elastic-mechanical properties of a composite material as a function of the standalone properties of the matrix and the reinforcement. They are applicable to a wide range of reinforcement shapes -continuous fibers, short fibers, whiskers, spheres- and have been extensively shown to fit the experimental data very well. More specifically, Halpin and Tsai demonstrated that the property of a composite,

Pc, could be expressed in terms of the corresponding property of the matrix, Pm, and the reinforcing phase, Pf, according to the following relationships [68]:

$$P_c = P_m \left(\frac{1+\zeta \eta v_f}{1-\eta v_f} \right)$$

$$\eta = \frac{\frac{P_f}{P_m} - 1}{\frac{P_f}{P_m} + \zeta}$$

The factor ζ describes the influence of the reinforcing phase's geometry on the property under evaluation. In the case of oriented whiskers -the relevant case for this work- it is equal to:

$$\zeta = 2\left(\frac{1}{d}\right) + 40 v_f^{10}$$

d stands for the diameter of the fibers.

I used the Halpin-Tsai model to predict the Young's moduli of the developed formulations. Not only did this give me useful insight on the potential of the various materials, but the comparison with the experimental values helped me assess the process quality. Assuming the exactness of the initial hypotheses[6], suboptimal experimental results generally imply process-related defects.

As seen before, the reinforcements used in this research do not have a precise length but rather a wide length distribution. Given the non-linearity of the Halpin-Tsai equations, using the average particle length in the model is not correct and would induce errors in the results. To address this issue, I used the previously obtained

[6] Owens Corning was the only manufacturer giving precise information about the mechanical performance of their reinforcement (Young's modulus: 80 GPa). As already mentioned before, I based my calculations for the other formulations on the typical Young's modulus values for S- and E-glass (85 and 75 GPa respectively, taken from AZO Materials' datasheets [15]-[56]).

distributions to calculate a more precise estimate, weighing the Young's modulus for each length class on that class's relative frequency.

Italdry Fil 100

As expected, the tensile tests show a similar increase both in the Young's modulus and in the ultimate tensile strength as the fiber content grows. The values are, however, considerably lower than expected and predicted by the theoretical models. The values for the Young's modulus obtained from the samples printed on the 3DRag V1 at 50 wt% fiber are lower than those of the non-filled, cast resin (2,8 GPa), as reported by the research group's previous work, conducted by fellow researcher Elena Paracchini. Samples printed on the Delta 40x70 showed a slight performance increase. This could be due the intrinsically higher performance of the machine leading to less defects (voids, mainly) or to the smaller nozzle used on the Delta (0,609 mm vs 1,54 mm). A smaller bead (whose dimension is directly dependent on the nozzle size) could reduce the intrinsic inter-bead void distribution and facilitate the photopolymerization process, since a shorter light travel path would imply less absorption and diffusion phenomena, permitting a higher photoinitiator activation rate. If the low mechanical performance were imputable to low conversion rates and not to the presence of defects in the samples, it would imply insufficient polymerization for all printed specimens.

It is interesting to notice the effect of a thermal treatment. The samples showed a twofold increase in Young's modulus, with values very close to the theoretical predictions and well inside the tolerances of the Halpin-Tsai model (complete accordance in case of the 60 wt% samples) and a threefold increase in ultimate tensile strength, reaching considerably high values.

In accordance with the literature, the elongation at break values decrease with the increasing fiber content [69]. As already observed for the UTS and Young's moduli, there is an increase when switching from the 3DRag V1 to the Delta 40x70 setup, followed by a very relevant (~50%) increase when the thermal treatment is added.

Similar improvements in the mechanical performance of UV-curable resins have been reported in literature and linked to reductions in unreacted monomer content and increased cross-linking [70]–[72].

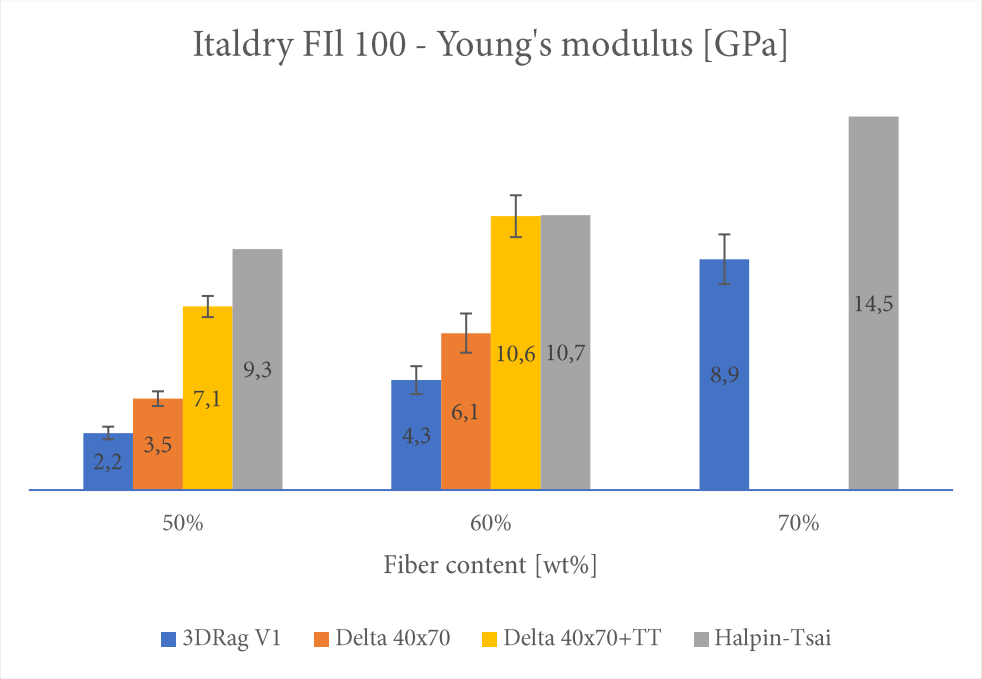

Chart 3.5 Young's modulus values of Italdry Fil 100 based samples with different filler contents compared to the theoretical predictions of the Halpin-Tsai model.

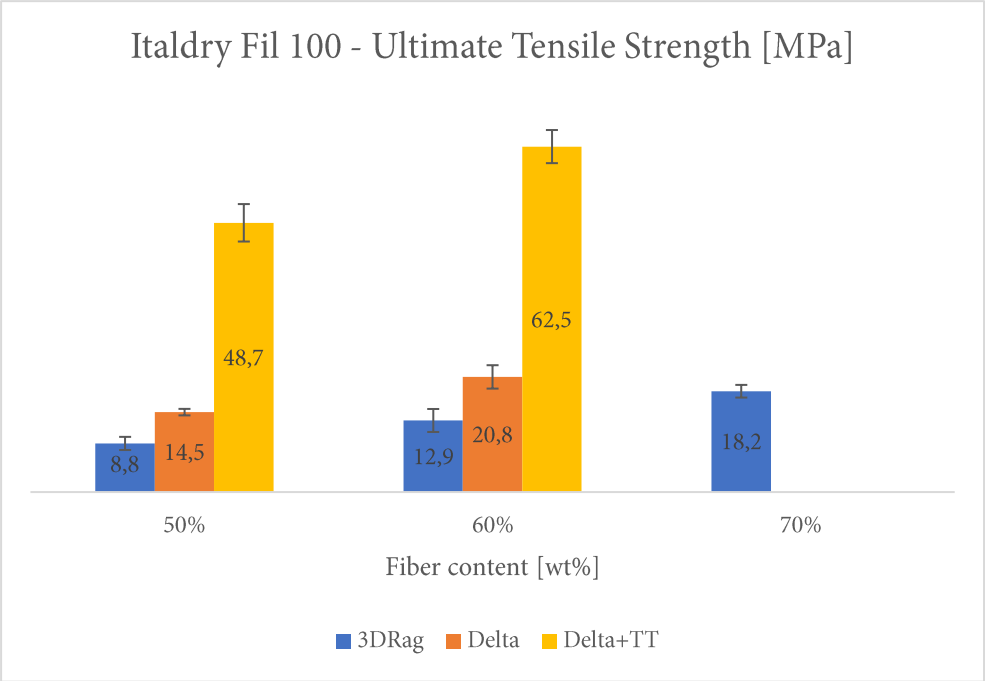

Chart 3.7 Ultimate tensile strength values of Italdry Fil 100 based samples with different filler contents..

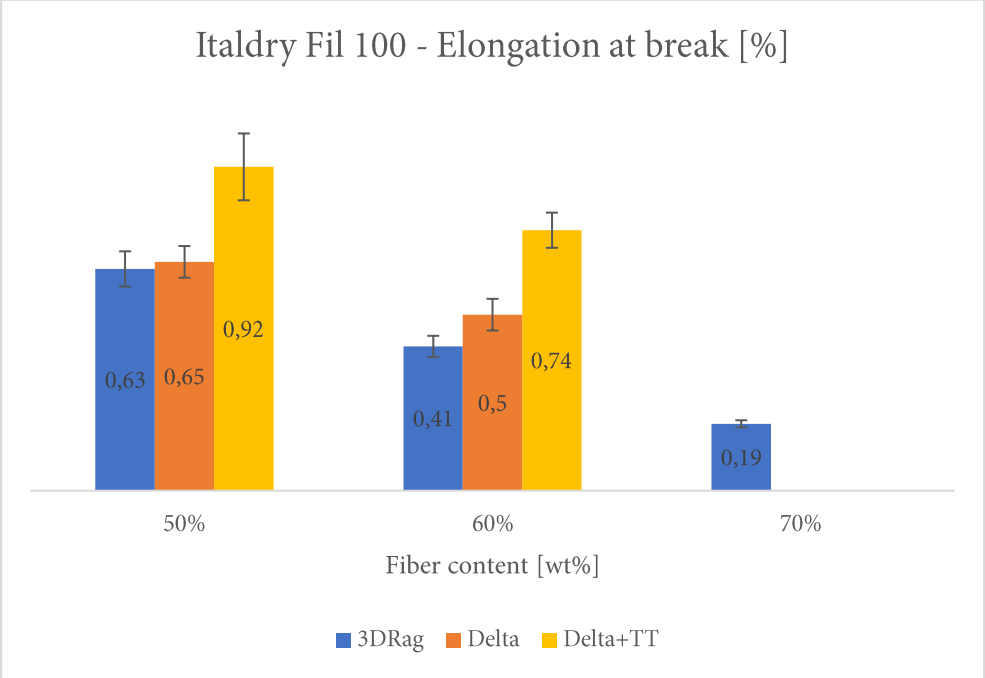

Chart 3.6 Elongation at break values of Italdry Fil 100 based samples with different filler contents.

The shapes of the σ-ε curves (see appendix) further underline the difference between treated and untreated samples. The untreated samples show marked viscoelastic effects and small-scale yielding. This statement holds for both 3DRag V1 and Delta 40x70 samples. The thermal treatment, on the other hand, visibly changes the behaviour of the materials. The curves display a completely fragile behaviour.

Visual inspection showed that the fracture surfaces of the thermally treated samples are of fragile nature. SEM imaging underlined an array of voids -air bubbles, mainly- that most likely were the cause of crack initiation and propagation. The somewhat relevant differences in performance between the samples can be attributed to the poor control over said defects. SEM imaging also indicated predominant pull-out of the fibers, with no observable fiber fracture. It follows that the fiber-matrix adhesion is somewhat poor.

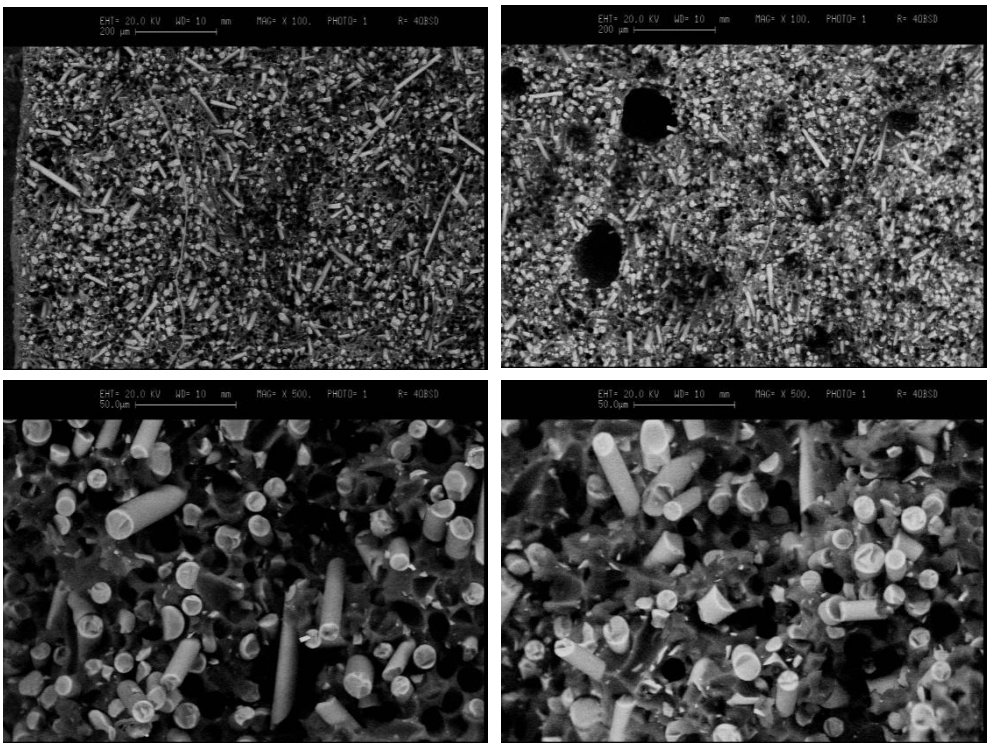

Figure 3.6 SEM images of SR60V (left) and SR60VTT (right) fractures surfaces. Preferential fiber alignement, voids (air inclusions) and marked pull-out phenomena can be observed. No discontinuities directly attributable to the layered manufacturing are visible, indicating good interlayer adhesion.

Owens Corning 737BC

The main difference of these fibers compared to Italdry Fil 100 lies in the silane sizing. An improved matrix-fiber adhesion is expected, and its evaluation was the main reason behind this specific reinforcement's selection. I decide to narrow the characterization the 60 wt% fiber formulation, equivalent to a fiber volume fraction of 0.40, since the initial experimentation with Italdry Fil 100 reinforcement indicated that this was the overall most promising fiber content.

The samples were printed on the 3DRag V2 setup. Similarly to what happened with the Italdry Fil 100 samples made with the 3DRag V1 setup, the specimens underperformed compared to the Halpin-Tsai model predictions. The Young's modulus measured at 1,91±0,40 GPa modulus, 82% less than the predicted 10,68 GPa. The ultimate tensile strength was 18,13±1,25 MPa and the elongation at break was 1,27±0,28%.

Interestingly, the thermal treatment did not yield the same result as for the Italdry Fil 100 samples. The UTS and the elongation at break showed a notable increase (+39% and +82% respectively), as with the Italdry formulations. The Young's modulus, however, saw a 16% decrease. This could be linked to a high defect presence in the material. The thermal treatment's improvement of the conversion rate of the matrix would reduce the plasticizer effect of the non-converted monomer [73], improving both maximum tensile stress and elongation at break, while at the same time emphasizing the void dependant stiffness reduction [74]. This hypothesis is further supported by the σ-ε curves of both annealed and non-annealed formulations (see appendix), which, as was the case with the previous reinforcement, show a marked brittle behaviour correlated with the thermal treatment, while the non-treated samples show marked small-scale yielding phenomena. The more ductile and brittle nature of the fractures seem to be validated by visual inspection.

SEM imaging shows a prevalent pull-out of the fibers, with no visible differences in the fracture mechanisms compared to the Italdry Fil 100 based samples. It follows that this silane sizing is inefficient in combination with the used acrylate resin.

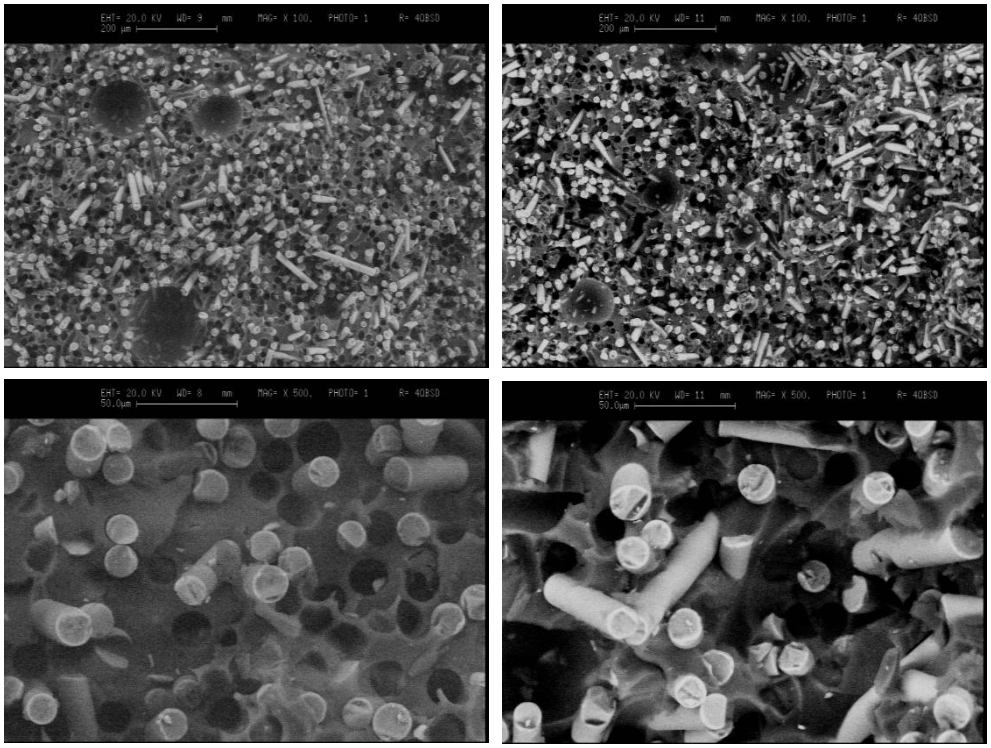

Figure 3.7 SEM images of SR60OC (left) and SR60OCTT (right) fractures surfaces. Pull-out phenomena are still clearly visible, indicating that the silane sizing has not led to notable changes in the fiber-matrix adhesion.

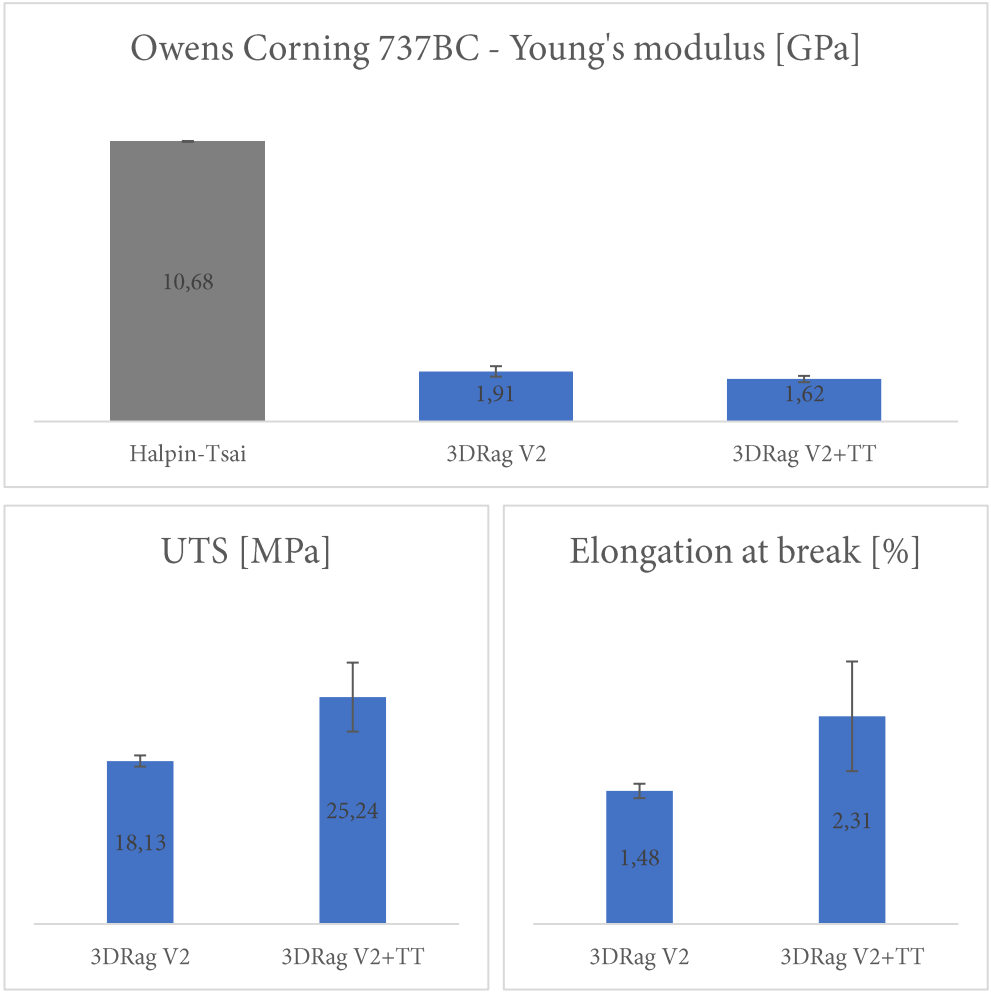

Chart 3.8 Mechanical properties of SR60OC and SR60OCTT samples.

Rivierasca

The recycled material provided by Rivierasca is prevalently made of polyester matrix fragments (glass content≈12 wt%). This is expected to show in the mechanical properties of the material with accordingly low values. Even though multiple formulations were developed, I selected only the most promising one for tensile testing, which was the 45 wt% filler mixture. Specimens were printed on the 3DRag

V1. The material is a homogenous grey paste with red hues (due to the presence of iron oxide in the filler).

The tested samples exhibit a good accordance with the Halpin-Tsai prediction regarding the Young's modulus. The discrepancy with the experimental results is inside the model's tolerances. The material exhibits a prevalently fragile behaviour, with a relatively low elongation at break. Visual inspection of the fracture surfaces confirms the fragile nature. Defects, mainly air inclusions, are visible and seem to have acted as crack nucleation sites. Once again, the poor control over the presence of these voids has contributed to the high variance of the results.

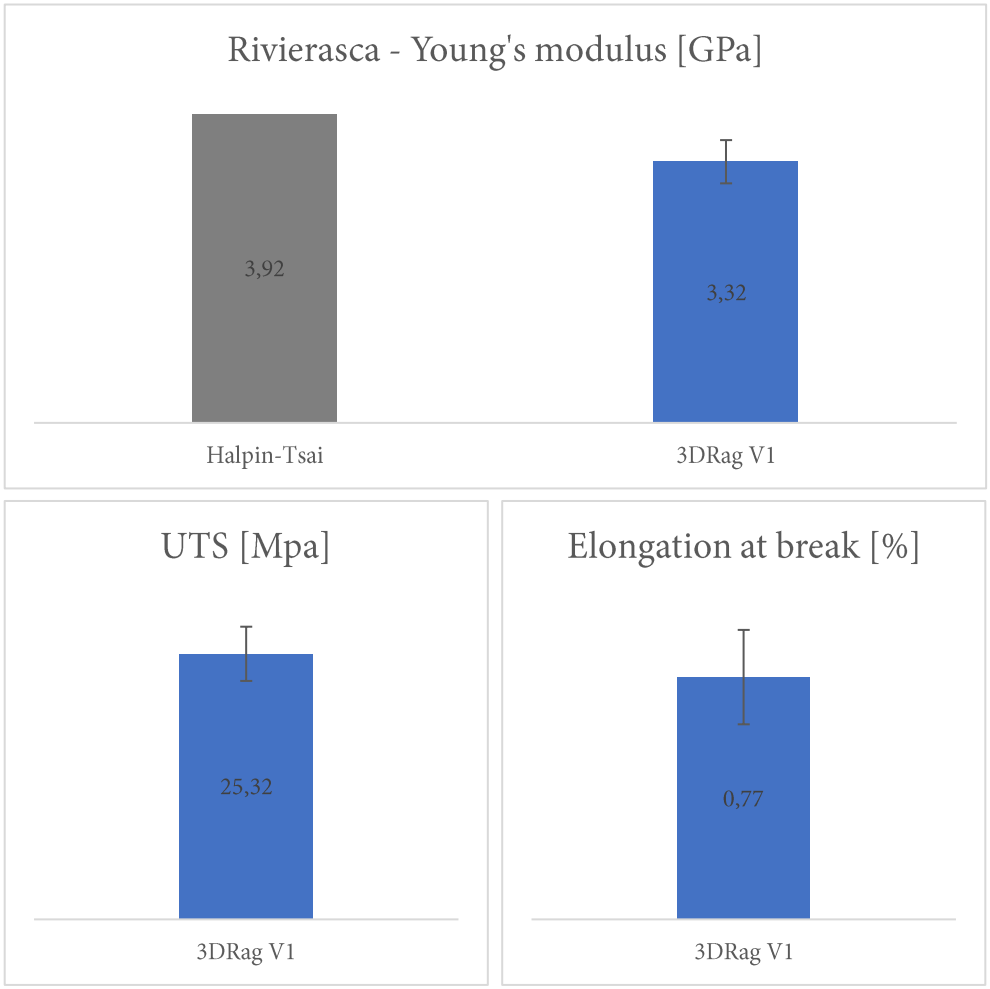

Chart 3.9 Mechanical properties of 20DR45 samples.

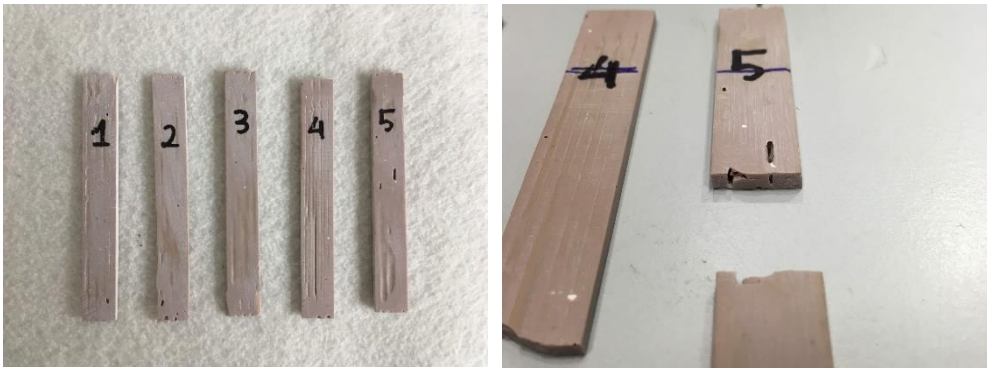

Figure 3.8 20DR45 tensile test specimens. It is possible to notice how fractures outside of the valid zone are a rather common occurrence and how there are various defects which often act as crack nucleation site (see sample 5). Fragile behaviour can be noted. These samples were printed on the 3DRag V1.

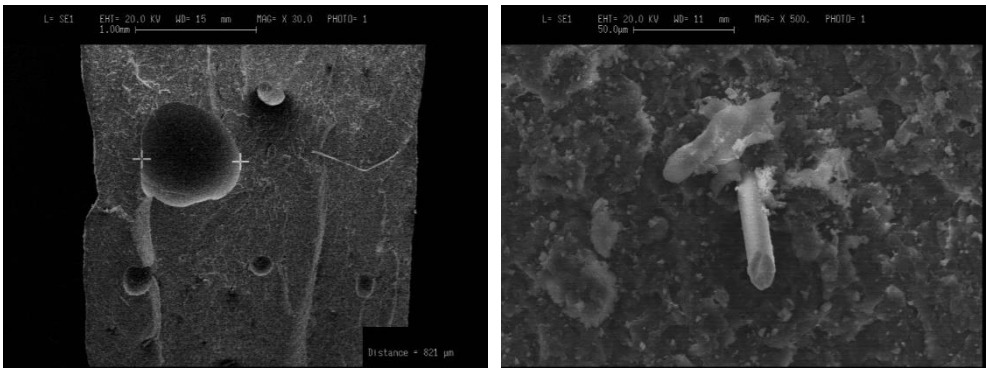

Figure 3.9 SEM imaging of 20DR45 fracture surfaces. The numbero of visible glass fibers is considerably low. Large voids are observable.

Gamesa

This second type of recycled material is expected to show improved performance in comparison with Rivierasca's, mainly because of the higher glass content. In order to be able to directly compare the two materials, the formulation was prepared with the same filler volume fraction (0,42). The specimens were printed on the 3DRag V2. The material is almost black in colour.

The darkness of the paste seemed to block a relevant amount of UV light. The conversion rate immediately after printing was visibly low. It was high enough, however, to guarantee the structural stability necessary to move the specimens to the oven for the activation of the thermal polymerization process without damage.

Interestingly enough, despite the relevant differences both in the filler and in the resin system nature, the 20DR57G and 20DR57GTT specimens printed with the 3DRag V2 setup displayed the same behaviour as the other batches printed on the same machine, namely the SR60OC and SR60OCTT. The supplementary thermal treatment reduced the elastic modulus (-62%), while increasing both the ultimate tensile strength (+39%) and the elongation at break (+318%). Observing the same behaviour on two different materials manufactured on the same setup seems to further endorse the previously made hypothesis: the thermal treatment may increase the conversion rate, improving the elastic behaviour while at the same time enhancing the detrimental influence of the defects on the elastic modulus. Again, the shapes of the σ-ε curves seem to confirm this (see appendix). The untreated samples show a mainly ductile behaviour with marked viscoelastic effects, while the thermally treated ones exhibit a typically fragile behaviour.

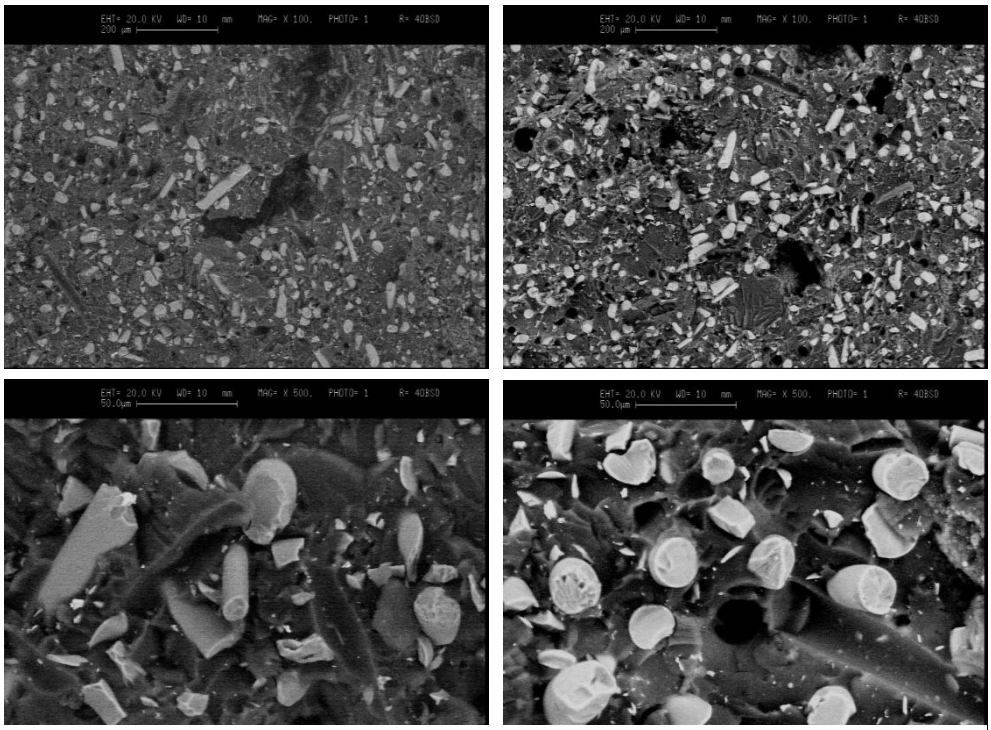

Figure 3.10 SEM imaging of 20D57G (left) and 20D57GTT (right) fracture surfaces. The higher glass content compared to Rivierasca based samples can be appreciated. Smaller fibers and glass fragments are visible.

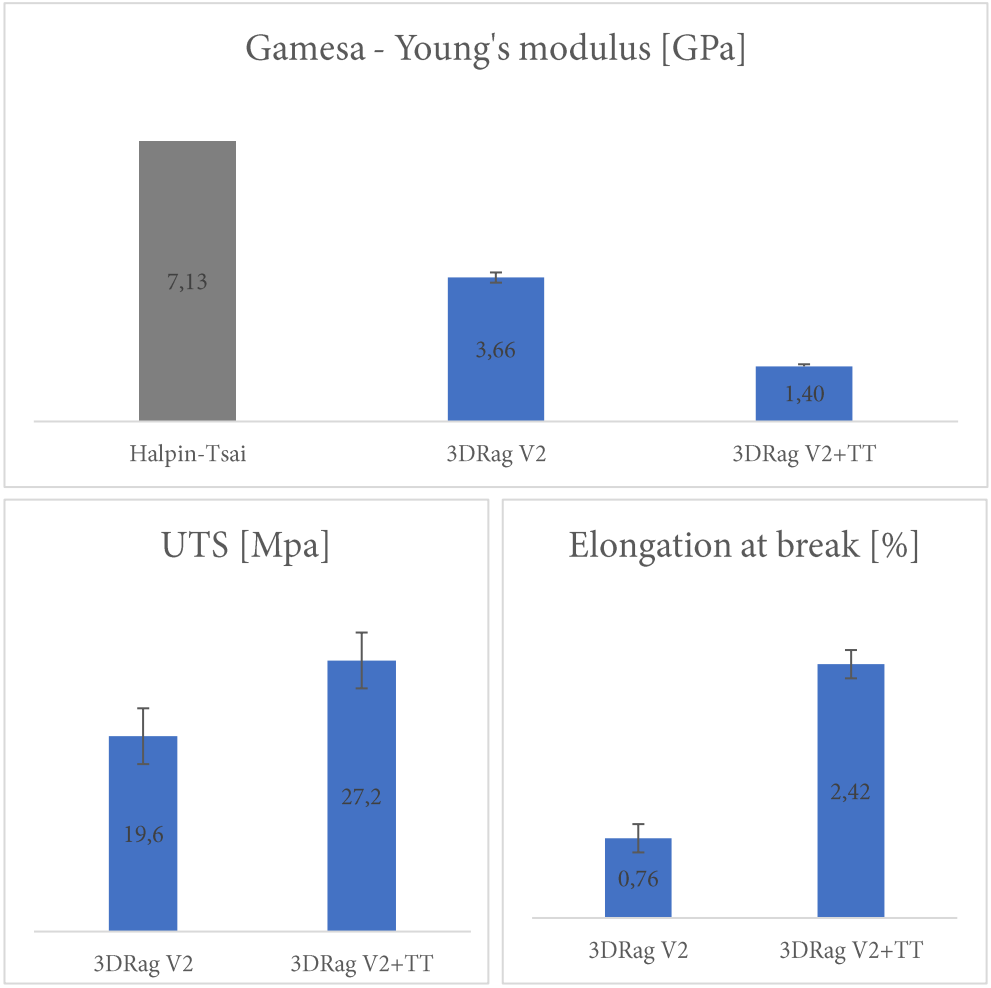

Chart 3.10 Mechanical properties of 20DR57G and 20DR57GTT samples.

Due to testing equipment limitations, compression tests were not doable. However, the behaviour under compressive stress of a material is of paramount important for tooling applications, since the typically dominant stresses in autoclave applications are of compressive nature. Given the brittle nature of the developed materials and based on the literature [75], an initial estimate for the compression strength could be set, conservatively, at 140% of the tensile strength.

	Machine	E [GPa]		UTS [MPa]	ε [%]
		Predicted	Experimental		
SR50V	3DRag V1	9,3	2,21±0,25	8,79± 1,19	0,63±0,05
SR50V	Delta	9,3	3,54±0,29	14,45±0,59	0,65±0,05
SR50VTT	Delta	9,3	7,11±0,41	48,68±3,39	0,92±0,1
SR60V	3DRag V1	10,7	4,26±0,54	12,94±2,08	0,41±0,03
SR60V	Delta	10,7	6,08±0,76	20,82±2,21	0,50±0,05
SR60VTT	Delta	10,7	10,7±1,62	62,46±3,00	0,74±0,05
SR70V	3DRag V1	14,5	8,9±1,93	18,23±1,15	0,19±0,02
SR60OC	3DRag V2	10,7	1,91±0,20	18,13±1,24	1,48±0,28
SR60OCTT	3DRag V2	10,7	1,62±0,12	25,24±3,84	2,31±0,61
20DR45	3DRag V1	3,9	3,32±0,28	25,32±2,59	0,77±0,15
20DR57G	3DRag V2	7,1	3,66±0,53	19,6±2,8	0,76±0,14
20DR57GTT	3DRag V2	7,1	1,40±0,15	27,2±4,6	2,42±0,38

Table 3.3 Summary of the tested samples' mechanical properties.

3.4 Process control

3.4.1 Gel content

Increasing light diffusion due to increasing fiber content and fillers absorbing in the relevant wavelengths increased the gel content. The addition of dicumyl peroxide as a thermal free-radical initiator partially solved the issue. The Italdry Fil 100 based SR70VT formulation showed a lower gel content in comparison to the mixture bearing only photoinitiator, and the Rivierasca based 20DR45 formulation showed a gel content reduction after the thermal initiator activation step. However, in both

cases residual monomer was detectable. A possible explanation to this could be the occlusion of the free radicals produced by the homolytic cleavage of dicumyl peroxide. The low mobility inside the already formed polymer network hinders the continuation of the chain-growth process. What seemed to successfully address this issue, on the other hand, was a thermal treatment of the materials at higher temperatures, as can be seen from the extremely low gel content of the SR60VTT sample. Similar phenomena have been reported in literature [76].

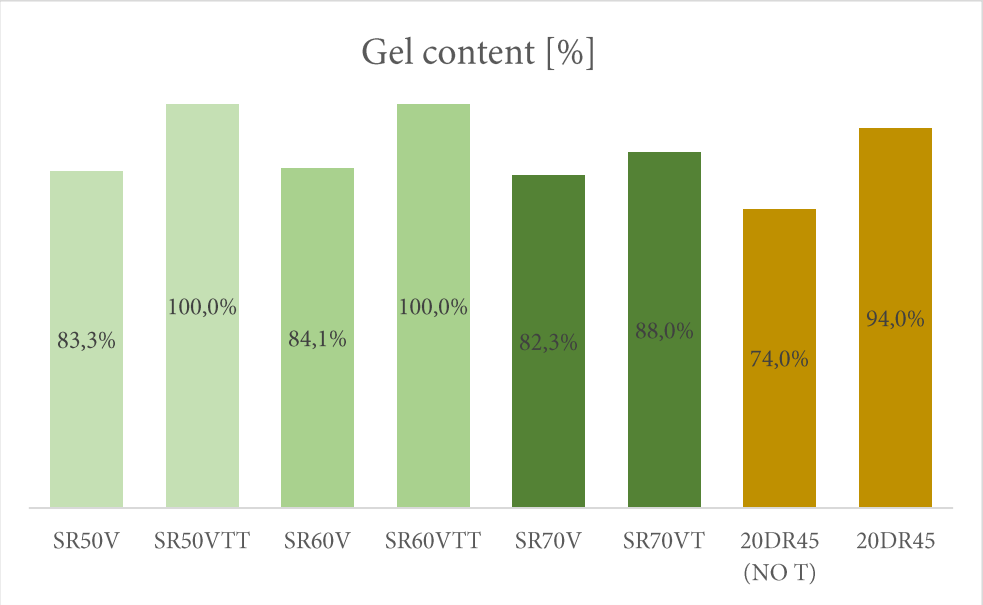

Chart 3.11 Gel content measurements of various samples.

3.4.2 UV-DSC

Italdry Fil 100

The value of the normalized integrals weighed on the active part of the formulation (the resin system) decreases with increasing fiber content, indicating a partial hindering of the monomer conversion process by the glass fiber, possibly due to light diffusion phenomena. Some residual level of heat production upon UV irradiation is observable in the printed samples, indicating ongoing free-radical production and consequent monomer conversion (see Chart 3.14).

Darocur vs. TPO-L

Darocur 1173 based samples show a marked heat reduction with the increase of the recycled material content, indicating a stronger susceptibility to filler-induced light hindering mechanisms. TPO-L, on the other hand, remains stable, with little to no heat reduction. Additionally, TPO-L displays shorter heat flow stabilization times (0.5 and 0.7 min vs. 0.4 and 1.2 min for 10 wt% and 30 wt% filler formulations, respectively). Hence, it seems to be the better choice as photoinitiator, and has been used for all formulations (see Chart 3.12).

Rivierasca

The stronger inhibition of the photopolymerization process of the recycled material compared to pristine glass fiber is confirmed by the decreasing trend of the values of the normalized heat emitted by the paste and by the printed material. A drastic decrease is notable with 55 wt% filler content. Thus, 45 wt% was identified as the maximum acceptable filler content (see Chart 3.13).

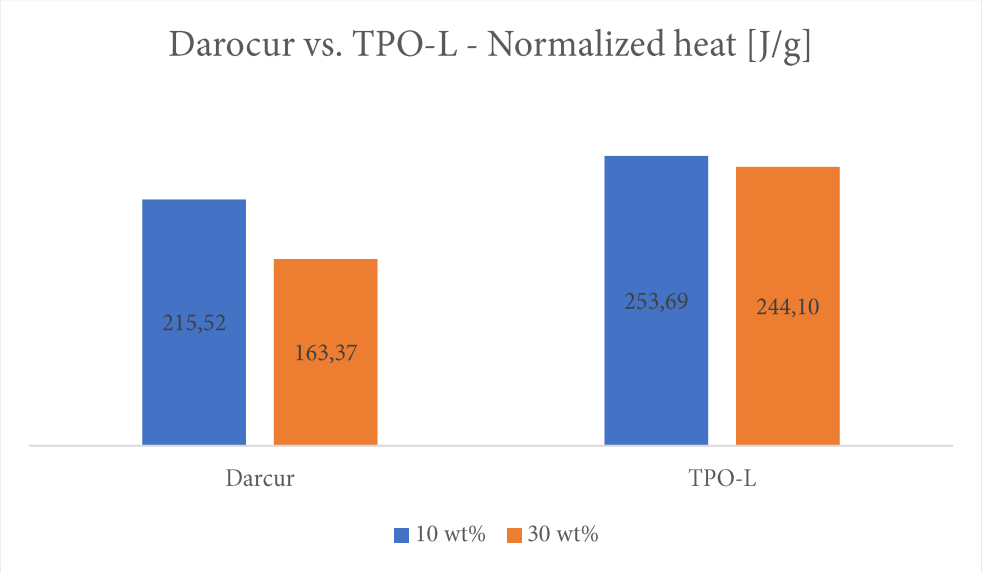

Chart 3.12 Comparison of UV-DSC normalized heat measurements of Darocur 1173 and TPO-L.

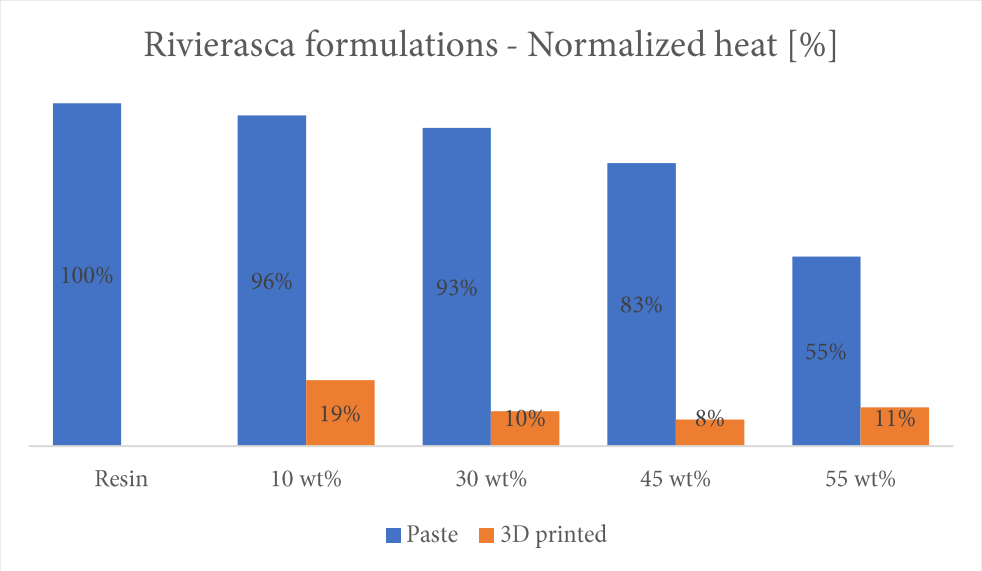

Chart 3.13 Analysis of the effect of different Rivierasca filler contents on the UV-DSC normalized heat measurements. The formulations are based on resin system C with different filler wt%.

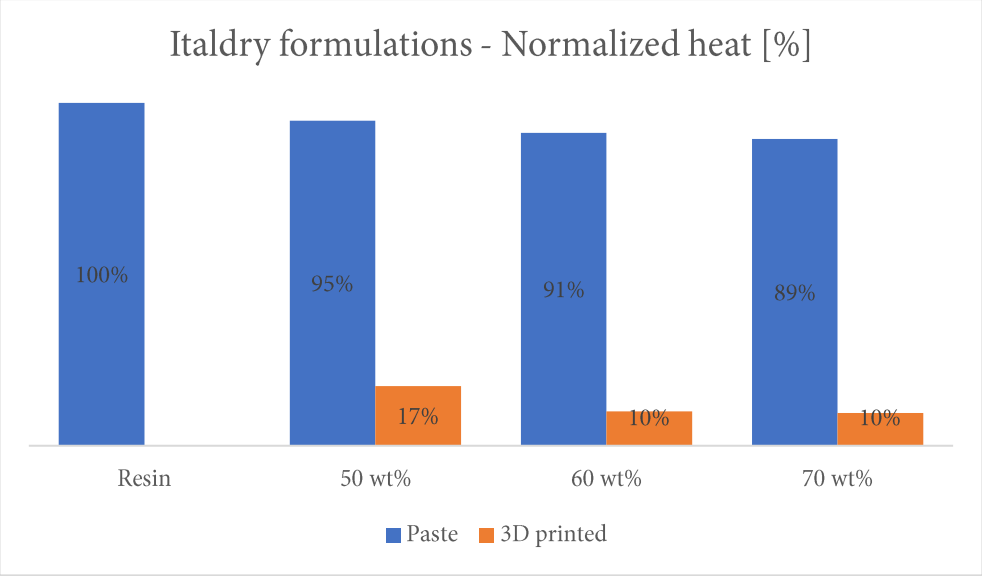

Chart 3.14 Analysis of the effect of different Italdry Fil 100 filler contents on the UV-DSC normalized heat measurements. The samples are SR50V, SR60V, SR70V.

3.4.3 FT-IR

The infrared absorption of thermally treated and untreated SR60V and SR60VTT samples were analysed, to assess the presence of thermal damage.

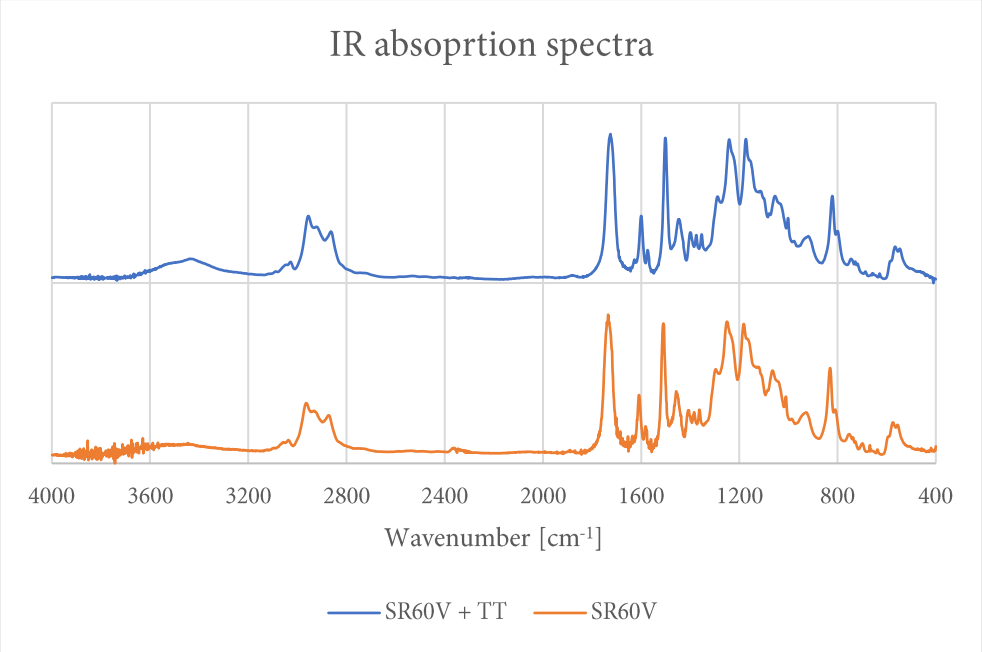

Chart 3.15 IR absorption spectra of two SR60V samples, with and without thermal treatment. The major difference lies in the broad absorption region at 3650-3250 cm-1, a possible sign thermal degradation of the polymer.

The degradation of the material due to prolonged exposition to high temperatures had to be carefully evaluated. The samples exhibit a light yellow shift in colour upon visual inspection, a typical sign of polymer degradation. FT-IR analysis shows the appearance of a broad absorption region at 3650-3250 cm^{-1}, characteristic of hydrogen-bonded hydroxyl groups of the alcohol type [77], which have been linked to thermal degradation of polymers with consequent radical production and cross-linking [78]. While this hypothesis seems to offer some valid support to the previous observations, definitive conclusions cannot be drawn, and an in-deep evaluation of the thermal degradation mechanism and its influence on the material is necessary.

3.5 Thermal behaviour

The properties of aluminium and the two analysed thermoplastic samples were taken from *Ansys Granta Materials Database*.

3.5.1 DMA/TMA

The coefficient of thermal expansion was initially measured on an aluminium sample to verify the correctness of measurements taken on a DMA instrument in TMA mode. The extrapolated value of $23{,}3 \cdot 10^{-6}$ is in line with the literature.

3.5.1.1 Thermoplastic samples

Carbon fiber filled polyamide

The CTE is in the 18-23·10^{-6} 1/K range. The T_g is visible at around 60 °C, in accordance with the literature.

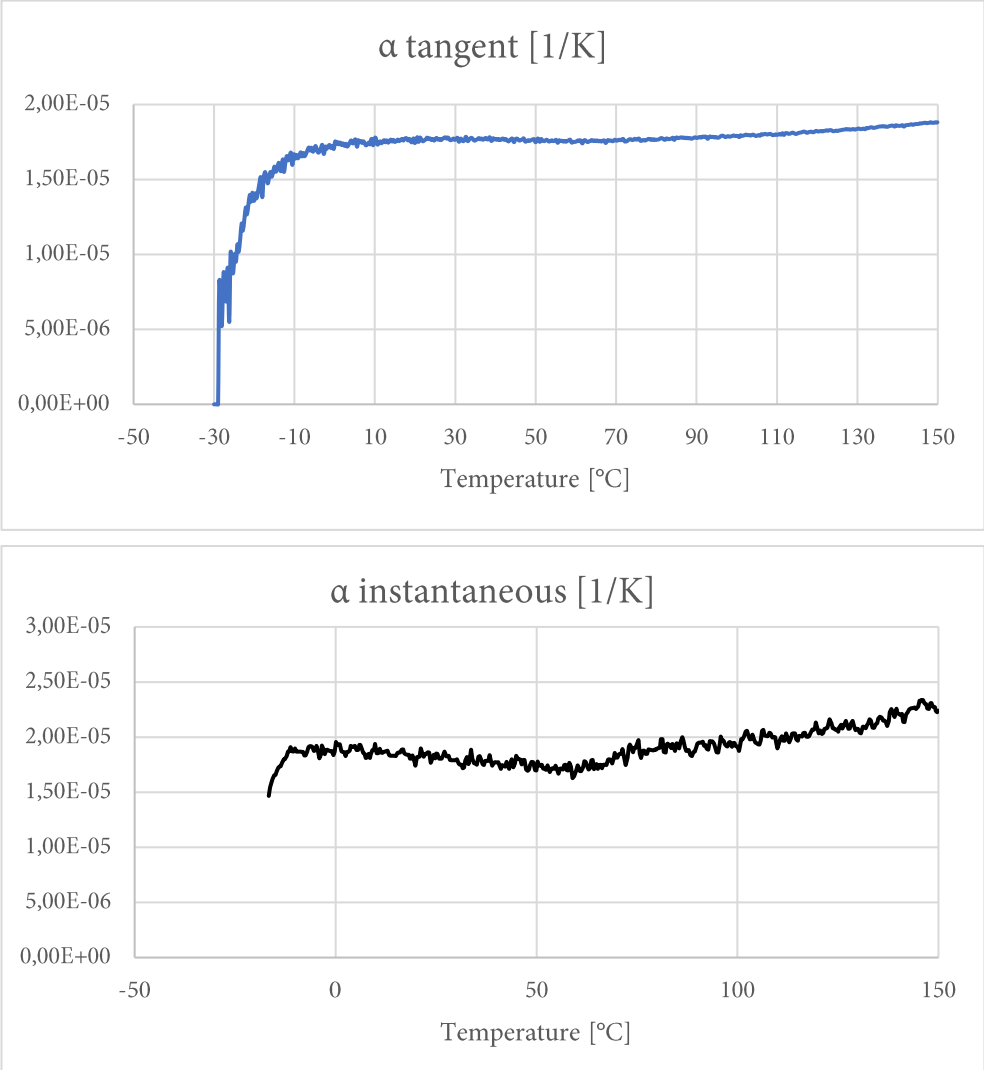

Chart 3.16 CF-PA samples CTE measurements.

Polyphenylene sulphide

The CTE is in the 20-28·10^{-6} 1/K range. The T_g is visible at around 90 °C, in accordance with the literature.

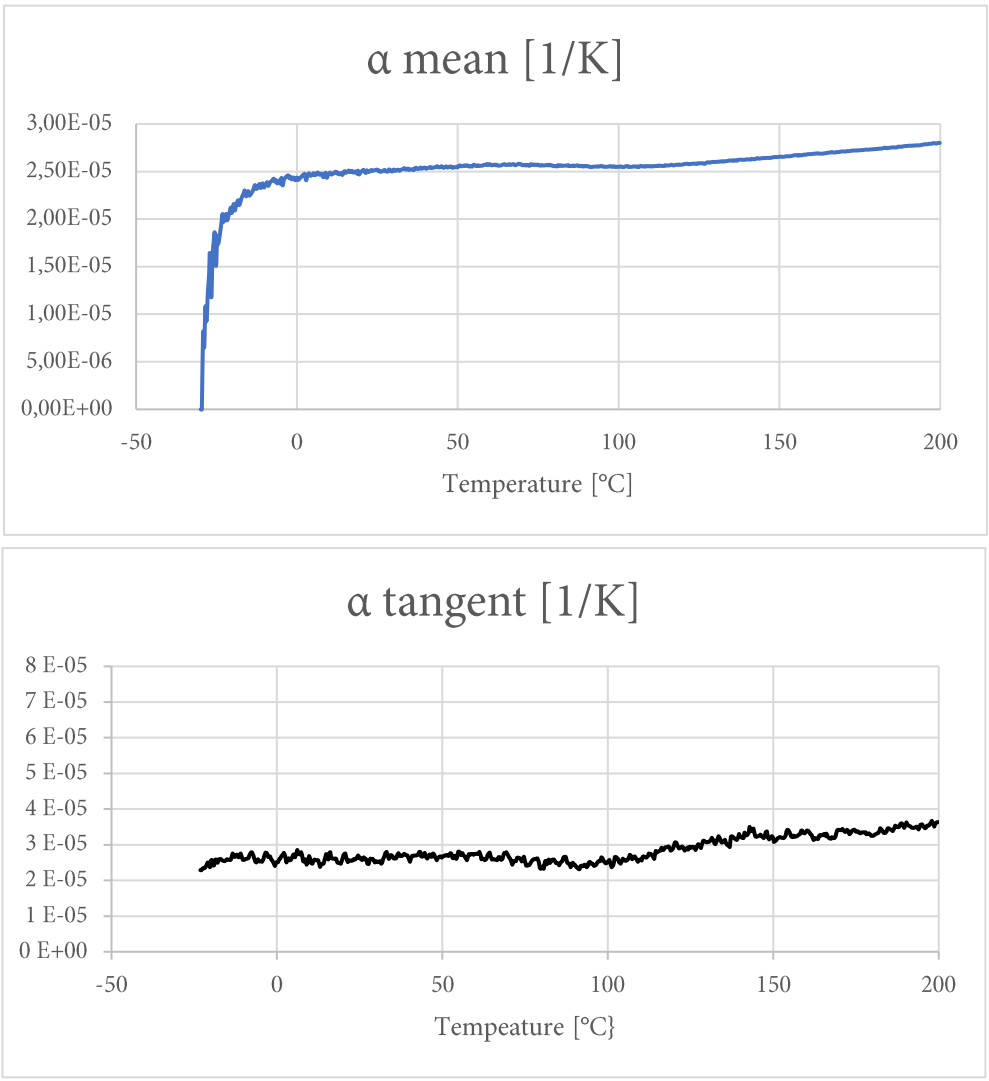

Chart 3.17 PPS samples CTE measurements.

Italdry Fil 100

The measurements show a marked stabilizing effect of glass fiber on the CTE. The values do not change drastically with the increasing fiber volume fraction; they do, however, show increased stability and tend to plateau at around $18 \cdot 10^{-6}$ 1/K. The glass transition temperature is visible at around 110 °C.

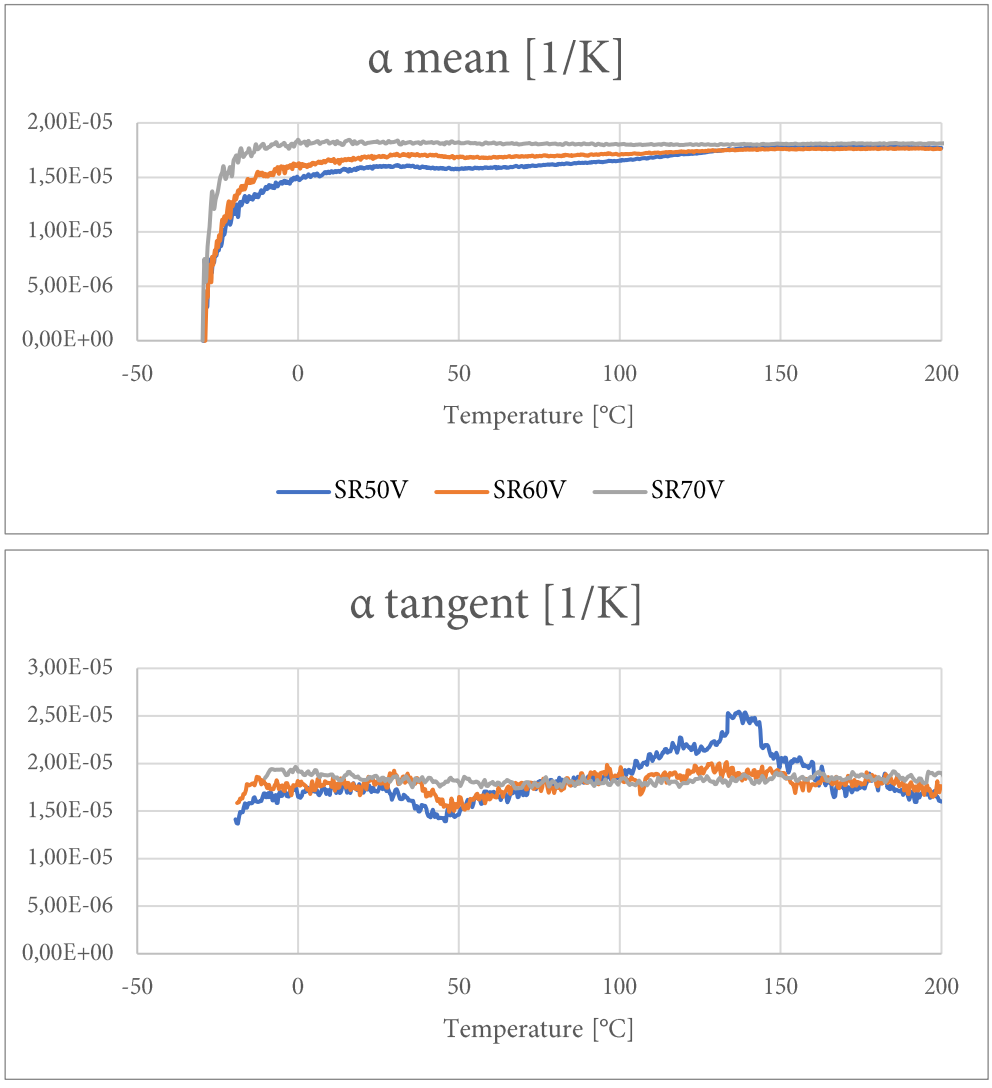

Chart 3.18 SR50V, SR60V and SR70V samples CTE measurements.

Owens Corning 737BC

Compared to the formulation with the same content of Italdry Fil 100 glass fiber, SR60V, the same general behaviour is identifiable. However, the SR60OC formulation shows an increased variability of the α values as a function of temperature. A possible explanation could entail putting this variation in relation with the lower mechanical properties described before, hypothesizing a dependence on the higher defect content of the samples.

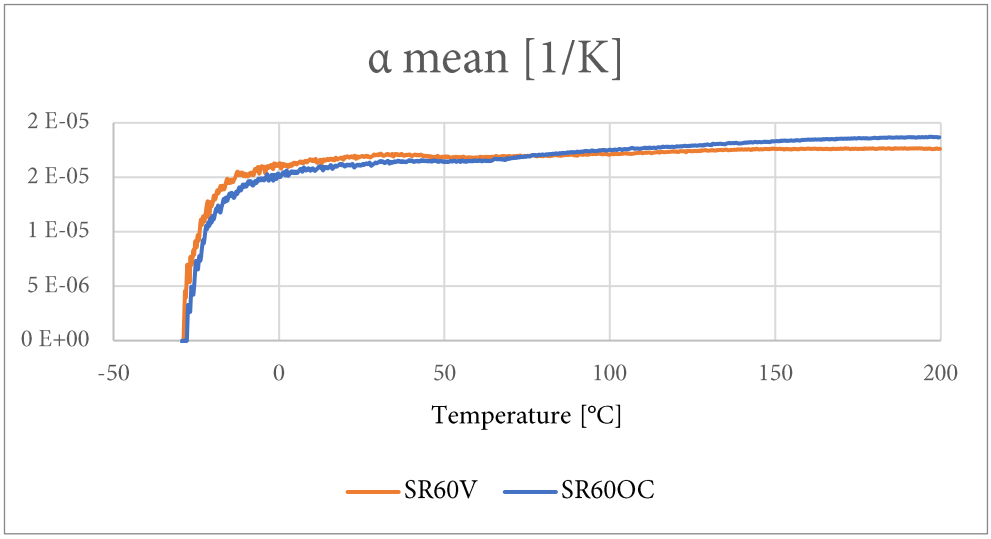

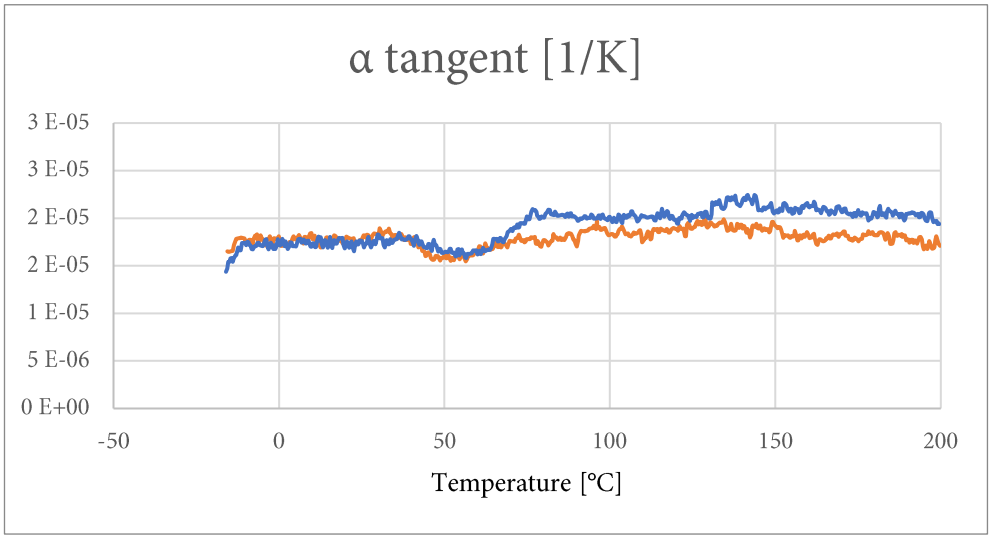

Chart 3.19 SR60V and SR60OC samples CTE measurements.

Rivierasca

The CTE is in the 20-30·10^{-6} 1/K range. The T_g of the matrix appears at around 110 °C. A second peak at around 70 °C could be associated with a phenomenon in the recycled material's matrix.

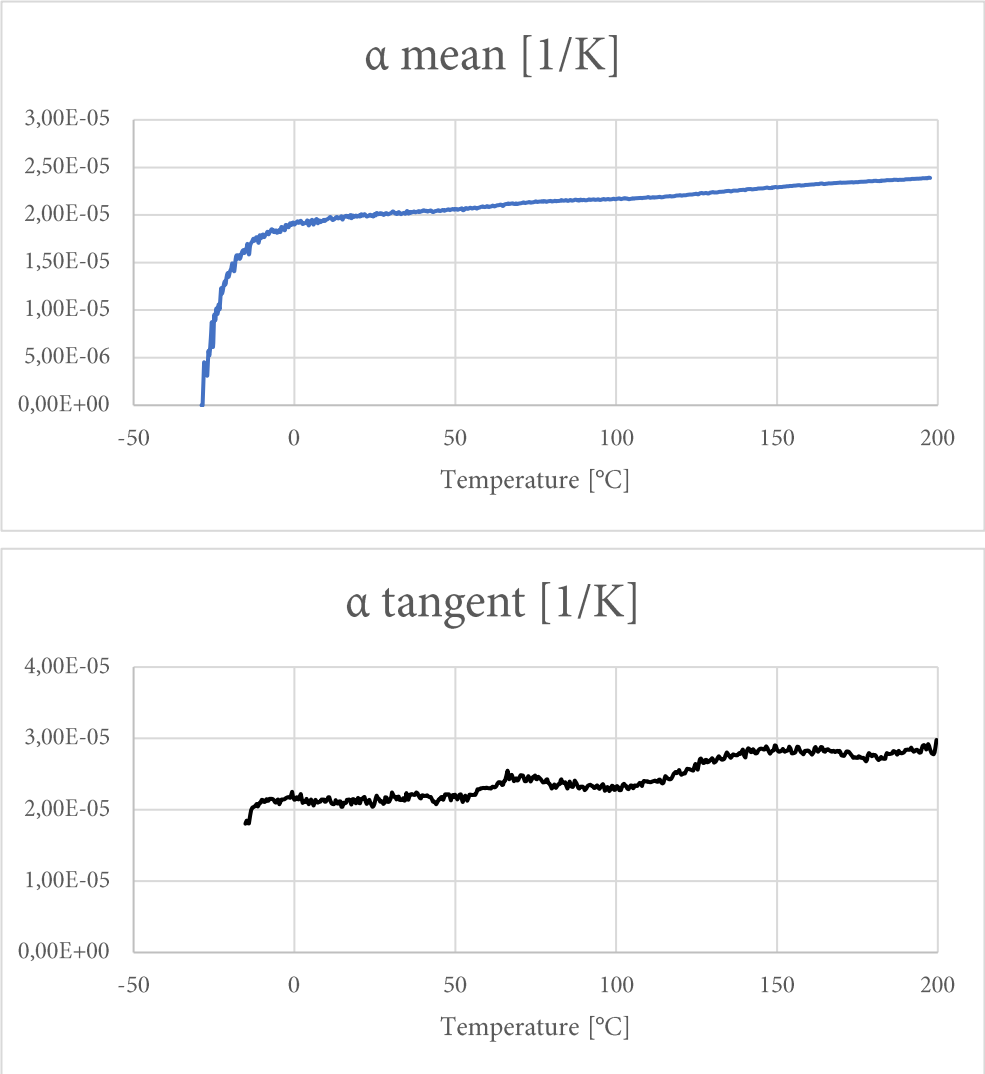

Chart 3.20 20DR45 samples CTE measurements.

Gamesa

Gamesa's recycled material improves the thermal stability of the formulation. This is probably due to the higher glass content and to the subsequent reduction in polyester matrix impurities. The peak at 70 °C disappears, endorsing the hypothesis of a relation with the recycled material's matrix. The glass transition remains visible at around 110 °C.

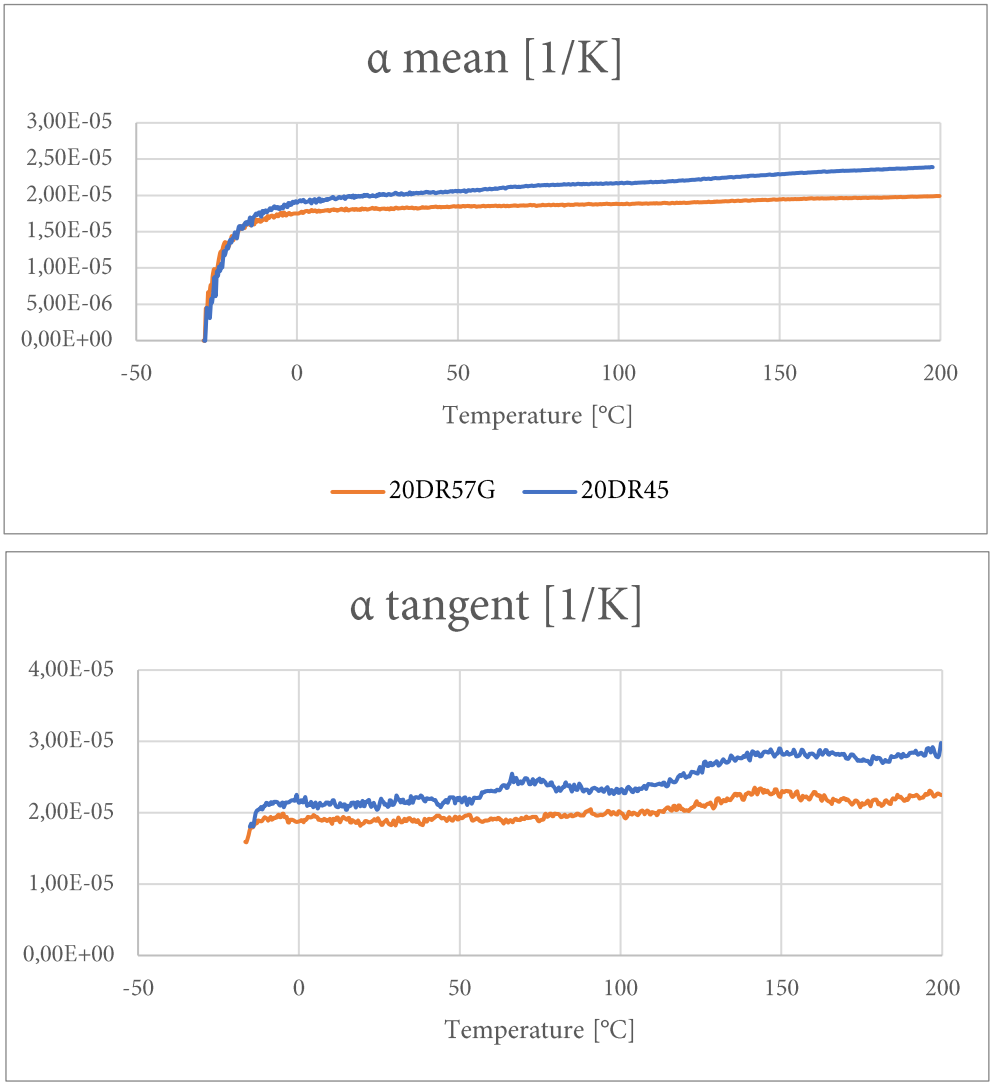

Chart 3.21 20DR45 and 20DR57G samples CTE measurements.

3.5.2 TGA

Italdry Fil 100

In both thermally treated and untreated samples, two well defined weight loss steps are observable, one at 444-449 °C and a second one at 538-546 °C. Both seem to indicate thermal decomposition with formation of gaseous reaction products.

The untreated sample show an additional weight loss step at 273 °C. A connection with unreacted monomer is plausible and would further corroborate the hypothesis of a completion of the polymerization process through the thermal treatment.

Rivierasca

TGA analysis of 20DR45 samples shows the two main thermal decomposition steps of the polymer matrix encountered with the Italdry formulations. The temperature variations (~10°C for the first step and ~30°C) are relevant enough to not be considered experimental fluctuations. They can be justified by the presence of 1,4-butanediol dimethacrylate in the 20DR45 samples and the changes in the polymer network it implies.

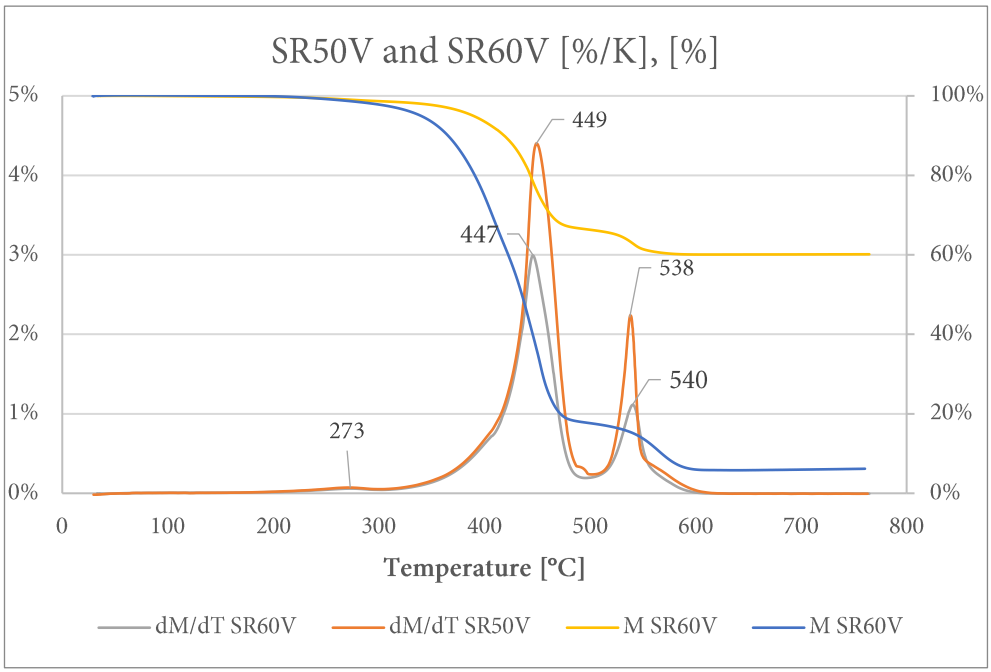

Chart 3.22 SR50V and SR60V samples TGA analysis.

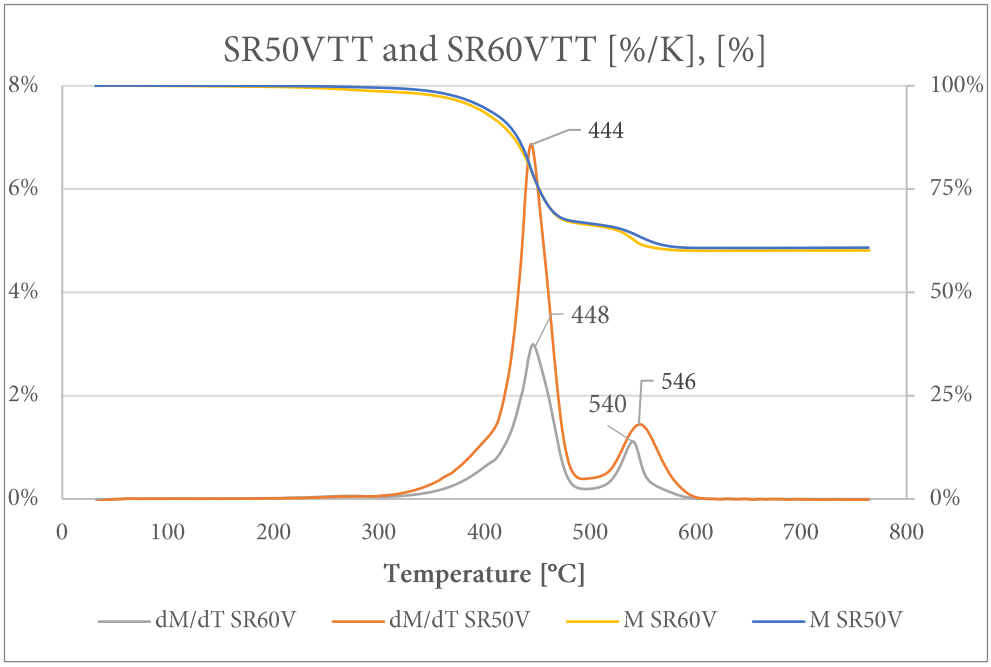

Chart 3.23 SR50VTT and SR60VTT samples TGA analysis.

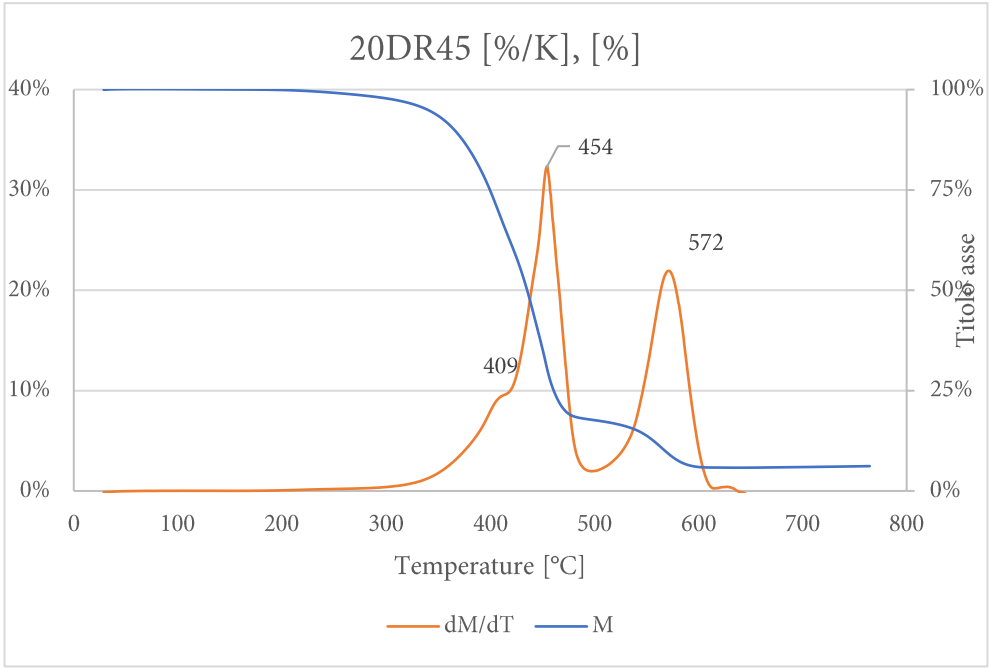

Chart 3.24 20DR45 samples TGA analysis.

3.5.3 DSC

Italdry Fil 100

Calorimetric analyses on SR50V, SR60V and SR70V show a glass transition temperature at around 120 °C, in line with TMA measurements, and an exothermic peak around 180 °C, probably related with reticulation processes of the remaining monomer. This hypothesis is corroborated by the analyses on the thermally treated samples, SR50VTT and SR60VTT, which exhibit a similar T_g but do not show the exothermic peak at higher temperature.

Rivierasca

Calorimetric analyses on the post-printing 20DR45 samples, prior to the thermal treatment, show an exothermic peak corresponding with the activation of the dicumyl peroxide in the first run at 10 K/min and a T_g at values between 110 °C and 120 °C in the second run, at 20 K/min. These values are in line with the TMA results. There is a broadening of the exothermic peak towards lower temperatures correlated with the increase in recycled material.

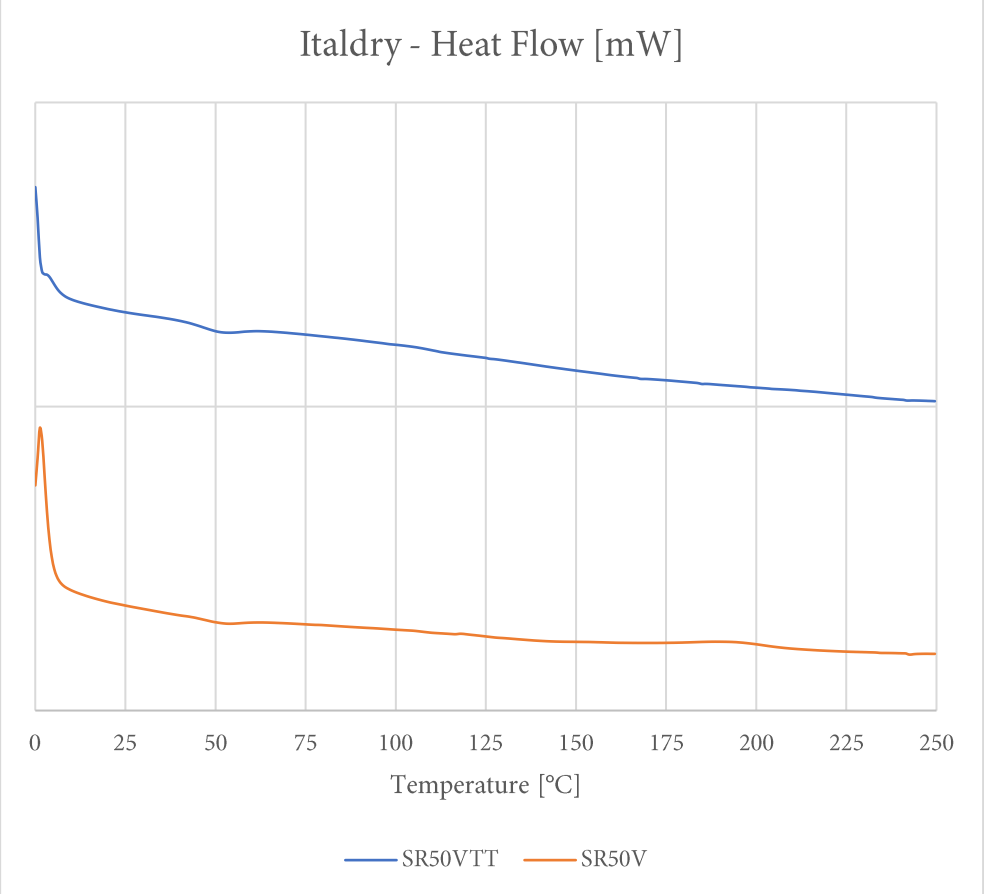

Chart 3.25 DSC analysis of SR50V and SR50VTT samples.

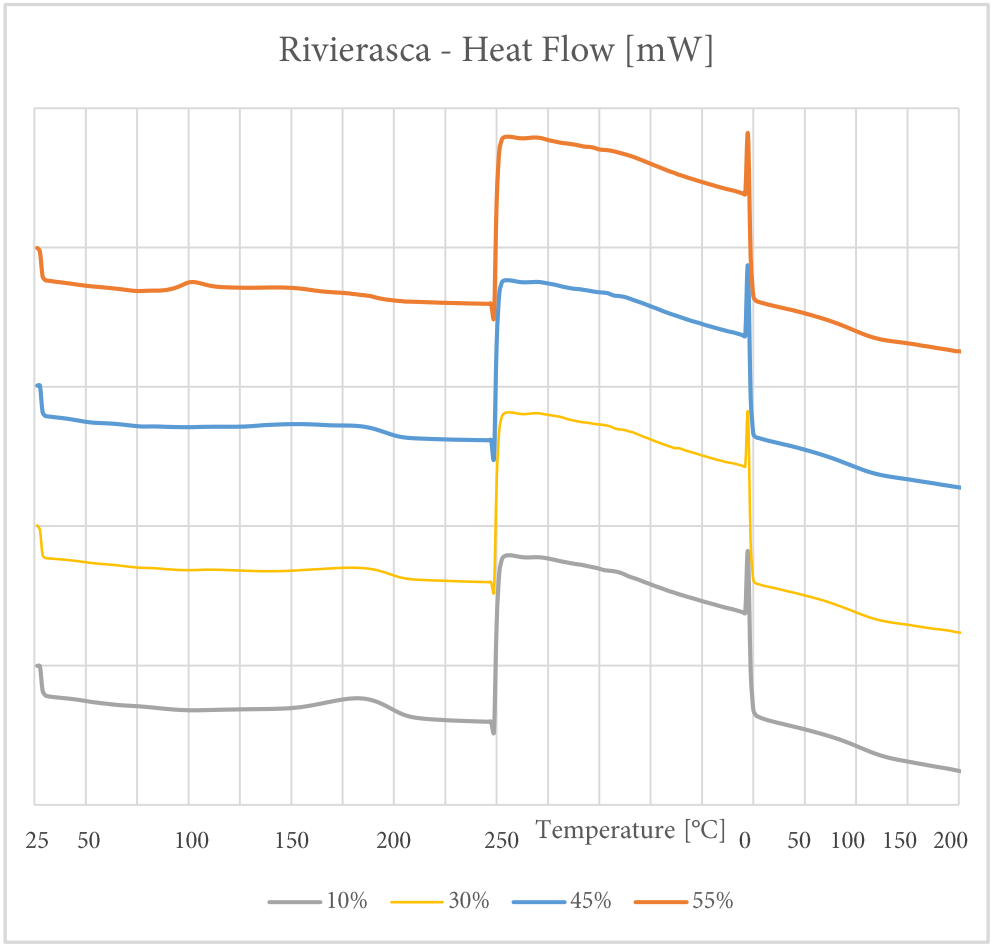

Chart 3.26 DSC analysis of resin system C formulations with different Rivierasca filler wt%.

3.6 Print quality

3.6.1 Formulations

Italdry Fil 100

As expected, the viscosity increases with the fiber content. 70% in weight was identified as the upper limit for the Italdry Fil 100 mixtures. With increasing fiber content, the high viscosity of the material impedes an even distribution inside the reservoir. Air bubbles accumulate, leading to momentary interruptions of the extrusion, often followed by a sudden excessive material output, most likely due to pressure build up in the nozzle. Vacuum-based degassing or similar techniques should be applied. 60% in weight was the most balanced fiber content overall: the material exhibited high enough viscosity to allow for the deposition of precise beads without excessive deformation in the instants prior to polymerization, while maintaining a high ease of use. Low fiber content formulations are less prone to clogging; they do, however, tend to deform excessively during bead deposition, leading to a generally worse print quality, especially in case of overhangs or top layers combined with sparse infills.

Owens Corning 737 BC

Given the similar nature of the reinforcements, I maintained the fiber content of the Italdry Fil 100 formulation exhibiting the best print behaviour: 60 wt%. As expected, the formulation yielded comparable ease of use and characteristics.

Rivierasca

Extensive trials were done to assess the rheological behaviour and print characteristics of various formulations based on Rivierasca's recycled material. The implementation of 1,4-butanediol dimethylacrylate as diluent and the effects of the filler content on the rheology were investigated during previous work of the research group. The formulation with 45 wt% filler was deemed the most satisfactory. The filler volume fraction, in this case, is equal to 42%. This value is very close to what was considered the ideal glass fiber content for the pristine glass fiber mixtures (40%). It is possible that a filler volume fraction of around 40% is the generally ideal

value. With due precautions, this information could be useful for the preparation of future formulations.

Gamesa

Based on the previous information, the formulation selected for trial had a 57 wt% filler content, equal to a filler volume fraction of 42%. The filler exhibits a higher wetting compared to Rivierasca's recycled material, which greatly facilitates the formulation preparation. As mentioned before, the very dark colour of the mixture somewhat hinders the photopolymerization process.

3.6.2 Machines

The Delta 40x70 was a great improvement over the initial 3DRag V1 setup. Not only does it feature a bigger build volume and a high capacity material reservoir; it also exhibits higher precision in the deposition process, low nozzle pressure, constant, controllable flow, and retraction capabilities. After an accurate fine tuning procedure, it is possible to achieve a satisfying print quality, as can be seen from Figure 3.9.

On the other hand, large quantities of air in the material reservoir tend to form air bubbles which cause momentary flow interruptions and nozzle clogging in the worst cases. The print quality would greatly benefit from additional control over the air presence in the mixture. The control over the polymerization process is somewhat poor. Direct irradiation of the nozzle causes undesired polymerization in certain key moments of the process, such as retractions or flowless movements, which may lead to the formation of imperfections and residues on top of the layer, which in turn can affect the deposition of the following layer either by remaining entrapped, effectively creating defects which could subsequently act as crack nucleation sites, or by altering the correct deposition process, negatively affecting the precision. Additionally, opposed to FDM processes where the hot end effectively melts any defects encountered on its way and smooths the layer, these defects tend to sum up during the printing process. It is of paramount importance to have complete control over the flow, the retraction, the layer height and the nozzle height to avoid these phenomena as much as possible. In any case, further developments to the UV irradiation system are necessary. One viable solution could be a more controlled and

targeted light emission, possibly via lasers, pointing only at the already deposited bead or turning off at specific moments. A hybrid technology, implementing a mechanical levelling process between different layers could also be beneficial.

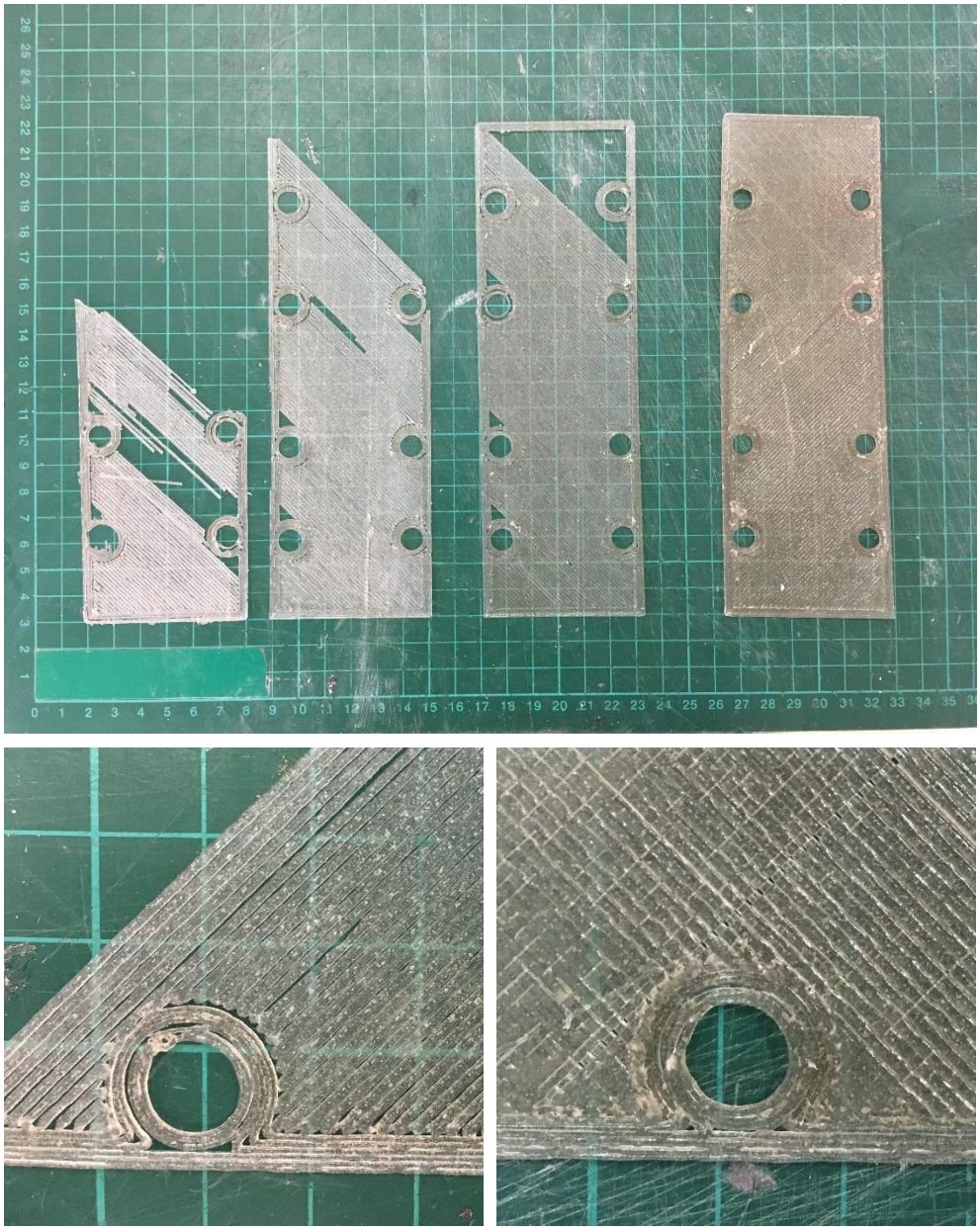

Figure 3.9 Print quality improvement on the Delta 40x70 system after flow, retraction and overlap adjustements. The bottom left pictures shows insufficient bead overlap and flow. On the right, the same feature after the fine tuning. The formulation used in this case was SR60V.

3.6.3 Nozzles

Just as for FDM processes, the nozzle plays a vital role in the material deposition process for LDM systems. Wider diameters allow for higher material-throughput and are less prone to clogging; smaller nozzles, however, mitigate the typical geometrical defects associated with material deposition processes, such as stair stepping, surface roughness or minimum corner diameter, and generally contribute to reducing the void content.

It was noticed that even though the plastic nozzle TT14-RIGID-PK is advertised as UV-shielding, it does not provide sufficient protection from near-visible UV-light such as that used in this experimentation. The material repeatedly polymerized inside the nozzle, effectively clogging it. Covering the nozzle with black tape or heat shrinking sleeves proved to be a viable solution. Special care had to be taken, however, to precisely cover the nozzle exactly up to the tip. Less coverage and the last millimetres of the nozzle would not be protected from UV-light, leading to clogging; excessive coverage and the tape, or sleeve, would protrude from the nozzle's tip and hinder a correct material deposition process by partially blocking the hole and scratching and deforming the deposited, not yet polymerized bead. It would also act as preferential adhesion site for the material, which would start building up on it, leading to huge material deposits that, while not actively blocking the extrusion, would completely alter the deposition process and lead to very notable print defects.

The conical nozzles generally proved to be a better alternative to cylindrical ones. Their internal chamber geometry reduces backpressure build-up and stabilizes the state of the fluid at the tip. this allows for a more constant flow, less clogging and a generally more precise extrusion. The 3DRag system worked best with the 1.54 mm conical plastic nozzle. The conical metal ones were too small in diameter. The machine was not able to achieve precise flow, probably due to elastic deformation in the syringe piston due to the excessive pressure caused by the smaller nozzle dimensions. On the other hand, these nozzles were the best option for the Delta system. In this case, the higher torque and rigidity of the system, combined with the conceptually different feeding mechanism that was able to achieve constant and precise flow in most working conditions, allowed to successfully use the 0.609 mm and 1.08 mm nozzles, greatly improving the print quality.

4. Case Study

To demonstrate the possible applications of the described technologies to composite tooling, a mold for vacuum assisted hand-layup was manufactured. In-field testing was the most efficient way to evaluate the real functionality of our processes, identify the main issues and understand how to tackle them. It generated extensive information that allowed to lay down a precise application-driven roadmap for future developments. This tool was generated in collaboration with Swiss high-end bicycle manufacturing company BMC.

The model tool was designed to contain some of the functional features typical of composite production processes, in this case, holes for the connection with a second mold, as is often the case in applications such as RTM or compression moulding, and a cut for the application of a valve, similar to those usually seen in bladder moulding processes. The part had an approximate dimension of 200x60x40 mm and was printed on the Delta 40x70 machine with the conical 0.608 mm nozzle, a 0.5 mm layer height and a 20 mm/s speed.

I opted for the SR60V material, which was deemed optimal for initial trials, due to its high performance and ease of use. The part was printed with five bottoms, tops and walls and 60% triangular infill[7] to ensure the necessary rigidity to withstand the vacuum bag pressure. I purposely exaggerated these values to avoid any possible damage to the part. For future projects, using lower values could reduce material use and print time without significantly affecting the mechanical properties.

The post-processing of the part comprehended polishing of the part with coarse, medium and fine grit sandpaper and the application of the gelcoat, specifically developed for tooling applications. According to the manufacturer's specifications, after a 24 hours curing time at room temperature a subsequent thermal treatment was undertaken (8 h @ 80 °C + 8 h @ 140 °C) to increase the T_g of the gelcoat to around 140 °C, in line with that of the material itself.

---

[7] Triangular infill was proven to be the most efficient infill type for simple uniaxial compressive stress states by fellow researcher Niccolò Spotti's work.

Figure 4.1 The mold immediately after printing (left), with clearly visible residual material deposits, and after their removal (right).

Figure 4.2 The mold after polishing (left) and gelcoat application (right).

Figure 4.3 Two Hexforce 200 g/m^2 3k 2/2 twill plies and the prepared vacuum bag.

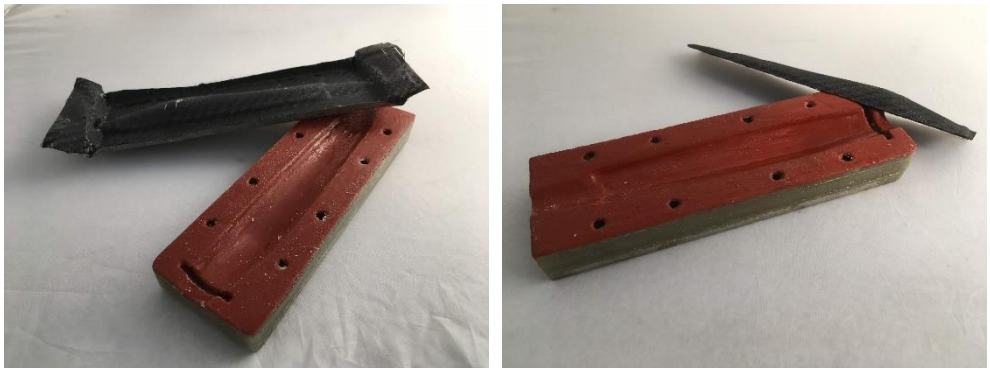

Figure 4.4 Laminated part before (left) and after excess material removal (right).

Figure 4.5 The finished mold and part. On the right, comparison with a PETG mold for room temperature applications.

5. Conclusions and Future Developments

5.1 Conclusions

In this research work, various photopolymerizable composite materials for LDM based additive manufacturing processes were developed. A diacrylate monomer was combined with two different free radical photoinitiators, one of which was deemed more efficient and used throughout the whole experimentation, and, according to the needs, with a dimethacrylate diluent and a free radical peroxide thermal initiator. Four different reinforcements were tested: two types of pristine hammer-milled glass fibers, one of which unsized and one with a silane sizing, and two types of recycled glass fibers, one obtained from corrugated construction panels, and one from dismissed wind turbines post-processed via hammer-milling by the CNR. Both recycled materials were obtained in the framework of the European FiberEUse project.

The length distributions of the reinforcements were carefully evaluated via optical microscopy to collect the necessary data for a precise application of the Halpin-Tsai equations. The mechanical properties of the materials were evaluated and the obtained results were compared to the theoretical predictions. The fracture surfaces were analysed through scanning electron microscopy.

The effectiveness and efficiency of the processes were evaluated via gel content measurements, differential scanning photocalorimetry and infrared absorption.

To assess the applicability of these materials to composite tooling applications, accurate evaluations of the thermal properties were of paramount importance. The coefficients of thermal expansion were evaluated in the 0-250 °C range via thermomechanical analysis. Glass transition temperatures and thermal stability were assessed via differential scanning calorimetry and thermogravimetric analysis.

Various conclusions were drawn:

- SEM analyses of the fracture surfaces showed that the silane sizing is ineffective with this acrylate matrix. No significant changes between the two pristine glass fiber based formulations were observed, and pull-out of the fibers was the prevalent failure mechanism in both cases.

- The printers' ultraviolet LED system by itself yielded insufficient monomer conversion rates in all formulations. While this effect was, as expected, especially marked for the recycled materials, which have a higher absorbance in the relevant wavelengths compared to pristine glass fibers, all materials exhibited insufficient gel content values and subpar mechanical performances.
- This issue was addressed by the addition of a high temperature post-cure thermal treatment, which led to notably higher monomer conversion rates and drastically increased mechanical performances, with one particular formulation's elastic modulus exactly matching the theoretical predictions.
- Compared to Rivierasca's recycled material, formulations based on Gamesa's showed appreciable performance increases in both mechanical performance and coefficient of thermal expansion. These improvements are mainly imputable to the higher glass content of the second filler.
- Glass transition temperatures were around 110 °C for all formulations.
- A stabilizing effect of the glass fibers on the coefficients of thermal expansion was noted. In all cases, the thermal expansion coefficients were significantly lower than those of the thermoplastic materials currently used for additive manufactured solutions for composite tooling applications, indicating a great potential in this field.

Overall, this technology proved to have a decisive advantage in comparison to the current solutions offered on the market. The results presented herein are very encouraging and provide clear indications for the future work and a sound basis for further developments.

5.2 Future Developments

- The thermal treatment introduced during this work was greatly beneficial to the performances of the materials. Initial evaluations of the thermal damage were done, but a more in-depth analysis is necessary to fully understand the ongoing mechanisms.
- Dynamic mechanical thermal analysis (DMTA) is necessary to gain better insight in the viscoelastic behaviour of the materials at higher temperatures.

- Future work should be directed at the development of a compatible sizing, which would drastically improve the mechanical performance of these composite materials.
- Studying the effects of nanofibers on the formulations would be of great interest. These particular fillers, with diameters smaller than 1 μm, have generally higher aspect ratios that would further improve the mechanical performance of the composite, and their very small size could be beneficial to the process, reducing clogging issues and possibly improving the printability of the mixtures.
- The machines should be improved regarding both the deposition and the polymerization control. As already mentioned before, precise layer heights are crucial for a precise, defect-free print. The z-values could be kept under control actively, by improving flow and deposition accuracy, or passively, by introducing a planar milling step in-between the layers. The polymerization process should be improved both regarding monomer conversion rates and precision. Active light sources should be studied, to achieve precise timing and dosing of the radiation. The presence of entrapped air in the material reservoir is another issue that should be addressed.
- An increase in the glass transition temperatures of these formulations is needed to expand their working temperature window, currently too low for the most demanding autoclave cycles. An epoxy-acrylate interpenetrated polymer network based on cationic initiation could be a viable solution.

6. Appendix

6.1 Tensile tests: stress-strain charts

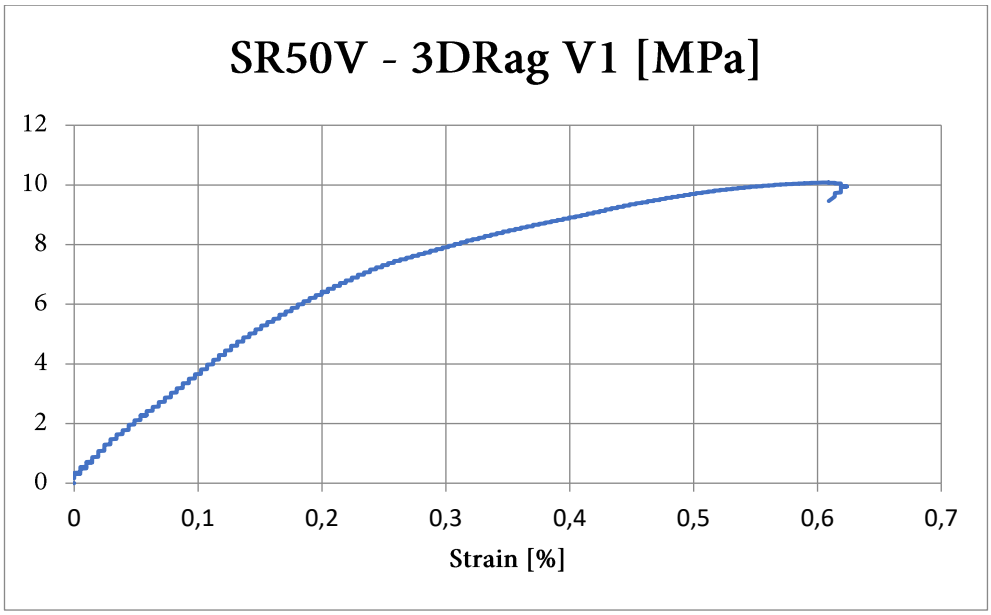

Chart 6.1 σ-ε chart: SR50V printed on the 3DRag V1.

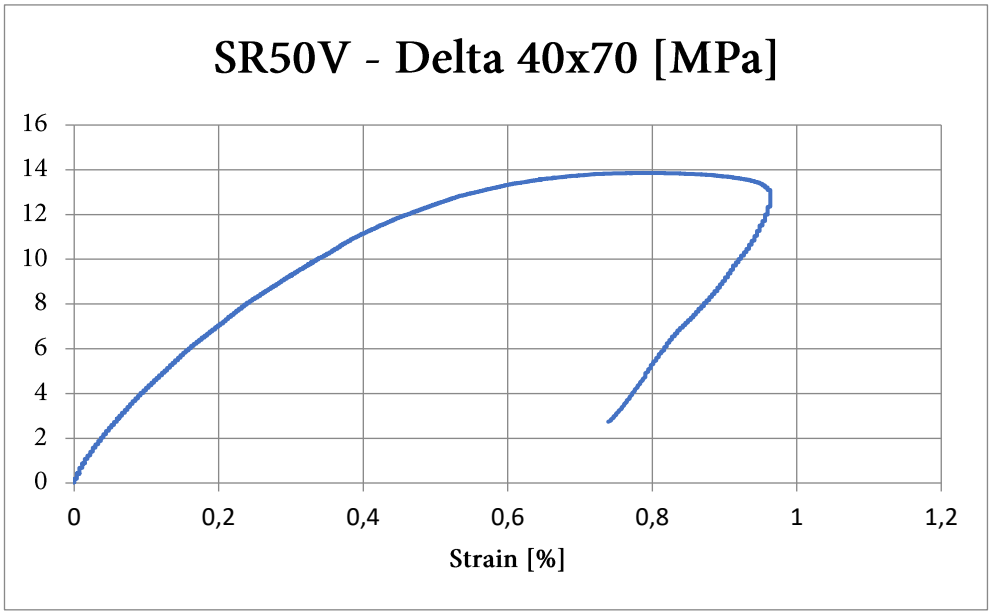

Chart 6.2 σ-ε chart: SR50V printed on the Delta 40x70.

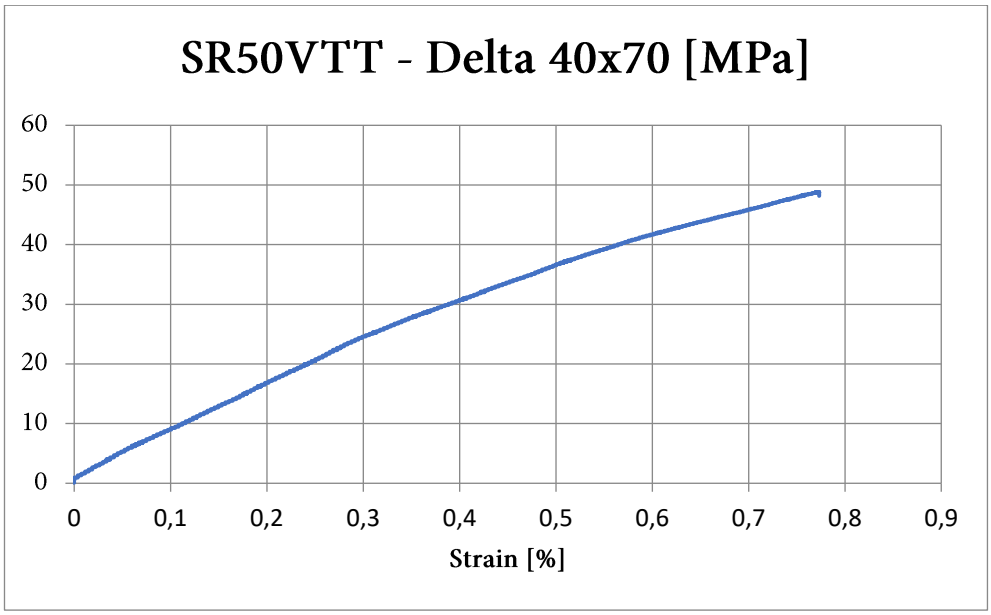

Chart 6.3 σ-ε chart: SR50VTT printed on the Delta 40x70.

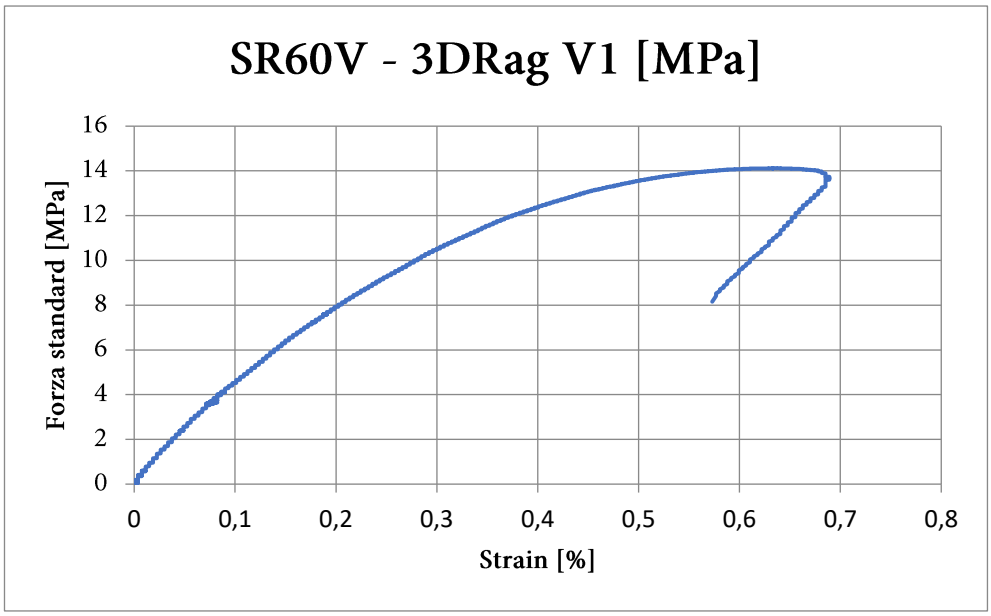

Chart 6.4 σ-ε chart: SR60V printed on the 3DRag V1.

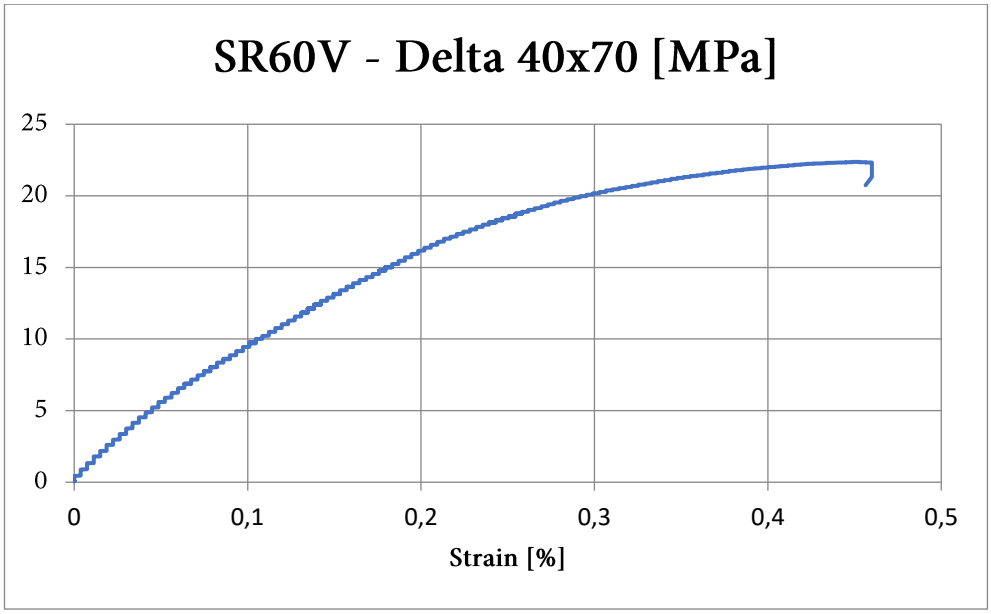

Chart 6.5 σ-ε chart: SR60V printed on the Delta 40x70.

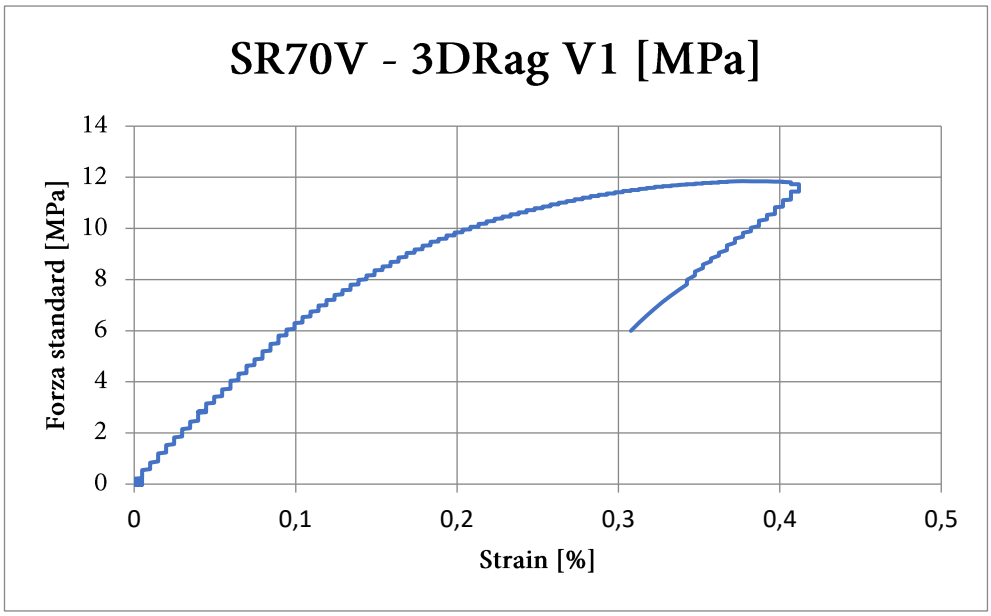

Chart 6.6 σ-ε chart: SR70V printed on the 3Drag V1.

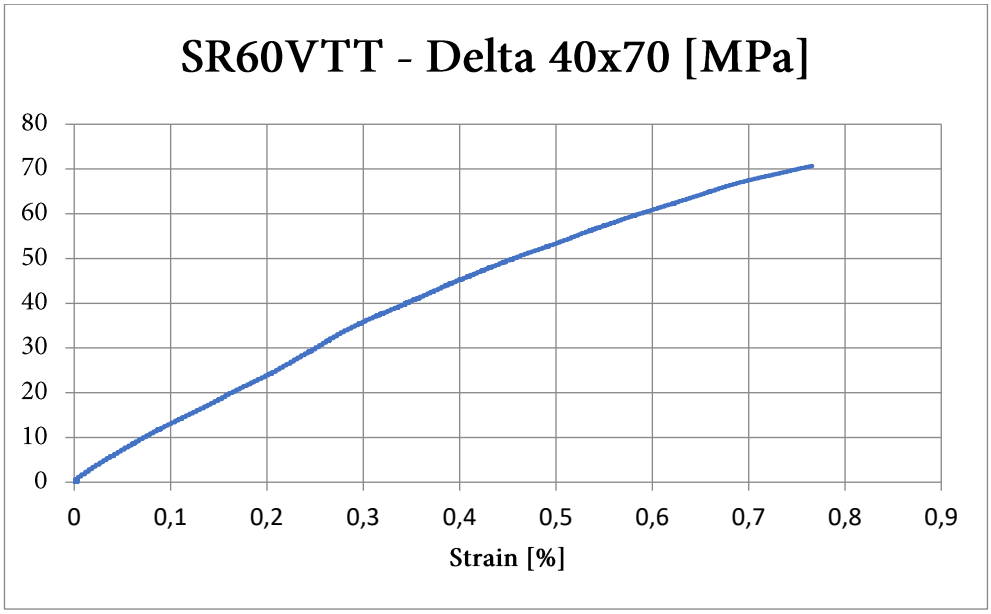

Chart 6.7 σ-ε chart: SR60VTT printed on the Delta 40x70.

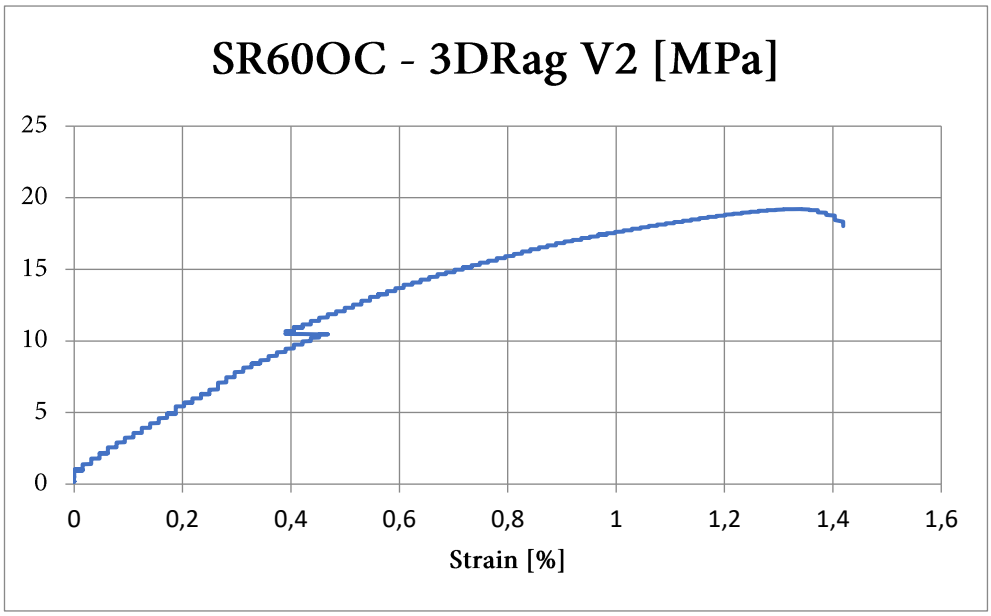

Chart 6.8 σ-ε chart: SR60OC printed on the 3DRag V2.

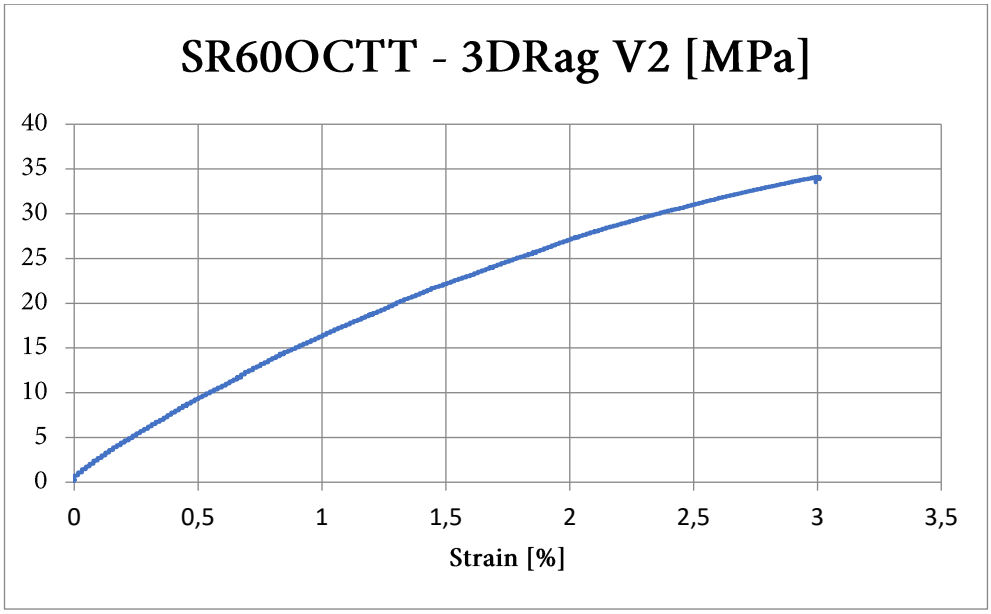

Chart 6.9 σ-ε chart: SR60OCTT printed on the 3DRag V2.

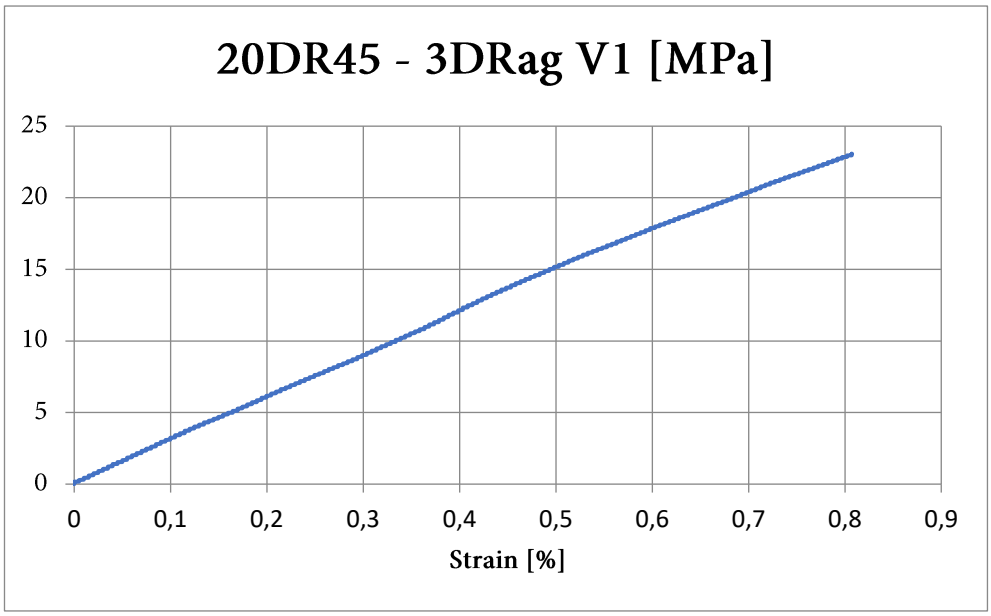

Chart 6.10 σ-ε chart: 20DR45 printed on the 3DRag V1.

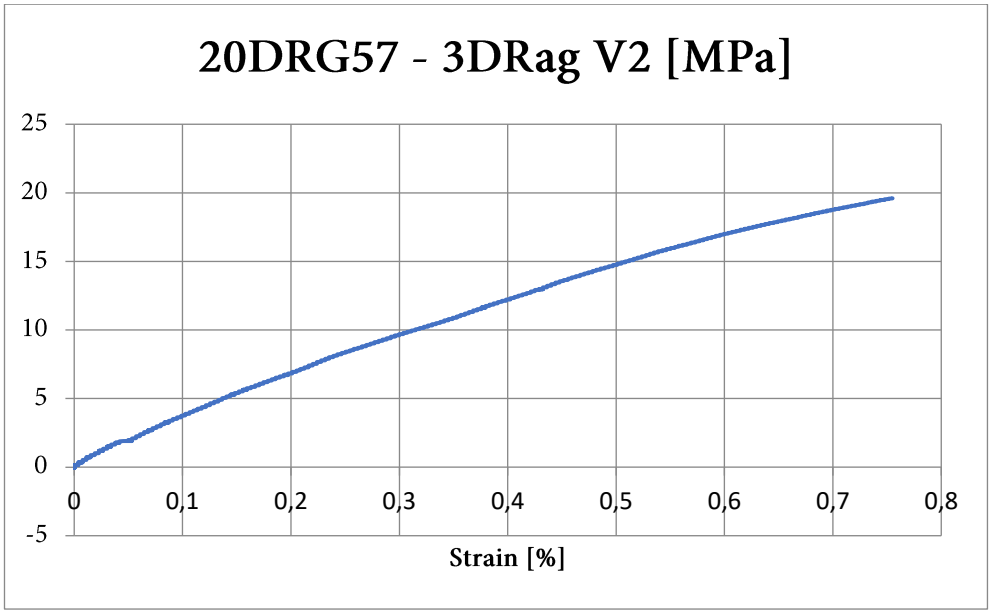

Chart 6.11 σ-ε chart: 20DR57G printed on the 3DRag V2.

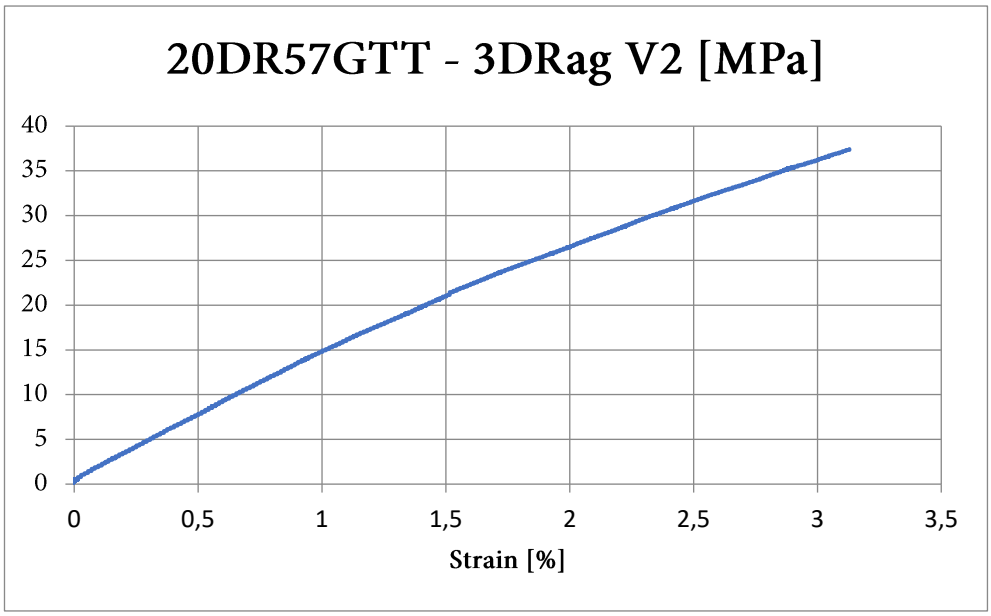

Chart 6.12 σ-ε chart: 20DR57GTT printed on the 3DRag V2.

6.2 TGA: glass content of Gamesa recycled material

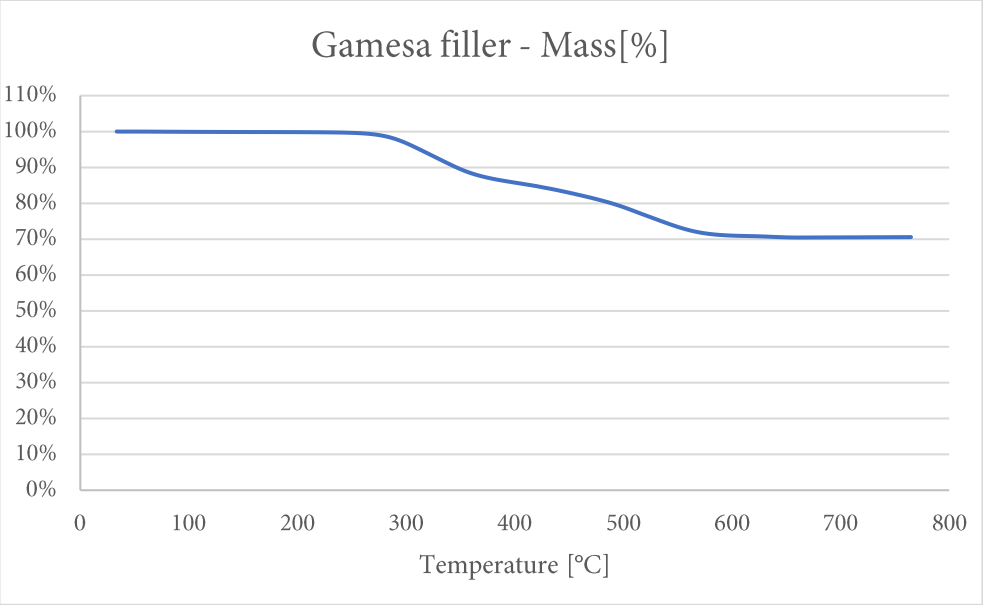

Chart 6.13 Glass content: Gamesa

Bibliography

[1] M. Hanlon, "Sailrocket runs 65.45 knots (75 mph) to smash World Speed Sailing Record," 2012. [Online]. Available: https://newatlas.com/new-world-speed-sailing-record-6537kts-75mph-121kmh/25065/. [Accessed: 01-Apr-2019].

[2] C. T. Herakovich, "Mechanics of composites : A historical review," *Mech. Res. Commun.*, vol. 41, pp. 1–20, 2012.

[3] G. A. Hassaan, "Mechanical Engineering in Ancient Egypt , Part 52 : Mud-Bricks Industry," vol. 3, no. 7, pp. 11–16, 2017.

[4] P. Brune, R. Perucchio, A. R. Ingraffea, and M. D. Jackson, "The toughness of imperial roman concrete," 2010.

[5] M. Ashby, "Materials-a brief history," *Philos. Mag. Lett.*, vol. 88, no. 9–10, pp. 749–755, 2008.

[6] P. Modigliani, "Method and Apparatus for the Production of Fibers from Molten Glass and Similar Meltable Materials," 2212448, 1937.

[7] S. Selvaraju and S. Ilaiyavel, "Applications of Composites in Marine Industry," *J. Eng. Res. Stud.*, pp. 89–91, 2011.

[8] A. I. Taub, P. E. Krajewski, A. A. Luo, and J. N. Owens, "The Evolution of Technology for Materials Processing over the Last 50 Years: The Automotive Example," *Jom*, vol. 59, no. 2, pp. 58–62, 2007.

[9] K. J. Leeg, G. Grove, D. A. Yeomans, S. Ana, and W. E. J. Ripley, "High temperature Resistant Materials Containing Boron and Method of Manufacturing Thereof," US2992960, 1958.

[10] R. B. Millington and R. C. Nordberg, "Process for preparing carbon fibers," US3294489A, 1961.

[11] P. McMullen, "FIbre/resin composites for aircraft primary structures: a short history, 1936-1984," *Composites*, vol. 15, no. 3, pp. 222–230, 1984.

[12] T. K. Das, P. Ghosh, and N. C. Das, "Preparation, development, outcomes,

and application versatility of carbon fiber-based polymer composites: a review," *Adv. Compos. Hybrid Mater.*, 2019.

[13] T. Roberts, "Rapid growth forecast for carbon fibre market," *Reinf. Plast.*, pp. 10–13, 2007.

[14] S. K. Mazumdar, *Composites Manufacturing: Materials, Product and Process Engineering*. Taylor & Francis, 2002.

[15] S. C. Ma and T. L. Yu, "The glass transition temperature of crosslinked unsaturated polyester," *J. Polym. Eng.*, vol. 12, no. 3, pp. 179–196, 1993.

[16] R. Stewart, "Carbon fibre composites poised for dramatic growth," *Reinf. Plast.*, vol. 53, no. 4, pp. 16–21, 2009.

[17] M. K. Thompson *et al.*, "Design for Additive Manufacturing: Trends, opportunities, considerations, and constraints," *CIRP Ann. - Manuf. Technol.*, vol. 65, no. 2, pp. 737–760, 2016.

[18] E. Atzeni and A. Salmi, "Economics of additive manufacturing for end-usable metal parts," *Int. J. Adv. Manuf. Technol.*, vol. 62, no. 9–12, pp. 1147–1155, 2012.

[19] I. Gibson and D. Rosen, *Additive Manufacturing Technologies*, Second Edi. Springer, 2015.

[20] J.-C. André, A. le Mehauté, and O. De Witte, "Dispositif pour réaliser un modèle de pièce industrielle," FR2567668, 1984.

[21] Y. Marutani, "学术图书馆数据馆员职业发展状况的调查与分析," JP19910134126, 1984.

[22] W. E. Masters, "Computer Automated Manufacturing Process and System," US4665492, 1984.

[23] C. W. Hull, "Apparatus for Production of Three Dimensional Objects By Stereolitography," US4575330, 1984.

[24] C. W. Hull, "Method and apparatus for production of three-dimensional objects by stereolitography," EP0171069 A2, 1985.

[25] S. S. Crump, "Apparatus and Method for Creating Three-Dimensional Objects," US5121329, 1992.

[26] R. Gault and D. . Pham, "A comparison of rapid prototyping technologies," *Int. J. Mach. Tools Manuf.*, vol. 38, no. 10–11, pp. 1257–1287, 1998.

[27] "Space in Images - 2014 - 04 - Additive Manufacturing process," *2014*. [Online]. Available: https://www.esa.int/spaceinimages/Images/2014/04/Additive_Manufacturing_process. [Accessed: 02-Apr-2019].

[28] B. E. Kelly, I. Bhattacharya, H. Heidari, M. Shusteff, C. M. Spadaccini, and H. K. Taylor, "Volumetric Additive Manufacturing via Tomographic R econstruction," *Science (80-.).*, vol. 126, no. 1, p. 21, 2019.

[29] S. Kim *et al.*, "Additive manufacturing of hydrogel-based materials for next-generation implantable medical devices," *Sci. Robot.*, vol. 2, no. 2, p. eaah6451, 2017.

[30] X.-H. Qin, A. Ovsianikov, J. Stampfl, and R. Liska, "Qin_Review on Additive Manufacturing of Hydrogels for Tissue Engineering.pdf," *BioNanoMat*, vol. 15, no. 3–4, pp. 49–70, 2014.

[31] A. B. Varotsis, "Introduction to SLA 3D Printing | 3D Hubs." [Online]. Available: https://www.3dhubs.com/knowledge-base/introduction-sla-3d-printing. [Accessed: 01-Apr-2019].

[32] A. B. Varotsis, "Introduction to SLS 3D Printing | 3D Hubs." [Online]. Available: https://www.3dhubs.com/knowledge-base/introduction-sls-3d-printing. [Accessed: 01-Apr-2019].

[33] A. B. Varotsis, "Introduction to FDM 3D printing | 3D Hubs." [Online]. Available: https://www.3dhubs.com/knowledge-base/introduction-fdm-3d-printing. [Accessed: 01-Apr-2019].

[34] "Thermwood LSAM - Large Scale Additive Manufacturing." [Online]. Available: http://www.thermwood.com/lsam_landing_page.htm. [Accessed: 02-Apr-2019].

[35] B. P. Conner *et al.*, "Making sense of 3-D printing: Creating a map of additive manufacturing products and services," *Addit. Manuf.*, vol. 1, pp. 64–76, 2014.

[36] N. Hopkinson and P. Dickens, "Analysis of rapid manufacturing — using layer," *Proc. Inst. Mech. Eng. Part C J. Eng. Manuf.*, vol. 217, pp. 31–39, 2003.

[37] M. Ruffo, C. Tuck, and R. Hague, "Cost estimation for rapid manufacturing - Laser sintering production for low to medium volumes," *Proc. Inst. Mech. Eng. Part B J. Eng. Manuf.*, vol. 220, no. 9, pp. 1417–1427, 2006.

[38] D. Thomsen, R. Stickles, C. Cooper, M. Foust, and W. Dodds, "Development of the GE Aviation Low Emissions TAPS Combustor for Next Generation Aircraft Engines," no. January, pp. 1–9, 2014.

[39] L. E. Murr, S. M. Gaytan, E. Martinez, F. Medina, and R. B. Wicker, "Next generation orthopaedic implants by additive manufacturing using electron beam melting," *Int. J. Biomater.*, vol. 2012, 2012.

[40] B. H. Wong, R. P. Scholz, and D. L. Turpin, "Invisalign A to Z," *Am. J. Orthod. Dentofac. Orthop.*, vol. 121, no. 5, pp. 540–541, 2002.

[41] L. Portolés Griñan, J. Delgado Gordillo, V. Petrovic, O. Jordá Ferrando, J. Ramón Blasco Puchades, and J. Vicente Haro Gonzalez, "Additive layered manufacturing: sectors of industrial application shown through case studies," *Int. J. Prod. Res.*, vol. 49, no. 4, pp. 1061–1079, 2010.

[42] D. E. Cooper, M. Stanford, K. A. Kibble, and G. J. Gibbons, "Additive Manufacturing for product improvement at Red Bull Technology," *Mater. Des.*, vol. 41, pp. 226–230, 2012.

[43] A. Kochan, "Rapid prototyping helps Renault F1 team UK improve championship prospects," *Assem. Autom.*, vol. 23, no. 4, pp. 336–339, 2003.

[44] "La "Adler Group s.r.l." di Paolo Scudieri: una realtà mondiale - la Repubblica.it," *2016*. [Online]. Available: https://ricerca.repubblica.it/repubblica/archivio/repubblica/2016/02/13/la-adler-group-srl-di-paolo-scudieri-una-realta-mondialeNapoli04.html. [Accessed: 02-Apr-2019].

[45] F. Uliano, "Comunicato Stampa FIM-CISL FCA produzione 3° trimestre 2018," 2018.

[46] D. Catchpole, "Boeing Stages Launch of 777X Production | Air Transport News: Aviation International News," *2017*. [Online]. Available: https://www.ainonline.com/aviation-news/air-transport/2017-10-24/boeing-stages-launch-777x-production. [Accessed: 02-Apr-2019].

[47] P. Parandoush and D. Lin, "A review on additive manufacturing of polymer-

fiber composites," *Compos. Struct.*, vol. 182, pp. 36–53, 2017.

[48] B. Brenken, E. Barocio, A. Favaloro, V. Kunc, and R. B. Pipes, "Fused Filament Fabrication of Fiber-Reinforced Polymers: A Review," *Addit. Manuf.*, vol. 21, no. February, pp. 1–16, 2018.

[49] G. T. Mark and A. S. Gozdz, "Three Dimensional Printer For Fiber Reinforced Composite Filament Fabrication," 9126367 B1, 2015.

[50] Stratasys.Inc, "FDM for Composite Tooling 2 . 0," 2018.

[51] "polyetherimide information and properties," 2001. [Online]. Available: http://www.polymerprocessing.com/polymers/PEI.html. [Accessed: 04-Apr-2019].

[52] J. G. Drobny, *Specialty Thermoplastics*. Springer, 2015.

[53] L. J. Love and C. Duty, "Cincinnati big area additive manufacturing (BAAM)," *Oak Ridge Natl. Lab.*, pp. 1–11, 2015.

[54] T. Z. Sudbury, ingfie R. Sprld, V. Kunc, and C. Duty, "An assessment of additive manufactured molds for hand-laid fiber reinforced composites," *Int. J. Adv. Manuf. Technol.*, vol. 90, no. 5–8, pp. 1659–1664, 2017.

[55] V. Kunc, "The Development of High Temperature Thermoplastic Composite Materials for Additive Manufactured Autoclave Tooling," *Oak Ridge Natl. Lab.*, 2017.

[56] G. Griffini, M. Invernizzi, M. Levi, G. Natale, G. Postiglione, and S. Turri, "3D-printable CFR polymer composites with dual-cure sequential IPNs," *Polymer (Guildf).*, vol. 91, pp. 174–179, 2016.

[57] M. Invernizzi, G. Natale, M. Levi, S. Turri, and G. Griffini, "UV-assisted 3D printing of glass and carbon fiber-reinforced dual-cure polymer composites," *Materials (Basel).*, vol. 9, no. 7, 2016.

[58] A. Zolfagharian, A. Z. Kouzani, S. Y. Khoo, A. A. A. Moghadam, I. Gibson, and A. Kaynak, "Evolution of 3D printed soft actuators," *Sensors Actuators, A Phys.*, vol. 250, pp. 258–272, 2016.

[59] B. Mosadegh, G. Xiong, S. Dunham, and J. K. Min, "Current progress in 3D printing for cardiovascular tissue engineering," *Biomed. Mater.*, vol. 10, no. 3, 2015.

[60] X. Li *et al.*, "3D-printed biopolymers for tissue engineering application," *Int. J. Polym. Sci.*, vol. 2014, 2014.

[61] "Properties: S-Glass Fibre." [Online]. Available: https://www.azom.com/properties.aspx?ArticleID=769. [Accessed: 02-Apr-2019].

[62] "Properties: E-Glass Fibre." [Online]. Available: https://www.azom.com/properties.aspx?ArticleID=764. [Accessed: 02-Apr-2019].

[63] ASTM, "Astm D3039/D3039M," *Annu. B. ASTM Stand.*, pp. 1–13, 2014.

[64] ASTM International, "Standard test method for tensile properties of plastics," *ASTM Int.*, vol. 08, pp. 46–58, 2003.

[65] R. N. Kay, "Effect of Raster Orientation on the Structural Properties of Components Fabricated by Fused Deposition Modeling," p. 165, 2014.

[66] W. Conshohocken, "Standard Test Method for Temperature Calibration of Thermomechanical Analyzers 1," *Current*, vol. i, pp. 5–8, 1998.

[67] ASTM International, "Standard Test Method for Linear Thermal Expansion of Solid Materials With a Push-Rod Dilatometer," *ASTM Stand. E228-17*, vol. 11, no. April, pp. 1–7, 2017.

[68] J. C. Halpin, S. T. Louis, J. L. Kardos, J. C.Halpin, S. T. Louis, and J. L.Kardos, "The Halpin-Tsai Equations: A Review," *Polym. Eng. Sci.*, vol. 16, no. 5, pp. 344–352, 1976.

[69] E. J. Barbero, *Introduction to Composite Materials Design*, Second Edi. 2011.

[70] Y. H. Bagis and F. A. Rueggeberg, "The effect of post-cure heating on residual, unreacted monomer in a commercial resin composite," *Dent. Mater.*, vol. 16, no. 4, pp. 244–247, 2000.

[71] S. A. J. Wendt, "The effect of heat used as a secondary cure upon the physical properties of three composite resins. I. Diametral tensile strength, compressive strength, and marginal dimensional stability," *Quintessence Int. (Berl).*, vol. 18, no. 4, pp. 265–271, 1987.

[72] E. ASMUSSEN, "Restorative resins: hardness and strength vs. quantity of remaining double bonds," *Eur. J. Oral Sci.*, vol. 90, no. 6, pp. 484–489, 1982.

[73] C. I. Vallo, P. E. Montemartini, and T. R. Cuadrado, "Effect of residual monomer content on some properties of a poly(methyl methacrylate)-based bone cement," *J. Appl. Polym. Sci.*, vol. 69, no. 7, pp. 1367–1383, 2002.

[74] H. Huang and R. Talreja, "Effects of void geometry on elastic properties of unidirectional fiber reinforced composites," *Compos. Sci. Technol.*, vol. 65, no. 13, pp. 1964–1981, 2005.

[75] R. M. (Richard M. . Christensen, *Theory of viscoelasticity : an introduction*, 2nd Editio. Academic Press, 1982.

[76] C. H. Bamford and A. D. Jenkins, "Studies in polymerization IX . The occlusion of free radicals by polymers: physical factors determining the concentration and behaviour of trapped radicals," *Proc. R. Soc. London. Ser. A. Math. Phys. Sci.*, vol. 228, no. 1173, pp. 220–237, 1955.

[77] George Socrates, *Infrared and Raman Characteristic Group Frequencies Contents*. 2004.

[78] G. G. Cameron and F. Davie, "The Oxidative Thermal Degradation of Poly (Methyl Acrylate)," *Chem*, vol. 26, pp. 200–207, 1972.

[79] "F900 & F900 PRO 3D Printers for Large Build Manufacturing | Stratasys." [Online]. Available: https://www.stratasys.com/3d-printers/stratasys-f900. [Accessed: 01-Apr-2019].

[80] "ULTEM™ 1010 resin: The Strongest FDM 3D Printing Material | Stratasys." [Online]. Available: https://www.stratasys.com/materials/search/ultem1010. [Accessed: 01-Apr-2019].

[81] J. Sloan, "Thermwood 3D prints large boat hull pattern: CompositesWorld," 2017. [Online]. Available: https://www.compositesworld.com/blog/post/thermwood-3d-prints-large-boat-hull-pattern. [Accessed: 02-Apr-2019].

[82] S. Black, "Boeing and Thermwood : CompositesWorld," 2018. [Online]. Available: https://www.compositesworld.com/articles/boeing-and-thermwood. [Accessed: 02-Apr-2019].

[83] J. Sloan, "CAMX 2017 preview: Thermwood : CompositesWorld," 2017. [Online]. Available: https://www.compositesworld.com/articles/camx-2017-preview-thermwood. [Accessed: 02-Apr-2019].

[84] H. Caliendo, “LM Industries Accelerating 3D-Printed Vehicles : Plastics Technology,” *2018*. [Online]. Available: https://www.ptonline.com/articles/lm-industries-accelerating-3d-printed-vehicles. [Accessed: 02-Apr-2019].

[85] “UONBI Learning - Size Reduction Equipment.” [Online]. Available: https://learning.uonbi.ac.ke/courses/SCH405/scormPackages/path_2/53_size_reduction.html. [Accessed: 01-Apr-2019].